

This is to certify that the

dissertation entitled

Cyclic Evolution of a Magmatic System: The Paintbrush Tuff, SW Nevada Volcanic Field

presented by

Timothy P. Flood

has been accepted towards fulfillment of the requirements for

Doctoral degree in Geology

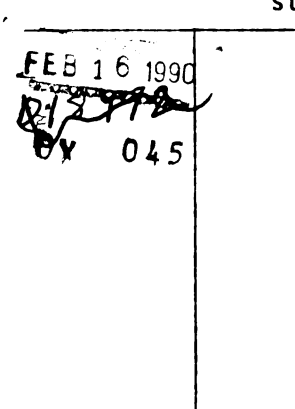
Major professor

MSU is an Affirmative Action/Equal Opportunity Institution

0-12771



RETURNING MATERIALS:
Place in book drop to
remove this checkout from
your record. FINES will
be charged if book is
returned after the date
stamped below.



CYCLIC EVOLUTION OF A MAGMATIC SYSTEM: THE PAINTBRUSH TUFF, SW NEVADA VOLCANIC FIELD

Ву

Timothy P. Flood

A DISSERTATION

Submitted to
Michigan State University
in partial fulfillment of the requirements
for the degree of

DOCTOR OF PHILOSOPHY

Department of Geological Sciences

1987

ABSTRACT

CYCLIC EVOLUTION OF A MAGMATIC SYSTEM: THE PAINTBRUSH TUFF, SW NEVADA VOLCANIC FIELD

By

Timothy P. Flood

The chemical and thermal evolution of a single magmatic system is recorded in a series of four ash-flow sheets, the Paintbrush Tuff, that were erupted from the same caldera within a span of 600,000 years. The chemistry of individual glassy pumices, collected from the tops and bottoms of the ash-flow sheets, are used to quantitatively evaluate possible fractionation mechanisms, such as magma mixing and fractional crystallization. The glassy pumices are used because they most nearly approximate the magma in the chamber.

The Topopah Spring Member (TPT) was the first ash-flow sheet (>1200km³) to be erupted. Prior to eruption of the TPT, a sharp compositional interface existed in the magma chamber between a high-silica rhyolite and a quartz latite. The Pah Canyon Member (TPP) was the second ash-flow sheet (<40km³) to be erupted. The magma that was the source for the TPP formed by mixing of the contrasting magma types represented in the TPT. The magma mixing was most likely due to disruption of the compositional interface during eruption of the TPT.

The Yucca Mountain Member (TPY) was the third ash-flow sheet (<20km3) to be erupted, and represents the reestablishment of a high-silica rhyolite in the system. This high-silica rhyolite is best modeled by 15% to 24% fractional crystallization from the TPP. The Tiva Canyon Member (TPC) is the fourth ash-flow sheet (>1000km3) to be erupted, and it consists of three compositional modes, a higher-silica rhyolite, rhyolite, and quartz latite. The high-silica rhyolite of the TPY is an early eruptive phase of the higher-silica rhyolite of the TPC and their origins are the same. The rhyolite most likely formed by a combination of fractional crystallization and magma mixing of the TPP and the quartz latite of the TPC. Alternatively, the rhyolite may have formed by fractional crystallization and magma mixing of the higher-silica rhyolite and the quartz latite of the TPC, or by fractional crystallization from the TPC. The origin of the quartz latite has not been determined.

All of the chemical variation within the Paintbrush Tuff can be accounted for by fractional crystallization or magma mixing operating alone and/or in conjunction. No other fractionation processes need be invoked. Also, volume estimates based on quantitative modeling reveal that the size of the ash-flow sheets do not reflect the size of their associated reservoirs.

ACKNOWLEDGMENTS

This thesis is dedicated to my family, in particular my father Frank and my mother Florence, who have contributed unmitigated moral and financial support, and tolerated my many years of avoiding the real world. Special commendation also goes to Kim Elias who shared the many frustrations and successes pursuant to this degree, and assisted in the final preparation of the manuscript.

I would like to acknowledge those geologists who took an interest in my career over the years, and assisted me along the way. Tom Vogel, my Ph.D. advisor, is commended for going above and beyond the call of duty in providing moral, professional and financial support. Ralph Marsden, recently deceased, was a geologist of great moral and professional stature who personified the concept of integrity, and passed it on via example to many of his students. Gene and Sally LaBerge acted as my geologic godparents throughout my career. It is always an understatement to try and thank ones parents, be they family or professional. John Tinker was my first geology instructor. He sparked my interest in geology. Dick Ojakangas was my M.S. advisor, and he taught me that a geologist can be very professional and also have a lot of fun.

I would also like to acknowledge my committee members Frank Byers Jr., John Wilband, Dave Long and Bill Cambray for their overall help and critical review of my thesis.

John Wilband is especially thanked for the use of his excellent computer programs.

I acknowledge the fellow students who have contributed to this degree. Mike and Beth Miller fed me often and helped me survive my first year at MSU. My fellow ash-flow tuffists, Ben Schuraytz, Jim Mills and Tim Rose, provided lively and critical discussions related to my work. John "Wad" Nelson and Deke have been excellent housemates. Bill Sack, Keith Hill, and many others are thanked for their friendship.

I acknowledge the support and critical discussions of other geologists working with the Paintbrush Tuff. Frank Byers Jr. has reviewed my thesis and has served as an inspiration with his continuing enthusiasm. Rick Warren, Dave Broxton, Bob Scott and Lee Younker contributed critical reviews, lively discussions and helped me clarify ideas related to my thesis.

I am grateful for the continued support of Lawrence
Livermore National Research Laboratory, especially Lee
Younker and the Basic Energy Sciences Program, as well as,
Larry Schwartz and the Containment Program, and, Larry
Ramspott and Virginia Oversby and the Waste Isolation
Program. Rick Ryerson is thanked for his assistance in
collecting microprobe data. Michigan State University
provided a teaching and research assistantship for my tenure
at MSU.

TABLE OF CONTENTS

LIST OF FIGURES	
LIST OF TABLES	
INTRODUCTION	. 1
REGIONAL GEOLOGY	. 5
NOMENCLATURE	. 10
SAMPLING AND ANALYTICAL METHODS	. 11
DATA	. 32
Chemistry	. 32
Mineralogy	. 36
Temperature Estimates	. 39
Pressure Estimates	. 42
Comparison of Topopah Spring and Tiva Canyon Members	. 44
	. 44
Canyon Members	
Canyon Members	. 50
Canyon Members	. 50
Canyon Members	. 50 . 50 . 50
Canyon Members	. 50 . 50 . 50 . 59
Canyon Members	. 50 . 50 . 50 . 59 . 64 . 67
Canyon Members	. 50 . 50 . 50 . 59 . 64 . 67
Canyon Members	. 50 . 50 . 50 . 59 . 64 . 67 . 70 . 71

TABLE OF CONTENTS (continued)

ORIGIN OF T	HE TIVA	CANYON	MEMBE	R .	 		•	• •	. 84
Introd	uction .				 				. 84
_	ison of he Highe								
	anyon Me								. 85
	of Ryo								
	ejection ractions		_	_					
	ummary .								
VOLUME RELA	TIONSHIE				 	•	•		. 103
DISCUSSION					 				. 107
CONCLUSIONS	• • •				 		•		. 114
Future	Conside	ration	s		 		•		. 116
APPENDICES					 				. 120
REFERENCES					 				. 142

LIST OF FIGURES

Figure	1.	Location map of SW Nevada volcanic field including the Timber Mountain-Oasis Valley caldera complex	6
Figure	2.	Generalized stratigraphic column of the four ash-flow sheets of the Paintbrush Tuff	9
Fi g ure	3.	Estimated temperatures and oxygen fugacities for the Topopah Spring and Pah Canyon Members	41
Figure	4.	Plots of La, Ba, and Hf against SiO2 for the Topopah Spring and Tiva Canyon Members	46
Figure	5.	Plots of La, Ba, and Hf against Zr for the Topopah Spring and Tiva Canyon Members	47
Fi <i>g</i> ure	6.	Average chondrite-normalized rare-earth element profiles of the Topopah Spring and Tiva Canyon Members	48
Figure	7.	Plots of La, Zr, and Hf against SiO2 for the Topopah Spring and Pah Canyon Members	52
Figure	8.	Plots of La, Sc and Hf against Zr for the Topopah Spring and Pah Canyon Members	53
Figure	9.	Ratio-ratio plots to evaluate magma mixing	54
Figure	10.	Chondrite-normalized rare-earth element profiles of the Topopah Spring and Pah Canyon Members	56

LIST OF FIGURES (continued)

Figure	11.	Comparison of magma mixing and fractional crystallization: Predicted and actual values of Ba, Rb, Sr, Eu	62
Figure	12.	Comparison of magma mixing and fractional crystallization: Predicted and actual values of Ba, Rb, Sr, Eu	63
Fi g ure	13.	Plots of La, Sc, and Hf against SiO2 for the Pah Canyon and Yucca Mountain Members	72
Figure	14.	Plots of La, Sc, and Hf against Zr for the Pah Canyon and Yucca Mountain Members	73
Figure	15.	Average chondrite-normalized rare-earth element profiles of the Pah Canyon and Yucca Mountain Members	74
Figure	16.	Fractional crystallization: Predicted and actual values of Ba, Rb, Sr, Eu	79
Figure	17.	Fractional crystallization: Predicted and actual values of Ba, Rb, Sr, Eu	80
Figure	18.	Fractional crystallization: Predicted and actual values of Ba, Rb, Sr, Eu	81
Figure	19.	Fractional crystallization: Predicted and actual values of Ba, Rb, Sr, Eu	82
Figure	20.	Plots of La, Sc, and Hf against SiO2 for the Yucca Mountain and Tiva Canyon Members	86

LIST OF FIGURES (continued)

Figure	21.	Plots of La, Sc, and Hf against Zr for the Yucca Mountain and Tiva Canyon Members	87
Figure	22.	Average chondrite-normalized rare-earth element profiles for the Yucca Mountain and Tiva Canyon Members	93
Figure	23.	Schematic illustration depicting the origin of the rhyolite of the Tiva Canyon Member by magma mixing and fractional crystallization	104
Figure	24.	Schematic illustration depicting alternate origin of the rhyolite of the Tiva Canyon Member by magma mixing and fractional crystallization	104
Figure	25	Schematic illustration depicting the origin of the rhyolite of the Tiva Canyon Member by fractional crystallization	104

LIST OF TABLES

Table	1.	Chemical analyses of pumices from the Topopah Spring Member		•	•	14
Table	2.	Chemical analyses of pumices from the Pah Canyon Member		•		18
Table	3.	Chemical analyses of pumices from the Yucca Mountain Member		•		21
Table	4.	Chemical analyses of pumices from the Tiva Canyon Member	•	•		25
Table	5.	Precision and accuracy of data	-	•	•	33
Table	6.	Modal phenocryst abundances of the Paintbrush Tuff		•	•	57
Table	7.	Predicted and actual trace element abundances in the Pah Canyon Member .	•	•		60
Table	8.	Distribution coefficients used for fractional crystallization modeling .	•			65
Table	9.	Comparison of the Yucca Mountain Member and the higher-silica rhyolite of the Tiva Canyon Member using a statistical T-test		•		90
Table	10.	Predicted and actual trace element abundances in the rhyolite of the Tiva Canyon Member				95

INTRODUCTION

Ash-flow sheets are important for understanding the evolution of high-level silicic magma systems because of their large erupted volume. They have been the subject of many investigations in recent years. Smith (1960) elucidated the basic concepts and terminology that would be the foundation for subsequent ash-flow sheet investigations. He outlined the idea that ash-flow tuffs and related calderas were the result of a rapid evacuation of the top of a magma chamber. Compositional and thermal variations within individual ash-flow sheets were noted by later workers (Smith and Bailey, 1966; Lipman et al., 1966). Some of the more comprehensive published data on compositionally zoned high-silica rhyolites has been compiled by recent workers (Smith, 1979; Hildreth, 1981; Mahood, 1981; Bacon et al., 1981; Crecraft et al., 1981; Whitney and Stormer, 1986; Schuraytz et al., 1986).

Glassy whole-pumices (crystals + liquid) found in ash-flow sheets are a useful tool for studying high-silica magmatic systems. The chemistry of glassy pumices represent a near approximation to the chemistry of the magma in the chamber minus volatiles. Pumices are better suited for studying high-level magmatic systems than lavas because pumices are derived from the upper part of the magma column, whereas lavas may erupt from unknown levels of the magma chamber. Further more, pumices are more representative of

the original magma than plutonic rocks that have been modified by crystallization processes. Chemical variation among pumices from the top of an ash-flow sheet may also represent the chemical variation throughout the entire ash-flow sheet (Schuraytz et al., 1983, 1986).

Smith (1979) proposed that ash-flow sheets, in a general way, record the inverted chemical and thermal variations in the magma chamber. Recent theoretical modeling of eruption dynamics however, (Blake, 1981; Spera, 1984; Blake and Ivey, 1986; Spera et al., 1986) has shown that the evacuation of magma from a reservoir during an ash-flow eruption is much more complex. For example, the occurrence of pumices of contrasting compositions at the top of ash-flow sheets is consistent with current models of eruption dynamics whereby different parts of the same magma body are erupted simultaneously. The origin of compositional gaps seen in some ash-flow sheets can also be theoretically modeled as the result of eruption dynamics (Spera et al., 1986).

The Paintbrush Tuff is well suited for studying the evolution of a magmatic system through time. The geologic field relationships are well known due to the extensive and excellent work of the U.S.G.S and others for the past 30 years (Byers et al., 1976a, 1976b; Scott et al., 1984; Warren and Byers, 1985, Schuraytz et al., 1986). Four major ash-flow sheets, erupted over a span of 600,000 years, provide periodic samplings of the chemical and thermal conditions of the evolving magmatic system. Specifically,

these conditions are recorded in glassy whole-pumices from the top and bottom of each of the four members. Pumices of contrasting composition occur in both the first and last ash-flow sheets that were erupted from the system. These represent magma from different parts of the magma chamber. Chemical and thermal data obtained from these pumices can be used to model and constrain fractionation processes that produced variations in the system through time.

The study of the evolution of the Paintbrush Tuff is significant because it is an investigation of the relationship between a series of ash-flow sheets from the same magmatic system. Many previous detailed studies have been done on individual ash-flow sheets that have attempted to model the <u>intrasheet</u> variation as the result of various fractionation mechanisms (for current bibliography, see Bacon and McBirney, 1985), however, this study attempts to model the mechanisms of evolution <u>between</u> ash-flow sheets from the same magmatic system. This is an attempt to model a magmatic system through time by assuming that the characteristics of each ash-flow sheet represent a view of the system at a particular instant in time.

Mechanisms responsible for the compositional variations seen in ash-flow sheets have been the subject of intensive research and debate. This investigation will concentrate on the mechanisms of magma mixing and fractional crystallization. These are processes that can be quantitatively evaluated. Other processes have been

proposed to account for the variation in high-level silicic systems, but these processes cannot be quantitatively evaluated. For example, Hildreth (1981) attributed the compositional variation of the Bishop Tuff, particularly the strong trace element variation, to mostly a liquid/liquid diffusional process he termed thermogravitational diffusion. Double diffusion convection is another liquid/liquid diffusional process, similar to thermogravitational diffusion, that has been experimentally modeled using saline solutions and theoretically applied to magma chambers (for review, see Turner and Campbell, 1986). A combination of liquid-liquid and crystal-liquid processes involving boundary layers has recently been invoked to explain compositional variations in high-silica magmas (Baker and McBirney, 1985; Sparks and Marshall, 1986).

The purpose of this investigation is to define the constraints on the chemical evolution of a magmatic system through time. The Paintbrush Tuff is well-suited to evaluate fractionation mechanisms because of the fact that; a) individual pumices from the four members of the Paintbrush Tuff represent magmatic conditions at the time of quenching, b) these four ash-flow sheets are part of the same magmatic system, therefore, fractionation mechanisms that may have operated in the system can be evaluated, c) comparison of chemical and mineralogical data, obtained from individual pumices from the different ash-flow sheets, can be used to constrain possible fractionation processes.

REGIONAL GEOLOGY

The Paintbrush Tuff is part of the Timber Mountain-Oasis Valley caldera complex, which lies in the southwestern Nevada volcanic field (Fig. 1). This volcanic field is located in the southern Great Basin of the western United States. The study area is located mostly on the Department of Energy's Nevada Test Site, about 100 km northwest of Las Vegas, Nevada.

The southwest Nevada volcanic field is an extensive volcanic plateau that developed in mid to late-Tertiary time (Noble et al., 1965; Christiansen et al., 1977). This field covered an area of 11,000km² and was most active in late Miocene and early Pliocene time, between 16 m.y. and 6 m.y. ago. More than 15 major ash-flow sheets and at least 8 collapse calderas have been identified in this field, largely by geologists of the U.S. Geological Survey (Ekren et al., 1971, Byers et al., 1976b).

The rocks of the southwest Nevada volcanic field have a rhyolite-basalt association, which is typical of the volcanism which accompanied the development of widespread extensional normal faulting along the margins of the Great Basin at this time (Christiansen and Lipman, 1972).

Rhyolite is the dominant volcanic rock type in this field, with subordinate amounts of basalt. A varied group of volcanic rocks have been noted, including: trachyandesites (Noble et al., 1965), peralkaline volcanic rocks (Noble et al., 1969; Noble et al., 1984) and calc-alkalic andesites

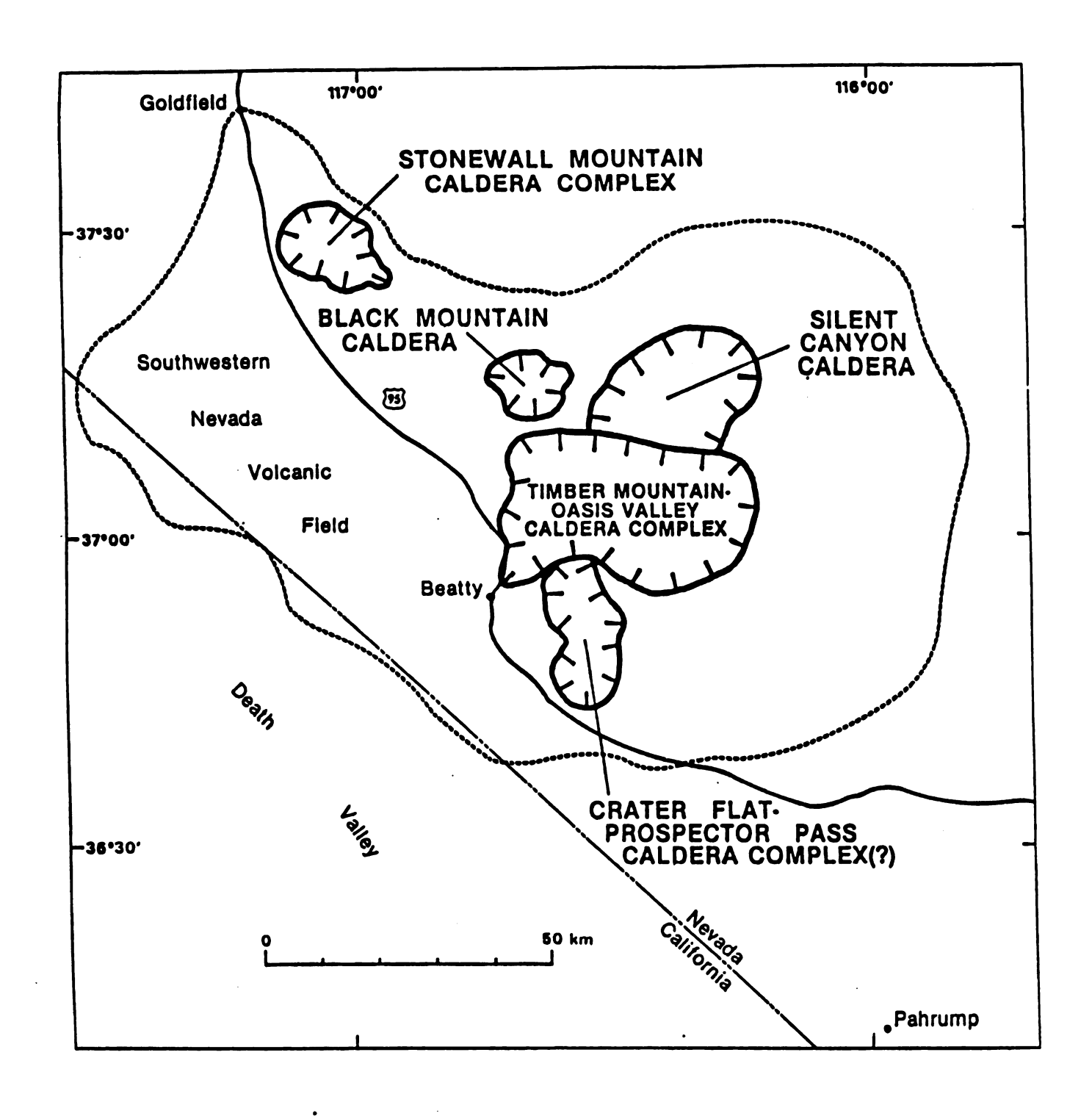


Figure 1. Location map of SW Nevada volcanic field including the Timber Mountain-Oasis Valley caldera complex (after Carr et al., 1984; and Noble et al., 1984).

to rhyodacites (Poole et al., 1966).

By the time of the first major eruptions from the southwest Nevada Volcanic field, some of the Basin and Range style structural and topographic features had been defined by extensional normal faulting (Ekren et al., 1968). Based on aerial distributions and thickness variations of extensive ash-flow sheets in the field, it was shown that Basin and Range normal faulting occurred before, during and after periods of major volcanic activity. However, the outlines of the present basins were formed mostly by normal faulting which overlapped or postdated the later stages of volcanism (Christiansen, et al., 1977).

The calc-alkaline part of the Timber Mountain-Oasis
Valley caldera complex belongs to the southwest Nevada
volcanic field (Fig. 1). This complex has been the subject
of intensive studies for over twenty years and these have
led to a much better understanding of high-level silicic
systems (Lipman et al., 1966; Noble and Hedge, 1969; Lipman,
1971; Lipman and Friedman, 1975; Byers et al., 1976a, 1976b;
Christiansen et al., 1977; Schuraytz et al., 1983; Scott et
al., 1984; Warren et al., 1984; Broxton et al., 1985; Flood
et al., 1985a, 1985b; Schuraytz et al., 1985; Warren and
Byers, 1985; Schuraytz et al., 1986).

The Timber Mountain-Oasis Valley caldera complex was active from 16 m.y. to 9 m.y. ago and was the source of nine voluminous rhyolitic ash-flow sheets and many smaller rhyolitic tuffs and lava flows (Byers et al., 1976b). The

caldera complex occupies a slightly elliptical area with a maximum diameter of 40 km, and was the source region for rocks with alkali-calcic, calc-alkaline and calcic affinities. The alkali-calcic Paintbrush Tuff is part of the Timber Mountain-Oasis Valley caldera complex and consists of four major ash-flow sheets, intercalated with lavas and minor pyroclastic fall material (Fig. 2). Topopah Spring Member was the first ash-flow sheet erupted (13.3 m.y.) and is a compound cooling unit (Lipman et al., 1966; Byers et al., 1976b). It has an estimated volume of >1200 km3 (Scott et al., 1984). The Pah Canyon and Yucca Mountain Members were the second and third ash-flow sheets erupted. Both are simple cooling units and relatively small in volume, <40 km3 and <20 km3, respectively (Byers et al., 1976b). The Tiva Canyon Member was the fourth ash-flow sheet erupted (12.7 m.y.) and is a compound cooling unit (Byers et al., 1976b). It has a volume of >1000 km³ (Scott et al., 1984).

These ash-flow sheets were all part of the same magmatic system, the Paintbrush Tuff, and were erupted from the Claim Canyon caldron (Byers et al., 1976b). Episodic subsidence occurred during or immediately following eruption of each ash-flow sheet, with the maximum subsidence of the Claim Canyon cauldron segment occurring during the late stages of eruption of the Tiva Canyon Member (Byers et al., 1976b). Christiansen et al. (1977) suggest that the Yucca Mountain and Tiva Canyon Members were erupted from an overlapping

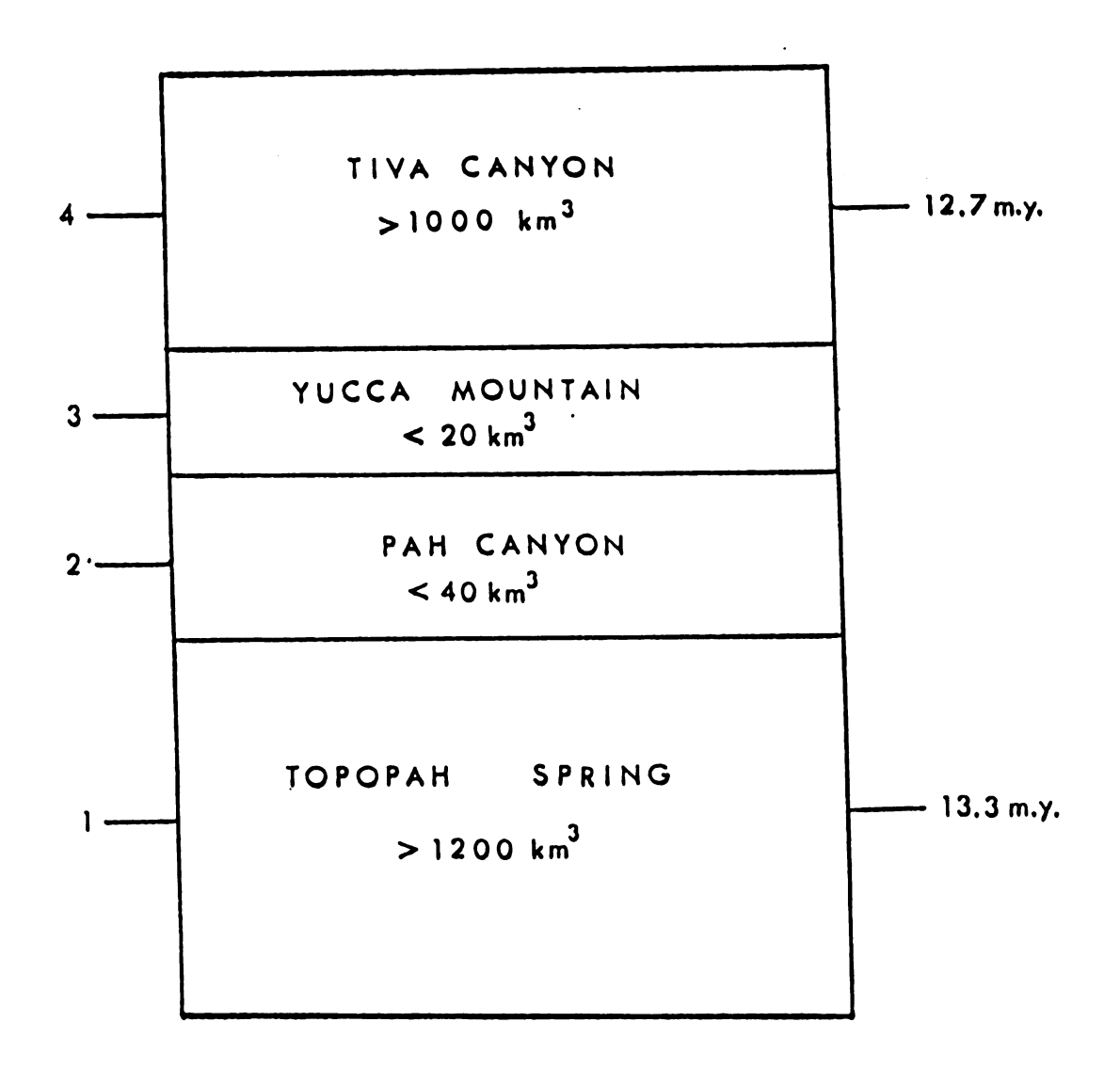


Figure 2. Generalized stratigraphic column of the four ash-flow sheets of the Paintbrush Tuff (after Byers et al., 1976a, 1976b)..

area including the Oasis Valley caldron segment and not the Claim Canyon caldron segment, even though the Claim Canyon segment did subside during the eruption of the Tiva Canyon Member.

A thorough and comprehensive review of the stratigraphy, petrography, and chemistry of the Paintbrush Tuff is summarized by Byers et al. (1976b) and Quinlivan and Byers (1977). This study adds to the known data base and will be discussed in greater detail in later chapters.

NOMENCLATURE

The terms quartz latite, rhyolite and high-silica rhyolite are used in this study to emphasize the chemical differences between groups of pumices. The terms are defined in a similar fashion by Byers et al. (1976b), where tuffs and lavas that range from approximately 65 to 72 percent SiO2 are called quartz latites; rocks ranging from about 72 to 76 percent SiO2 are called rhyolites; and rocks ranging from 76 to 78 percent SiO2 are called high-silica rhyolites. For the Tiva Canyon Member, the quartz latite ranges in SiO2 from 65.9 to 67.3 percent; the rhyolite from 71.0 to 72.6 percent SiO2; and a higher-silica rhyolite from 74.1 to 77.4 percent SiO2. No rocks occur in the gaps between the groups. For example, no observed pumices in the Tiva Canyon Member have a chemical composition in the range of 67.3 to 71.0 percent SiO2.

SAMPLING AND ANALYTICAL METHODS

All chemical data were obtained from individual, glassy pumices which were collected from the tops and bottoms of the ash-flow sheets. Pumices from the Topopah Spring Member were collected by Schuraytz, whereas the pumices from the Pah Canyon, Yucca Mountain, and Tiva Canyon Members were collected by the author. Sample locations for the upper three units are given in Appendix 1.

Sampling was designed to specifically sample the variation among the glassy pumices. Glassy pumices were chosen because they represent an instantaneous sampling of the unmodified magma from the magma chamber. That is, these glassy whole-pumices (glass + phenocrysts) most nearly represent the magma in the magma chamber, minus lost volatiles. These glassy pumices are also independent of later processes such as crystallization, devitrification, vapor phase alteration, and weathering. Pumices collected from the tops and bottoms of the ash-flow sheets represent the chemical variation of the whole ash-flow sheet. Schuraytz et al. (1983, 1985) determined that the chemical variation among the glassy pumices taken from the top of the Topopah Spring Member is as great as the variation seen throughout the entire ash-flow sheet. The same is true of the Tiva Canyon Member. This is consistent with an eruption sampling through a layered magma body, with the uppermost part of the ash-flow sheet representing all parts of the erupted magma body (Spera, 1984; Blake and Ivey, 1986).

Individual, glassy pumices that were collected from the tops and bottoms of the ash-flow sheets were the only samples used for this study. The Topopah Spring Member is represented by 21 major and trace element analyses of pumices, 11 from the base of the ash-flow sheet, and 10 from the top. The Pah Canyon Member is represented by 15 analyses, 6 from the base of the ash-flow sheet, and 9 from the top. The Yucca Mountain Member is represented by 25 analyses, 9 from the base of the ash-flow sheet and 16 from the top. The Tiva Canyon Member is represented by 46 analyses, 23 from the base of the ash-flow sheet and 23 from the top.

Ten major elements and nineteen trace elements were determined for each collected sample used in this study. The major elements plus Ba, Rb, and Sr were analyzed by a Rigaku (S-Max) automated X-ray fluorescence spectrometer (XRF) at Michigan State University. Major elements were determined using the Criss matrix absorbtion parameter (Criss, 1980). Trace elements were calculated using an internal reference peak to measure the matrix adsorption (Hagan, 1982). Concentrations were determined by linear least squares regression on U.S.G.S. standards. XRF analyses were performed on wafers made according (Appendix 2) to the method of Hagan (1982). All the major element analyses reported in this study were obtained from wafers made by the author, including the Topopah Spring Member. Powders of individual pumices from the Topopah Spring

Member, which were collected by Schuraytz, were obtained and prepared for analysis in the same manner as pumices collected by the author. All trace elements analyses, including the Topopah Spring Member, were done by instrumental neutron activation analyses (INNA) at Lawrence Livermore National Laboratoy under the direction of Robert Heft. Prior to analyses, all samples of glassy pumice were subjected to a soil carbonate leaching procedure (Appendix 2) to remove the secondary carbonate.

The chemistry of the glassy pumices used in this study may be found in Tables 1 to 4. Because of the secondary hydration of glassy pumice, all the values of the major elements have been normalized to one hundred percent. The accuracy and precision of the data is reported in Table 5.

The chemistry of the phenocrysts for all major phases of the Pah Canyon, Yucca Mountain, and Tiva Canyon Members was determined for this study. The minerals include; plagioclase, potassium feldspar, clinopyroxene, hornblende, biotite, magnetite, and ilmenite. All determinations were made at Lawrence Livermore National Research Laboratory using a JEOL 733 superprobe. The chemistry of a limited number of minerals for the Topopah Spring Member were determined by Schuraytz et al. (1986). An outline of the procedures used to obtain the mineral compositions, including preparation, is reported in Appendix 3. Summary histograms of the mineral characteristics for each unit are also given in Appendix 3.

TABLE 1. Chemical analyses of pumices from the Topopah Spring Member.

SAMPLE NO. FIELD I.D.		2 BB8-15B	3 BB8-15C	4 BB8-10	5 BB8-5	6 BB8-3A	7 BB8-3B
WT. X							
S102	77.1	75.9	77.3	76.5	78.7	77.7	76.3
Al2 O3	13.1	14.3	12.9	13.3	12.3	12.8	13.7
FeO	0.92	0.77	0.94	0.88	0.83	0.69	0.69
CaO	0.62	0.53	0.59	0.90	0.53	0.53	0.52
MgO	0.17	0.26	0.15	0.36	0.04	0.14	0.20
TiO2	0.11	0.13	0.11	0.11	0.09	0.11	0.16
MnO	0.09	0.15	0.08	0.08	0.07	0.08	0.06
Na ₂ O	2.74	2.78	2.92	2.58	2.42	2.62	2.75
K2 O	5.20	5.18	5.04	5.25	4.95	5.31	5.57
P2 O5	0.01	0.01	0.01	0.02	0.01	0.00	0.00
PPM							
Sc	2.2	2.3	2.3	2.2	2.3	2.1	1.9
Rb	195.1	194.1	186.6	192.1	186.5	205.2	215.7
Zr	163.5	177.4	131.3	153.6	107.5	159.7	206.9
Cs	5.4	5.5	5.1	5.6	5.1	5.9	6.0
Hf	5.4	6.4	4.9	5.3	4.5	5.4	7.1
Ta	1.4	1.5	1.4	1.4	1.3	1.4	1.4
Th	22.5	27.3	23.1	22.2	22.0	21.8	24.2
Ba	120	170	170	150	100	100	90
La	33.6	36.1	33.2	32.1	34.6	31.4	44.9
Ce	78.5	83.2	66.1	62.8	82.1	64.8	92.0
Sm	5.4	5.7	5.5	5.2	5.9	5.2	6.0
Eu	0.24	0.27	0.24	0.22	0.25	0.24	0.32
Tb	0.7	0.7	0.7	0.7	0.8	0.7	0.8
Yb	3.0	3.1	3.1	2.8	3.3	2.8	3.1
Lu	0.5	0.5	0.5	0.5	0.3	0.5	0.5

TABLE 1 (continued).

SAMPLE NO. FIELD I.D.	8 BB8-2	9 CP1-3A	10 CP1-2 E	11 CP1-1G	12 CP32B	13 LW1-A	14 LW2-5
WT. %							
SiO2 Al2O3 FeO CaO MgO TiO2 MnO Na2O K2O P2O5	78.0 12.5 0.98 0.54 0.10 0.09 0.10 2.64 5.05	77.1 12.9 0.81 0.55 0.16 0.09 0.07 3.19 5.05 0.00	77.0 13.0 0.76 0.53 0.23 0.09 0.07 2.89 5.34 0.00	77.1 12.8 0.79 0.54 0.15 0.09 0.08 2.92 5.53 0.00	69.7 16.9 2.03 0.38 0.49 0.49 0.05 3.22 6.65 0.08	69.4 16.0 1.57 1.28 0.43 0.41 0.11 3.83 6.90 0.08	71.4 15.1 1.29 0.90 0.24 0.32 0.10 3.25 7.35 0.03
PPM							
Sc Rb Zr Cs Hf Ta Th Ba	2.3 187.7 119.8 5.1 4.5 1.3 21.6	2.4 204.3 121.2 6.8 4.8 1.4 22.7	2.5 206.1 116.7 6.4 5.0 1.4 22.7	2.5 204.4 127.3 7.4 5.0 1.4 23.4	6.9 141.4 620.5 4.2 13.0 0.8 20.8	5.9 128.8 563.6 3.3 12.0 0.9 20.7	4.1 155.7 397.1 3.5 9.8 1.1 21.0
La Ce Sm Eu Tb Yb Lu	30.7 66.3 5.4 0.23 0.7 3.1 0.6	33.2 60.2 5.6 0.24 0.7 2.7 0.5	30.8 68.1 5.4 0.25 0.7 3.2 0.6	32.2 66.3 5.6 0.23 0.7 3.0	208.4 324.6 12.4 2.67 0.9 2.8 0.6	174.7 263.6 11.7 2.24 0.8 2.9 0.5	111.4 201.6 9.4 1.17 0.8 3.0 0.3

TABLE 1 (continued).

SAMPLE NO. FIELD I.D.		16 LW4-1A	17 LW4-1C	18 LW4-5B	19 LW410B	20 LW4-15B	21 LW4-15C
WT. %							
SiO2 Al2O3 FeO CaO MgO TiO2 MnO Na2O K2O P2O5	77.2 12.4 0.64 0.57 0.21 0.09 0.06 3.09 5.77 0.00	76.8 12.7 0.73 0.52 0.16 0.11 0.06 3.25 5.55 0.01	69.2 16.3 1.80 1.16 0.54 0.48 0.09 3.56 6.72 0.16	69.4 15.6 1.50 1.58 0.43 0.38 0.10 3.62 7.30 0.08	70.1 15.4 1.43 1.59 0.38 0.36 0.10 4.14 6.40 0.06	76.8 12.4 0.70 0.97 0.20 0.10 0.07 3.21 5.54 0.03	68.7 16.4 1.88 1.63 0.48 0.46 0.11 4.10 6.13 0.11
PPM							
Sc Rb Zr Cs Hf Ta Th Ba	2.3 188.9 112.2 5.1 4.6 1.3 22.0	2.4 182.8 136.9 4.8 4.9 1.3 21.7	7.0 134.1 618.4 4.0 12.8 0.8 20.5	5.2 135.7 500.6 2.7 11.3 0.9 19.7 490	4.8 155.6 486.8 3.1 11.3 0.9 20.4 350	2.1 180.6 152.6 4.9 5.0 1.3 22.0	6.3 123.3 659.4 2.7 13.8 0.8 18.4 2380
La Ce Sm Eu Tb Yb Lu	30.0 59.6 5.3 0.22 0.7 2.9	38.7 73.4 5.7 0.36 0.7 2.9 0.5	215.2 323.7 13.0 2.77 0.93 3.2 0.6	152.2 267.7 10.3 2.13 0.8 3.0 0.6	137.7 247.1 10.3 1.79 0.9 3.0 0.5	37.2 74.1 5.3 0.25 0.7 3.1 0.5	195.7 291.2 12.3 3.30 0.9 3.1 0.5

TABLE 2. Chemical analyses of pumices from the Pah Canyon Member.

SAMPLE NO FIELD I.D		23 P1B	24 P1C	25 P1D	26 P1E	27 P1F	28 P2AA
WT. %							
SiO2 Al203 FeO CaO MgO TiO2 MnO Na2O K2O P2O5	73.9 14.4 1.22 0.75 0.18 0.30 0.10 3.78 5.31 0.02	74.0 14.4 1.04 0.80 0.20 0.29 0.09 4.00 5.18 0.02	74.2 14.4 1.09 0.75 0.19 0.27 0.09 3.69 5.28 0.02	73.8 14.4 1.06 0.83 0.25 0.29 0.09 4.00 5.31 0.02	73.7 14.3 1.00 0.80 0.19 0.26 0.09 4.68 4.99 0.02	74.2 14.4 1.10 0.78 0.17 0.29 0.09 4.02 5.01 0.03	73.6 14.5 1.03 0.88 0.50 0.29 0.10 3.35 5.73 0.04
PPM				•			
Sc Rb Zr Cs Hf Ta Th Ba	4.2 176.4 304.3 4.5 7.8 1.2 20.6 1090	4.1 184.8 350.4 4.6 8.1 1.2 20.2 1080	3.9 182.8 262.9 4.7 8.2 1.3 20.2 1200	4.0 203.2 302.7 4.7 8.0 1.3 19.9 1200	3.9 194.4 314.4 4.7 7.9 1.3 20.4 970	4.2 193.8 355.3 4.7 8.3 1.3 20.4 1000	4.0 169.1 310.8 4.6 7.7 1.2 19.3
La Ce Sm Eu Tb Yb Lu	77.6 145.4 8.3 1.52 0.8 3.6 0.3	77.6 145.5 8.1 1.52 0.9 3.3 0.7	76.4 149.2 8.5 1.54 0.8 3.5 0.5	76.6 147.2 8.2 1.53 0.8 3.3 0.7	79.2 148.1 7.8 1.66 0.9 3.7 0.5	75.6 145.4 8.7 1.60 0.9 3.5 0.6	91.8 150.4 9.8 1.63 1.0 3.3

TABLE 2 (continued).

SAMPLE NO		30	31	32	33	34	35
FIELD I.D		P2C	P2D	P2 F	P2G	P2H	P5B
WT. X							
SiO2	73.1	72.9	74.0	72.8	74.0	73.9 14.3 1.10 0.89 0.83 0.31 0.09 3.13 5.39 0.04	74.1
Al2O3	14.7	14.7	14.2	14.7	14.2		14.3
FeO	1.35	1.33	0.92	1.37	1.19		1.11
CaO	0.84	0.82	0.83	0.77	0.87		0.81
MgO	0.55	0.57	0.40	0.49	0.59		0.35
TiO2	0.29	0.30	0.24	0.31	0.30		0.26
MnO	0.10	0.10	0.08	0.10	0.09		0.08
Na2O	3.29	3.40	3.49	3.41	3.18		3.45
K2O	5.74	5.94	5.81	6.02	5.59		5.49
P2O5	0.03	0.03	0.03	0.04	0.04		0.02
PPM							
Sc Rb Zr Cs Hf Ta Th Ba	4.0 161.2 315.1 3.9 7.3 1.2 18.5 1160	4.2 181.1 431.3 4.5 8.3 1.3 20.7	3.5 163.3 175.2 3.7 6.9 1.2 18.8 850	3.8 170.3 313.5 4.6 8.5 1.2 20.2 1180	4.0 157.0 276.5 3.7 7.8 1.1 18.2 1190	5.3 160.7 352.3 3.9 8.6 1.2 19.9	4.6 164.5 358.0 3.7 9.2 1.1 20.2
La	92.5	91.2	73.4	79.3	83.4	90.8	92.4
Ce	140.4	156.6	122.6	148.1	145.8	161.8	173.8
Sm	8.4	9.8	8.8	8.7	9.2	9.6	9.0
Eu	1.56	1.83	1.45	1.66	1.67	1.63	1.86
Tb	1.0	1.0	0.9	0.8	0.8	1.0	0.8
Yb	2.7	3.8	3.6	3.2	3.1	3.5	3.3
Lu	0.6	0.8	0.6	0.7	0.6	0.7	0.8

TABLE 2 (continued).

SAMPLE N	10. 36		
FIELD I.	D. P5E		
WT. %			
SiO2	73.2		
Al203	14.8		
FeO	1.27		
CaO	0.90		
MgO	0.28		
TiO2 MnO	0.33 0.10		
Na2O	3.41		
K2 O	5.68		
P2 O5	0.03		
PPM			
C _	4.4		
Sc Rb	4.4 167.5		
Zr	318.4		
Cs	3.7		
Hf	8.5		
Га	1.1		
Th	19.3		
Ba	1440		
La	93.4		
Ce	176.9		
S m	9.0		
<u>E</u> u	1.96		
ТЪ	0.9		
ΥЪ	3.3		
Lu	0.7		

TABLE 3. Chemical analyses of pumices from the Yucca Mountain Member.

SAMPLE NO. FIELD I.D.	37 Y3B	38 Y3C	39 Y3D	40 Y3F	41 Y3H	42 Y3I	43 Y1B
WT. X							
SiO2	77.0	76.4	77.2	77.4	76:7	77.2	76.8
Al203	12.9	12.8	12.6	12.5	12.6	12.7	12.9
FeO	0.61	0.72	0.62	0.68	0.87	0.73	0.76
CaO	0.28	0.35	0.31	0.28	0.36	0.32	0.28
MgO	0.12	0.20	0.08	0.04	0.13	0.05	0.26
TiO2	0.13	0.14	0.12	0.12	0.13	0.14	0.12
MnO	0.10	0.11	0.11	0.10	0.11	0.09	0.09
Na2 O	3.52	4.13	3.95	3.76	3.83	3.29	3.55
K2 O	5.36	5.11	5.06	5.11	5.20	5.72	5.20
P2 O5	0.01	0.01	0.01	0.01	0.01	0.01	0.01
PPM							
Sc	1.7	1.7	1.6	1.6	1.7	1.7	1.6
Rb	208.7	191.0	201.7	199.9	195.7	195.6	203.1
Zr	232.6	184.5	229.7	203.2	171.4	231.7	191.3
Cs	5.4	5.5	5.5	5.3	5.4	5.2	5.4
Hf	7.1	7.6	7.5	7.4	7.7	7.0	7.2
Ta	1.5	1.6	1.5	1.5	1.5	1.4	1.5
Th	24.1	24.7	24.0	24.5	23.9	23.3	24.4
Ba	0	100	65	0	80	130	5
La	30.8	30.1	32.0	29.9	33.2	30.0	30.6
Ce	60.1	63.3	65.8	60.0	66.2	58.6	54 .6
Sm	4.1	4.5	5.7	4.1	5.0	3.6	3.4
Eu	0.24	0.27	0.33	0.23	0.26	0.23	0.24
Тъ	0.7	0.7	0.9	0.7	0.8	0.7	0.6
ΥЪ	3.6	3.8	3.8	3.4	3.7	3.0	3.4
Lu	0.5	0.7	0.8	0.6	0.7	0.6	0.6

TABLE 3 (continued).

SAMPLE NO. FIELD I.D.	44 Y1C	45 Y1D	46 Y1BA	47 Y1BB	48 Y1BC	49 Y1BD	50 Y1BE
WT. X							
SiO2 Al2Os FeO CaO MgO TiO2 MnO Na2O K2O P2Os	76.9 12.9 0.66 0.29 0.31 0.13 0.10 3.52 5.20 0.01	76.7 12.7 0.90 0.33 0.13 0.13 0.10 3.83 5.15 0.01	76.1 12.6 0.88 0.44 0.55 0.15 0.12 2.86 6.23 0.03	76.8 12.6 0.73 0.26 0.20 0.14 0.09 3.38 5.72 0.01	75.8 12.4 0.90 0.31 0.11 0.13 0.10 3.74 6.44 0.01	76.8 12.4 0.79 0.28 0.42 0.13 0.09 3.24 5.76 0.01	76.7 12.6 0.84 0.33 0.15 0.13 0.09 3.64 5.52 0.01
PPM							
Sc Rb Zr Cs Hf Ta Th Ba	1.6 191.5 180.5 5.1 7.3 1.5 24.6	1.7 196.5 216.1 5.2 7.4 1.5 24.0	1.8 201.8 252.1 5.6 8.3 1.5 23.6	1.7 208.8 244.0 5.3 8.7 1.7 25.0	1.6 216.1 251.3 6.2 8.3 1.6 24.1	1.6 196.8 271.1 5.4 8.1 1.6 23.5	1.6 202.3 301.9 5.1 8.0 1.5 23.0
La Ce Sm Eu Tb Yb Lu	32.8 61.5 4.5 0.29 0.7 3.6 0.8	27.9 63.1 4.0 0.27 0.7 3.5 0.7	33.4 66.1 6.1 0.45 0.9 4.0	31.8 67.8 6.9 0.29 1.1 4.2 0.7	29.7 63.9 5.7 0.28 0.9 4.1 0.5	29.5 62.1 5.5 0.26 0.9 3.9 0.6	28.4 63.7 7.2 0.28 1.1 3.7 0.7

TABLE 3 (continued).

SAMPLE NO.	51	52	53	54	55	56	57
FIELD I.D.	Y1BF	Y1BG	Y1BH	Y4AA	Y4AB	Y4BB	Y4BD
WT. X							
SiO2	76.6	76.6	76.7	76.3	75.8	77.2	76.8
Al2O3	12.6	12.4	12.6	13.1	13.2	12.6	12.7
FeO	0.94	0.85	0.82	0.94	0.83	0.76	0.90
CaO	0.32	0.54	0.26	0.34	0.26	0.26	0.33
MgO	0.18	0.42	0.34	0.14	0.36	0.08	0.06
TiO2	0.13	0.13	0.13	0.13	0.15	0.13	0.13
MnO	0.09	0.11	0.09	0.08	0.11	0.10	0.07
Na2O	3.68	2.77	3.24	3.62	3.18	3.68	3.64
K2O	5.48	6.10	5.89	5.35	6.09	5.17	5.40
P2OS	0.00	0.02	0.01	0.01	0.00	0.01	0.01
PPM							
Sc Rb Zr Cs Hf Ta Th Ba	1.7 212.7 251.7 5.4 8.4 1.7 25.1	1.6 204.8 207.0 5.3 8.1 1.6 23.6 45	1.6 203.5 225.5 5.4 8.3 1.6 24.6 5	1.7 213.6 249.9 5.6 8.0 1.6 24.5 25	1.6 188.7 246.0 5.1 8.4 1.6 24.6	1.6 205.8 224.7 5.5 8.1 1.6 23.9	1.6 200.0 228.1 5.2 8.2 1.6 24.8
La	29.6	29.2	28.8	29.1	30.4	29.9	29.3
Ce	66.0	59.2	61.6	63.2	74.2	61.6	62.4
Sm	5.8	5.7	5.4	4.9	7.1	5.8	5.5
Eu	0.25	0.26	0.26	0.27	0.26	0.26	0.23
Tb	0.9	0.9	0.9	0.9	1.1	0.9	0.9
Yb	4.2	3.9	4.0	3.9	4.4	4.0	3.9
Lu	0.8	0.7	0.6	0.7	0.7	0.6	0.6

TABLE 3 (continued).

SAMPLE NO. FIELD I.D.		59 Y4BF	60 Y4BG	61 Y4BH
WT. %				
SiO2	76.6	76.8	76.9	77.1
A12O3	12.6	12.6	12.6	12.4
FeO	0.73	0.78	0.83	0.90
CaO	0.3 4 0.07	0.34 0.22	0.34 0.10	0.36 0.06
MgO TiO2	0.07	0.22	0.10	0.06
MnO		0.14	0.13	0.13
Na ₂ O	0.09 4.21	2.91	3.32	3.28
K2 O	5.23	6.07	5.72	5.65
P2 O5	0.01	0.01	0.01	0.01
1403	0.01	0.01	0.01	0.01
PPM				
Sc	1.6	1.6	1.7	1.7
Rb	192.1	227.2	209.2	164.2
Zr	208.4	220.6	263.5	261.0
Cs	5.4	6.8	5.7	6.2
Hf	8.0	8.2	8.1	8.0
Ta	1.6	1.6	1.6	1.3
Th	24.0	23.7	23.0	24.2
Ba	0	0	0	80
La	28.5	29.8	30.3	28.8
Ce	62.2	62.9	61.8	62.1
Sm	5.6	5.6	4.4	5.2
Eu	0.25	0.27	0.24	0.21
Tb	0.9	0.9	0.9	0.9
Yb	4.1	4.0	3.5	4.1
Lu	0.6	0.9	0.7	0.6

TABLE 4. Chemical analyses of pumices from the Yucca Mountain Member.

SAMPLE NO.		63	64	65	66	67	68
FIELD I.D.		C2BB	C2BC	C2BD	C2EA	C2EB	C2EC
WT. X							
SiO2	76.5	76.2	76.4	76.2	76.2	76.1	76.3
Al203	12.7	12.7	12.7	12.6	12.8	12.7	12.6
FeO	0.74	0.87	0.84	0.95	0.71	0.75	0.94
CaO	0.22	0.28	0.21	0.27	0.21	0.28	0.20
MgO	0.18	0.05	0.09	0.04	0.18	0.09	0.12
TiO2	0.14	0.14	0.14	0.14	0.14	0.14	0.14
MnO	0.09	0.08	0.06	0.08	0.08	0.07	0.11
Na20	3.08	2.85	2.68	2.64	2.92	2.58	2.93
K20	6.36	6.85	6.90	7.05	6.73	7.20	6.56
P205	0.01	0.00	0.01	0.01	0.01	0.01	0.00
PPM							
Sc Rb Zr Cs Hf Ta Th Ba	1.5 207.9 241.9 5.4 7.9 1.5 23.7	1.4 200.2 208.5 4.9 7.2 1.5 22.3	1.3 213.0 189.5 5.1 6.5 1.3 19.4 25	1.5 209.1 209.6 5.2 7.7 1.5 22.9	1.5 214.4 223.6 5.1 7.6 1.5 22.8	1.5 223.7 238.6 5.7 7.6 1.5 22.2	1.6 222.2 226.3 5.9 8.2 1.6 24.7
La	28.3	28.4	24.7	28.3	28.8	24.1	29.2
Ce	64.6	58.3	44.8	61.0	62.0	61.2	67.1
Sm	5.2	5.5	3.7	5.4	5.5	5.4	5.4
Eu	0.18	0.19	0.12	0.19	0.19	0.18	0.18
Tb	0.8	0.8	0.7	0.8	0.9	0.9	0.9
Yb	3.8	4.0	3.0	3.7	3.7	3.5	3.9
Lu	0.8	0.5	0.6	0.5	0.5	1.0	0.7

TABLE 4 (continued).

SAMPLE NO. FIELD I.D.	69 C2ED	70 C4B2	71 C4C2	72 C4D2	73 C4E2	74 C4F2	75 C4G2
WT. X							
SiO2 Al2O3 FeO CaO MgO TiO2 MnO Na2O K2O P2O5	76.0 12.9 0.98 0.19 0.27 0.14 0.08 3.03 6.38 0.01	76.1 12.9 0.86 0.23 0.16 0.14 0.06 2.80 6.70 0.01	75.4 13.5 0.80 0.21 0.78 0.15 0.09 3.58 5.53 0.01	76.0 13.1 0.71 0.25 0.29 0.14 0.09 2.70 6.67 0.01	75.2 13.6 0.91 0.18 0.56 0.15 0.11 2.92 6.37 0.01	75.9 13.0 0.84 0.22 0.29 0.14 0.08 2.91 6.56 0.01	75.5 13.5 0.93 0.17 0.61 0.15 0.08 2.84 6.23 0.01
PPM							
Sc Rb Zr Cs Hf Ta Th Ba	1.4 210.3 218.3 5.5 7.7 1.5 22.7	1.7 231.7 250.3 5.2 8.3 1.6 24.0	1.7 222.2 233.8 5.3 7.5 1.5 22.7	1.6 198.1 224.0 5.0 7.7 1.6 22.9	1.6 196.1 220.1 4.9 8.1 1.6 23.9	1.5 204.1 190.9 5.3 8.0 1.6 23.8	1.6 212.0 252.0 5.4 8.4 1.6 24.2
La Ce Sm Eu Tb Yb Lu	26.9 60.4 5.4 0.18 0.9 4.0 0.6	32.6 70.4 6.3 0.17 1.0 4.0 0.8	27.8 57.3 4.8 0.14 0.7 3.3 0.7	28.1 61.1 5.3 0.19 0.9 3.9 0.5	27.6 64.7 5.9 0.18 1.0 4.8 0.8	26.8 61.0 5.2 0.17 0.9 3.9 0.6	28.0 61.9 6.2 0.18 1.0 4.4

TABLE 4 (continued).

SAMPLE NO.	76	77	78	79	80	81	82
FIELD I.D.	C4H2	C5BI	C5BJ	C5BK	C5BL	C5BM	C5BN
WT. %							
SiO2	75.5	76.3	75.9	75.3	74.3	75.3	74.9
Al2O3	13.3	13.0	13.1	13.6	14.3	13.7	14.1
FeO	0.86	0.69	1.05	0.96	1.08	0.96	0.89
CaO	0.19	0.25	0.25	0.24	0.24	0.24	0.24
MgO	0.54	0.34	0.61	1.07	1.59	0.89	1.23
TiO2	0.15	0.14	0.14	0.15	0.17	0.14	0.16
MnO	0.07	0.10	0.11	0.11	0.12	0.11	0.12
Na2O	2.68	3.50	3.19	3.22	3.25	3.34	3.28
K2O	6.60	5.53	5.58	5.27	4.92	5.21	5.17
P2O5	0.01	0.01	0.01	0.01	0.01	0.01	0.02
PPM							
Sc Rb Zr Cs Hf Ta Th Ba	1.5 218.0 228.1 5.7 8.2 1.6 23.4	1.5 189.7 266.7 4.9 7.2 1.5 21.1	1.7 219.2 207.8 5.8 8.1 1.7 23.2 185	1.5 187.3 236.9 4.9 7.9 1.6 21.8	1.7 186.8 190.4 5.4 7.9 1.7 23.9	1.7 183.6 228.1 5.1 7.6 1.6 23.0 90	1.7 186.9 212.6 5.4 8.1 1.6 23.3 85
La	28.5	29.8	30.2	27.9	31.1	28.4	30.7
Ce	66.1	59.6	61.6	64.1	62.3	62.2	68.5
Sm	6.2	6.1	5.9	6.9	5.8	5.6	6.5
Eu	0.20	0.28	0.29	0.36	0.32	0.27	0.32
Tb	0.9	0.9	1.0	1.0	0.9	0.9	0.9
Yb	4.2	3.2	3.8	3.9	3.9	3.7	4.0
Lu	0.8	0.7	0.7	0.8	0.7	0.7	0.8

TABLE 4 (continued).

SAMPLE NO.	83	84	85	86	87	88	89
FIELD I.D.	C5BO	C5BP	C4AI	C4AK	C4AL	C4AM	C4AN
WT. X							
SiO2	75.9	75.2	75.6	75.1	74.1	65.9	71.7
Al2Os	12.4	13.8	12.8	13.1	13.8	17.4	15.0
FeO	1.01	1.03	1.06	0.97	1.01	1.99	1.21
CaO	0.34	0.22	0.43	0.36	0.61	2.07	0.70
MgO	1.43	0.99	0.07	0.45	0.30	0.77	0.21
TiO2	0.13	0.15	0.18	0.16	0.24	0.61	0.32
MnO	0.09	0.12	0.11	0.09	0.10	0.10	0.14
Na2O	3.15	3.05	3.10	3.06	3.13	4.33	4.17
K2O	5.46	5.42	6.61	6.65	6.56	6.66	6.53
P2O5	0.01	0.02	0.01	0.01	0.02	0.14	0.03
PPM							
Sc Rb Zr Cs Hf Ta Th Ba	1.5 185.9 264.2 5.0 7.6 1.5 21.2	1.6 196.3 206.9 5.4 7.3 1.5 22.3	1.6 173.3 213.4 4.7 8.1 1.5 22.5	1.5 177.5 194.1 4.9 7.7 1.6 23.8	3.3 162.3 372.3 4.2 8.8 1.3 20.9 285	7.2 76.54 887.0 1.5 16.5 0.6 12.6 2926	3.1 139.1 629.5 3.5 14.6 1.3 21.0
La	27.6	28.4	35.3	30.9	73.2	218.3	72.3
Ce	58.2	57.0	72.4	67.9	148.6	386.9	165.7
Sm	5.6	5.4	6.6	6.5	7.3	14.1	10.6
Eu	0.22	0.28	0.35	0.28	1.27	5.21	0.84
Tb	0.9	0.9	0.9	1.0	0.8	0.9	1.2
Yb	3.6	3.3	3.8	3.9	3.5	3.0	4.1
Lu	0.4	0.7	0.6	0.2	0.6	0.3	0.9

TABLE 4 (continued).

SAMPLE NO.		91	92	93	94	95	96
FIELD I.D.		C4AP	C1A6	C1A7	C1AA	C1AB	C1AC
WT. %							
SiO2	71.8	75.9	72.6	66.4	67.3	76.8	76.3
Al2O3	14.8	12.8	14.4	17.6	17.0	12.7	12.6
FeO	1.39	1.00	1.21	2.26	1.85	0.68	0.73
CaO	0.70	0.31	0.78	1.69	1.33	0.27	0.31
MgO	0.22	0.07	0.28	0.74	0.63	0.03	0.07
TiO2	0.34	0.14	0.28	0.61	0.62	0.15	0.16
MnO	0.15	0.09	0.12	0.12	0.15	0.06	0.06
Na2O	3.97	3.08	3.69	4.51	4.87	3.24	3.33
K2O	6.58	6.59	6.69	5.94	6.20	6.09	6.42
P2O5	0.02	0.01	0.03	0.15	0.08	0.01	0.01
PPM							
Sc Rb Zr Cs Hf Ta Th Ba	3.4 138.1 603.1 3.5 15.0 1.3 20.2 460	1.5 165.0 221.2 4.3 7.7 1.5 21.1	2.5 151.1 446.7 3.9 11.7 1.5 20.2 280	7.5 83.8 834.1 1.6 15.3 0.6 12.9 3134	7.3 181.7 802.4 3.8 14.9 0.7 15.2 1800	1.7 324.9 225.5 7.6 8.4 1.7 25.0	1.7 316.3 247.6 7.9 8.9 1.7 25.0
La	74.2	31.5	51.9	202.0	229.5	21.2	28.8
Ce	174.1	69.8	128.1	391.5	434.2	77.3	73.5
Sm	10.7	6.0	9.4	12.9	14.2	6.1	6.7
Eu	0.91	0.29	0.80	5.22	4.11	0.33	0.34
Tb	1.2	0.8	1.3	0.9	0.9	1.0	1.1
Yb	4.5	3.3	4.4	2.6	3.4	4.2	4.5
Lu	0.6	0.5	0.9	0.4	0.7	0.8	0.7

TABLE 4 (continued).

SAMPLE NO FIELD I.D		98 C1 AE	99 C2A1	100 C2A2	101 C2A3	102 C3A1	103 C3A2
WT. %							
SiO2 Al2O3 FeO CaO MgO TiO2 MnO Na2O K2O P2O5	66.8 17.8 1.97 1.41 0.60 0.61 0.14 4.25 6.40 0.07	76.8 12.6 0.68 0.28 0.03 0.14 0.07 3.06 6.33 0.01	76.5 12.7 0.82 0.31 0.04 0.14 0.09 3.26 6.14 0.01	77.4 12.5 0.68 0.31 0.12 0.12 0.10 3.69 5.06 0.01	76.5 12.7 0.82 0.30 0.03 0.14 0.09 3.27 6.18 0.01	76.1 13.1 0.92 0.30 0.30 0.15 0.06 2.76 6.26 0.01	76.1 12.9 0.92 0.32 0.48 0.14 0.09 2.71 6.31 0.01
PPM							
Sc Rb Zr Cs Hf Ta Th Ba	7.2 148.9 851.1 3.5 14.3 0.7 14.6 2626	1.6 243.2 220.3 5.6 7.9 1.6 25.4	1.7 280.6 275.4 5.7 8.7 1.7 25.2	2.4 296.5 326.8 5.9 10.3 1.6 21.9	1.5 271.1 256.1 5.5 8.0 1.6 24.5	1.8 186.7 239.5 4.9 7.8 1.6 23.9	1.6 171.3 278.0 4.5 8.2 1.6 22.9
La Ce Sm Eu Tb Yb Lu	208.0 389.4 12.6 4.55 0.9 3.1 0.7	30.1 70.0 5.3 0.28 0.9 3.9 0.8	29.6 69.3 5.3 0.30 0.9 4.3 0.8	51.2 124.9 10.6 0.67 1.4 4.9 0.9	27.0 64.1 5.2 0.26 0.9 3.9 0.7	34.0 69.5 5.9 0.28 0.9 3.7 0.7	38.7 74.1 6.9 0.39 0.9 4.1

TABLE 4 (continued).

SAMPLE NO. FIELD I.D.		105 C3A4	106 C4D	107 C3D	
WT. %					
SiO2	76.2	76.2	76.4	71.0	
A12O3	12.8	12.8	12.8	15.8	
FeO	0.86	0.86	0.95	1.67	
CaO	0.34	0.34	0.26	0.61	
MgO	0.28	0.45	0.24	0.56	
TiO2	0.15	0.15	0.14	0.41	
MnO Na2O	0.07 2.78	0.0 7 2.59	0.08 2.40	0.08 3.49	
Na20 320	6.49	2.59 6.48	2.40 6.71	6.31	
P2 O5	0.02	0.01	0.01	0.02	
203	0.02	0.01	0.01	0.02	
PPM					
Sc	1.7	1.9	1.6	4.5	
l b	179.8	189.3	199.1	129.3	
ir	239.1	257.9	223.4	611.5	
5	4.8	4.9	4.8	3.2	
lf	8.4	8.1	8.0	13.7	
'a	1.6	1.7	1.6	1.3	
Th .	23.7	24.7	23.8	18.9	
a	185	0	90	235	
a	38.0	39.6	35.3	105.7	
e	69.8	75.1	69.3	209.4	
m.	6.5	6.0	6.0	11.0	
u	0.32	0.33	0.35	1.07	
Ъ	0.9	1.0	0.9	1.0	
Ъ	3.9	3.9	4.0	3.6	
u	0.8	0.8	0.7	0.8	

DATA

Chemistry

For each whole-pumice sample, ten major element and sixteen trace element analyses were obtained (Tables 1 to 4). The ten major elements, reported as weight percent oxides, are; SiO2, Al2O3, FeO, CaO, MgO, TiO2, MnO, Na2O, K2O, P2O5. These elements along with Rb, Sr, Zr, and Ba were determined by XRF analysis. The trace elements, determined by INAA are: Sc, Cs, Hf, Ta, Th, La, Ce, Sm, Eu, Tb, Yb, Lu. The distribution of the elements in each of the four units of the Paintbrush Tuff is presented in Appendix 4. The accuracy and the precision of the data may be found in Table 5.

Ideally, the best elements to use for the purpose of evaluating magmatic processes have a wide range of concentration and show a high correlation with other elements (Cox et al., 1979, pg. 13), as well as good precision and accuracy. The major elements that best fit these requirements, expressed in weight percent oxide, are SiO2, TiO2, FeO, and MgO. SiO2 is the preferred major element used for quantitative and illustrative purposes because the Paintbrush Tuff is a high-silica system. It is also the only major element that is enriched in the system. Trace elements which fit the above requirements are La, Hf, Ba, and Zr. Most trace elements, including these, have an antithetic relationship with respect to silica content. The trace elements that increase with increasing silica content

TABLE 5. Precision and accuracy of data.

A. Concentration of U.S.G.S. standard G-1 determined by X-ray flourecence (XRF).

WT. %	Govindaraju (1984)	XRF	% stand. dev.	n
SiO2	72.64	72.04	0.41	8
Al2 03	14.04	14.13	0.25	8
FeO	1.74	1.80	1.45	8
CaO	1.39	1.36	1.70	8
MgO	0.38	0.37	6.70	8
TiO	0.26	0.26	0.39	8
MnO	0.03	0.03	3.33	8
Na ₂ O	3.32	3.23	3.61	8
K2 O	5.48	5.48	0.22	8
P2 O5	0.09	0.08	6.02	8

B. Concentration of U.S.G.S. standard G-2 determined by X-ray flourecence (XRF).

PPM	Govindaraju (1984)	XRF	% stand. dev.	n
Ba	1870-1900	1918	7.47	8
Rb	168	171	1.37	8
Sr	480	474	0.25	8

C. Concentrations of U.S.G.S. standard BCR-1 determined by instrumental neutron activation analysis (INNA).

	Govindaraju	INAA	% stand. dev.	n
PPM	(1984)			
Sc	33	34	4.24	7
Zr	185	168.5	14.60	6
Cs	0.95	0.98	7.21	7
Hf	4.7	5.45	5.55	7
Th	6.0	5.67	6.99	7
Ta	0.91	0.78	6.09	7
La	25	27.01	3.54	7
Ce	54	53.62	6.59	7
Sm	6.6	6.41	6.77	7
Eu	1.9	1.98	3.19	7
ТЪ	1.0	0.96	6.63	7
Yb	3.4	3.60	9.14	7
Lu	0.6	0.49	8.23	6

are Rb, Cs, Ta, and Th.

Out of necessity, some elements are used for evaluation purposes even though they are not as good to use as others. For example, in order for ratio/ratio plots to be illustrative (Fig. 9), two enriched and two depleted elements must be used. For this reason, Rb and Ta are used even though Rb is somewhat mobile (Appendix 3) and Ta has only a small variation in the system (Appendix 3).

The Topopah Spring Member is represented by twenty one major and trace element analyses. The chemical compositions of pumices fall into two distinct groups, a lower-silica quartz latite and a high-silica rhyolite (Table 1, Appendix 4). The lower silica group has a SiO2 range of 68.7% to 71.3%, a La range of 111 ppm to 208 ppm, and a Hf range of 10 ppm to 15 ppm. The higher silica grouping has a SiO2 range of 75.8% to 78.7%, a La range of 30 ppm to 39 ppm, and a Hf range of 4 ppm to 7 ppm. The chemical composition of the pumices from the base of the Topopah Spring ash-flow sheet all fall within the high-silica group. The chemical composition of pumices from the top of the ash-flow sheet fall within both groups.

The Pah Canyon Member is represented by fifteen major and trace element analyses. The chemical composition of pumices fall into one distinct group, and are intermediate in chemical composition between the high-silica rhyolite and quartz latite from the Topopah Spring Member (Tables 1 and 2, and Appendix 4). The significance of the intermediate

nature of the Pah Canyon Member relative to the Topopah Spring Member will be discussed in a later section. The range in chemical compositions for the Pah Canyon Member is small. For example, SiO2 varies from only 72.8% to 74.2%; La varies from only 73 ppm to 93 ppm; and Hf varies from only 7 ppm to 9 ppm.

The Yucca Mountain Member is represented by twenty three major and trace element analyses. The chemical composition of pumices have a very small range (Table 3, Appendix 4). For example, SiO2 varies from only 75.8% to 77.4%; La varies from only 28 ppm to 33 ppm; and Hf varies from only 7 ppm to 9 ppm.

The Tiva Canyon Member is represented by forty six major and trace element analyses. The chemical compositions of the pumices fall into three distinct groups, a lower-silica quartz latite, a rhyolite, and a higher-silica rhyolite (Table 4, Appendix 4). The higher-silica rhyolite of the Tiva Canyon Member is very similar to the high-silica rhyolite of the Yucca Mountain Member, and the relationship between these two units will be discussed in a later The quartz latite group has an SiO2 range of section. 65.9% to 67.3%, a La range of 202 ppm to 229 ppm, and a Zr range of 802 ppm to 887 ppm. The rhyolite group has an SiO2 range of 71.0% to 72.6%; a La range of 52 ppm to 106 ppm, and a Zr range of 447 ppm to 630 ppm. higher-silica rhyolite group has an SiO2 range of 74.1% to 77.4%, a La range of 21 ppm to 40 ppm, and a Zr range of 190 ppm to 372 ppm. Apparent silica gaps occur between 67.3% to 71.0% and 72.6% to 74.1%. Corresponding gaps occur in the trace element chemistry (Appendix 4).

Mineralogy

Systematic variations in the chemistry of the phenocrysts and their modal abundances have been noted by various workers for the Paintbrush Tuff (Byers et al., 1976b; Scott et al., 1984; Broxton et al., 1985; Warren et al., 1985). Compositional variations are most notable in mole percent Or and Cn in sanidine and An in plagioclase. Conspicuous modal variations of plagioclase and mafic phenocrysts were noted from unit to unit within the Paintbrush Tuff. Phenocryst compositions for the Topopah Spring Member have been determined by several workers (Byers et al., 1976b; Scott et al., 1984; Warren et al; 1984; Broxton et al., 1985) and the chemical compositions were determined for phenocrysts taken from whole-rock as well as pumices. All phenocryst compositions for the Pah Canyon, Yucca Mountain and Tiva Canyon Members used in this study were determined by the author from phenocrysts taken from individual pumices. All modal phenocryst data for the Paintbrush Tuff (Table 6) are taken from Byers et al., (1976b).

The most striking aspect of the mineralogy of the Paintbrush Tuff is the lack of quartz in the system. Quartz phenocrysts do not exceed 1% as total rock volume in any of the four ash-flow sheets of the Paintbrush Tuff (Byers et

al., 1976b). The remaining gross mineralogy of the system is similar from member to member, except that the Topopah Spring Member is a sphene-free unit (Byers et al., 1976b).

The variation in An contents of plagioclase is shown in Appendix 3. The Topopah Spring Member has an An content that varies from Ani 4 to Ani 0 in the high-silica rhyolite, while in the quartz latite the variation is from Ani 3 to Ani 7. The Pah Canyon Member has an An content that varies from Ani 4 to Ani 0. The Yucca Mountain Member and the higher-silica rhyolite portion of the Tiva Canyon Member has an An content that varies from Ani 0 to Ani 0, but only three analyses were obtained because of the low number of total phenocrysts in these units. The rhyolite of the Tiva Canyon Member has an An content that varies from Ani 2 to Ani 5, and for the quartz latite, the variation is from Ani 8 to Ani 3.

The variation of Or contents of sanidines is shown in Appendix 3. For the Topopah Spring Member, the variation is approximately Ors2 to Orss in the high-silica rhyolite, while in the quartz latite the variation is from approximately Or45 to Ors7. For the Pah Canyon Member, the variation is from Or47 to Ors5. For the Yucca Mountain and the higher-silica rhyolite portion of the Tiva Canyon Member, the variation is from approximately Ors0 to Or48, and Or28 to Ors2, respectively. For the rhyolite of the Tiva Canyon Member, the variation is from approximately Or21 to Or42, while for the quartz latite,

the variation is from Or28 to Or50.

The variation in mole percent Cn in sanidines is shown in Appendix 3. For the Topopah Spring Member, the variation is approximately 0.0 to 0.3 in the high-silica rhyolite, while the variation for the quartz latite is 2.4 to 3.9. In the Pah Canyon Member, the variation in mole percent Cn is 1.1 to 2.4. In the Yucca Mountain Member and the higher-silica rhyolite of the Tiva Canyon Member, the variation in mole percent BaO is, 0.1 to 0.4 and 0.0 to 0.3, respectively. In the rhyolite of the Tiva Canyon Member, the variation in mole percent BaO is approximately 0.1 to 0.2, while for the quartz latite the variation is 0.1 to 1.5.

The variation of the ferromagnesium minerals, as expressed by the Mg number of the analyzed biotite, amphiboles and clinopyroxenes within the Pah Canyon Member (Appendix 3), Yucca Mountain Member (Appendix 3) and the Tiva Canyon Member (Appendix 3) is small. Only limited phenocryst data from the Topopah Spring Member is available for these phenocryst types. Biotite is found as a mineral phase in the Pah Canyon Member, Yucca Mountain Member, and throughout the Tiva Canyon Member. Amphibole is found as a mineral phase in the Yucca Mountain Member and the higher-silica rhyolite of the Tiva Canyon Member. No amphibole is found in the Pah Canyon Member and the rhyolite and quartz latite of the Tiva Canyon Member. Clinopyroxene is found as a mineral phase in the Pah Canyon Member, the Yucca Mountain Member, and throughout the Tiva Canyon Member.

Temperatures

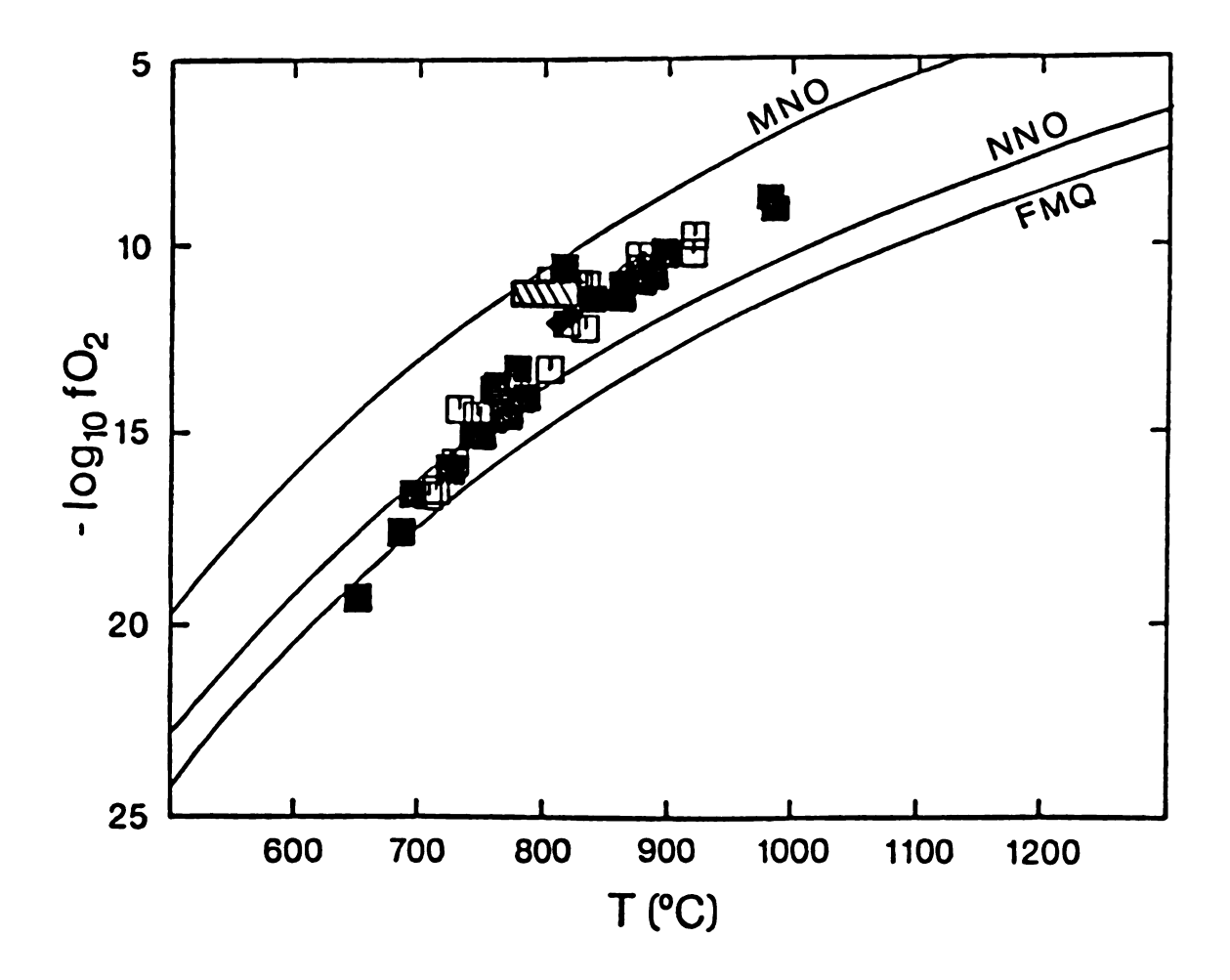
Estimates of magmatic temperatures for the Paintbrush Tuff were determined from individual glassy pumices using the magnetite/ilmenite geothermometer (Spencer and Lindsley, 1981). Schuraytz et al. (1986) determined the temperatures for the Topopah Spring Member, whereas temperatures for the Pah Canyon, Yucca Mountain and Tiva Canyon Members were determined by the author. The procedure used to calculate temperatures is the same as that outlined by Schuraytz et al. (1986) and is summarized in Appendix 5.

It should be emphasized that the temperatures and oxygen

fugacities reported herein are estimates only. This is due to a number of factors including: 1) The composition of the ulvospinel and ilmenite used in the calculations represent averages of several individual grains, with each individual grain itself representing an average of several analyses. 2) Exsolution was common in many of the grains, particularly in the Yucca Mountain and Tiva Canyon Members. To obtain a representative analysis, the microprobe beam was rastered over a large area of 100 microns squared. The Bence-Albee correction program assumes homogeneity of the analyzed area, and hence low totals for inhomogenous areas resulted. Many of the calculated oxygen fugacities fall outside the experimental range and therefore have to be estimates. The validity of the assumption that the magnetite and ilmenite grains formed in equilibrium with the surrounding glass. Schuraytz et al. (1986) gives a comprehensive review of the problems inherent when estimating temperatures from pumices using the magnetite/ilmenite geothermometer.

The temperatures determined for pumices from the Topopah Spring Member range from 620°C to 1000°C (Schuraytz et These temperatures fall into two distinct al., 1986). groups (Fig. 3) and are separated by a paucity of temperatures in the interval from 805°C to 883°C. The lower temperature group corresponds to the high-silica rhyolite, while the higher temperature group corresponds to the quartz latite. The trend of the temperatures from the high-silica, low temperature group are distinctly different from the trend of the temperatures of the quartz latite higher-temperature group (Fig. 3). The paucity of temperature data between the two groups also corresponds to chemical gaps. The interpretation of a sharp compositional interface existing in the magma chamber between the high-silica rhyolite and the quartz latite is based to a large degree on the change in slope of the temperatures from group to group, and the correlation of chemical gaps to the paucity of temperatures (Schuraytz et al., 1986) .

The Pah Canyon is represented by 20 temperature estimates, with temperatures clustering in a very narrow range from 763°C to 796°C. The log FO2 of the oxygen fugacities range from -11.27 to -12.14. These oxygen fugacities are outside the experimental range of Spencer and Lindsley (1981), and can be used as an estimate only. The temperatures of the Pah Canyon Member would correlate to the



- Pumice
- Tuff
- Pah Canyon

Figure 3. Estimated temperatures and oxygen fugacities for the Topopah Spring and Pah Canyon Members (after Schuraytz et al., 1986).

higher temperature end of the high-silica group in the Topopah Spring Member, but the corresponding oxygen fugacities would be higher (Fig. 3).

Temperature estimates for the Yucca Mountain and Tiva Canyon Members are limited because of the lack of magnetite/ilmenite grains suitable for determinations. The dominant titanium bearing phase for these two members is sphene. The Yucca Mountain Member is represented by only 2 temperature determinations, 691°C and 721°C, whereas the high-silica portion of the Tiva Canyon Member is represented by only one analysis, 734°C. The rhyolite of the Tiva Canyon Member is represented by only 3 temperature determinations which range from 755°C to 773°C, while the quartz latite is represented by only 2, 845°C and 863°C. The oxygen fugacities that correspond to some of these temperatures are also outside the experimental limits of Spencer and Lindsley (1981) and are used as estimates only.

Pressure

A method for determining the absolute pressure and depth of origin for the magmatic mineral assemblage of magnetite, ilmenite, plagioclase, and alkali feldspar has been proposed by Stormer and Whitney (1985). Their thesis is based on the experimental observation that the iron-titanium geothermometer is essentially independent of pressure, while the two-feldspar geothermometer is related to pressure, with

an added temperature correction with pressure by about 18°C/Kbar (Brown and Parsons, 1981). The two-feldspar geothermometer can be converted to a geobarometer when combined with a pressure-independent estimate of temperature such as an iron-titanium derived temperature. For example, if iron-titanium temperature estimates are 800°C and the two-feldspar temperature estimates are 700°C, the phenocrysts are interpreted to have equilibrated at approximately 6 kilobars pressure, equivalent to a depth of approximately 18 km. This procedure requires good analytical precision and reasonable certainty that the minerals formed in equilibrium. If estimates of the depth of mineral equilibration can be determined, then the depth of the reservoirs for large volume ash-flow eruptions can be inferred (Stormer and Whitney, 1985).

Pressure and depth of mineral equilibration was determined for the Pah Canyon Member. Similar estimates for the Topopah Spring Member are in progress (Schuraytz pers. commun., 1987), while estimates are not possible for the Yucca Mountain and Tiva Canyon Members because of the paucity of iron-titanium derived temperatures and the uncertainty of equilibrium of the phases at their time of formation. The Pah Canyon Member has temperature estimates from the two-feldspar and iron-titanium geothermometers that give nearly identical values, indicating equilibration at a very shallow depth. For example, for two samples of the Pah Canyon Member, the iron-titanium temperatures are 789°C

and 767°C, whereas the respective two-feldspar temperatures are 770°C and 765°C. This would indicate that the Pah Canyon magma equilibrated at approximately 1 kilobar pressure or at a depth of 3 kilometers.

Comparison of the Topopah Spring Member and the Tiva Canyon Member

The Topopah Spring Member and the Tiva Canyon Member are the first and last ash-flow sheets of the Paintbrush Tuff to be erupted, respectively. Both are compositionally zoned and large ash-flow sheets (>1200 km³ and >1000 km³, respectively). A comparison of these two units provides insights into the initial nature of the system (Topopah Spring Member) as well as a comparable glimpse of the system at a later stage (Tiva Canyon Member).

The Topopah Spring and Tiva Canyon Members both erupted contrasting magma types. The first material erupted from both members was high-silica rhyolite. The base of the Topopah Spring ash-flow sheet contains pumices only of high-silica rhyolite, while the top of the ash-flow sheet contains pumices of both quartz latite and high-silica rhyolite. The base of the Tiva Canyon ash-flow sheet, like the base of the Topopah Spring ash-flow sheet, contains pumices only of higher-silica rhyolite, while the top of the ash-flow sheet contains pumices of three distinct types, quartz latite, rhyolite, and higher-silica rhyolite.

Based on SiO2 ranges, the high-silica rhyolite of the Topopah Spring Member is slightly more evolved than the higher-silica rhyolite of the Tiva Canyon Member (Table 1; Figs. 4 and 5). Several elements are used to highlight differences between the two units. For example, SiO2 in the Topopah Spring Member varies from 75.8% to 78.7%, Hf varies from 4 ppm to 7 ppm, and Zr varies from 107 ppm to 326 ppm. For the higher-silica rhyolite of the Tiva Canyon Member, SiO2 varies from 74.3% to 77.4%, Hf varies from 7 ppm to 10 ppm, and Zr varies from 190 ppm to 326 ppm. concentrations of some elements are approximately the same for both members, for example, Ba and the HREE (tables 1 and 4; Figs. 4 and 6). The concentrations of some elements such as the LREE (Fig. 6) are antithetic to the behavior of most other elements and are higher in the Tiva Canyon Member than the Topopah Spring Member.

Modal phenocryst data (Table 6) can also be interpreted to suggest that the high-silica rhyolite of the Topopah Spring is more evolved than the higher-silica rhyolite of the Tiva Canyon Member. The high-silica rhyolites from both members are low in total phenocrysts, <5% for the Topopah Spring Member and <4% for the Tiva Canyon Member. The mafic phenocrysts in the high-silica rhyolite of the Topopah Spring Member are dominantly biotite, whereas amphibole and clinopyroxene occur subequally with biotite in the Tiva Canyon Member.

Based on SiO2 ranges, the quartz latite of the Tiva

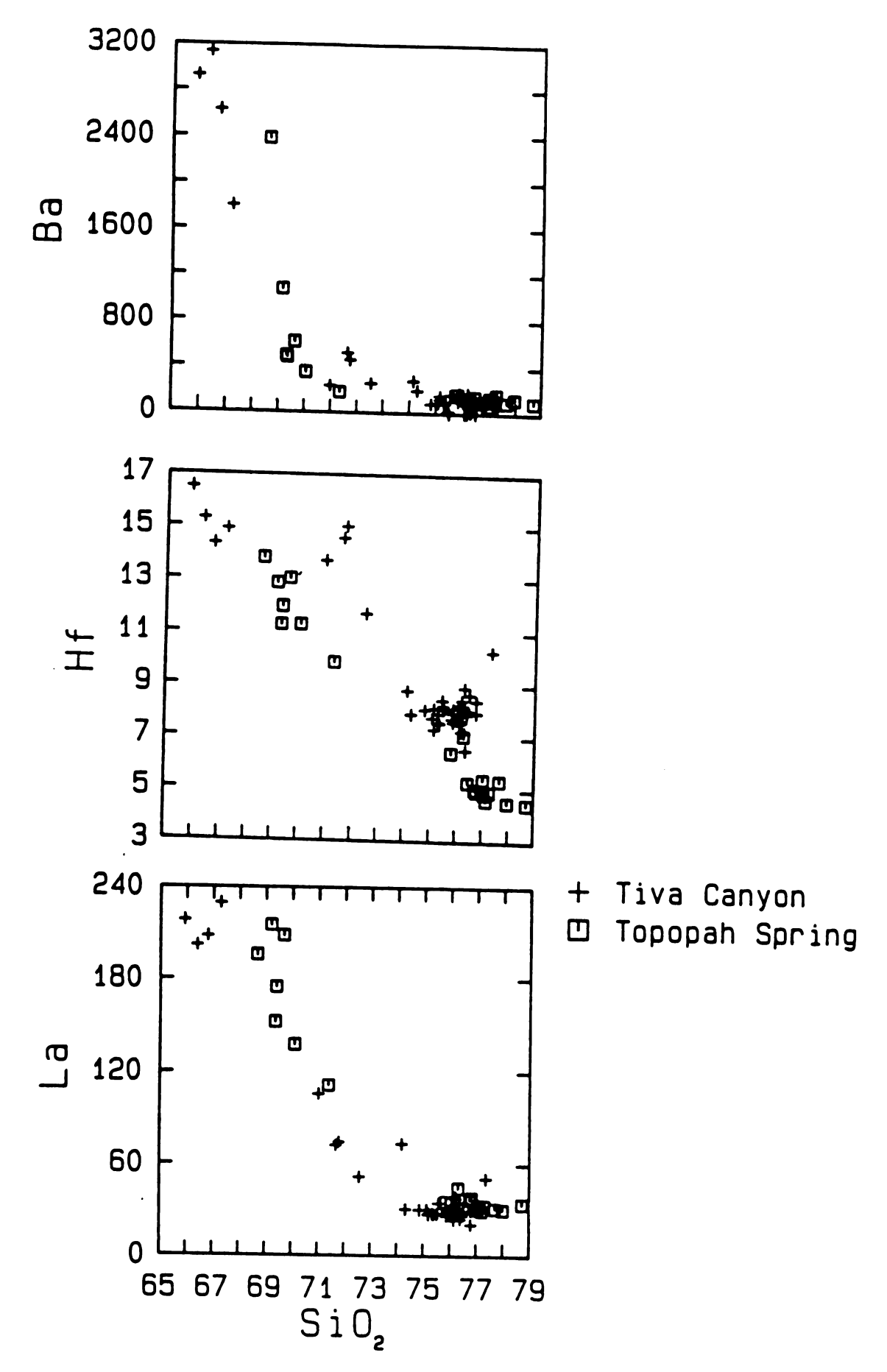


Figure 4. Plots of La, Hf and Ba against SiO2 for the Topopah Spring and Tiva Canyon Members.

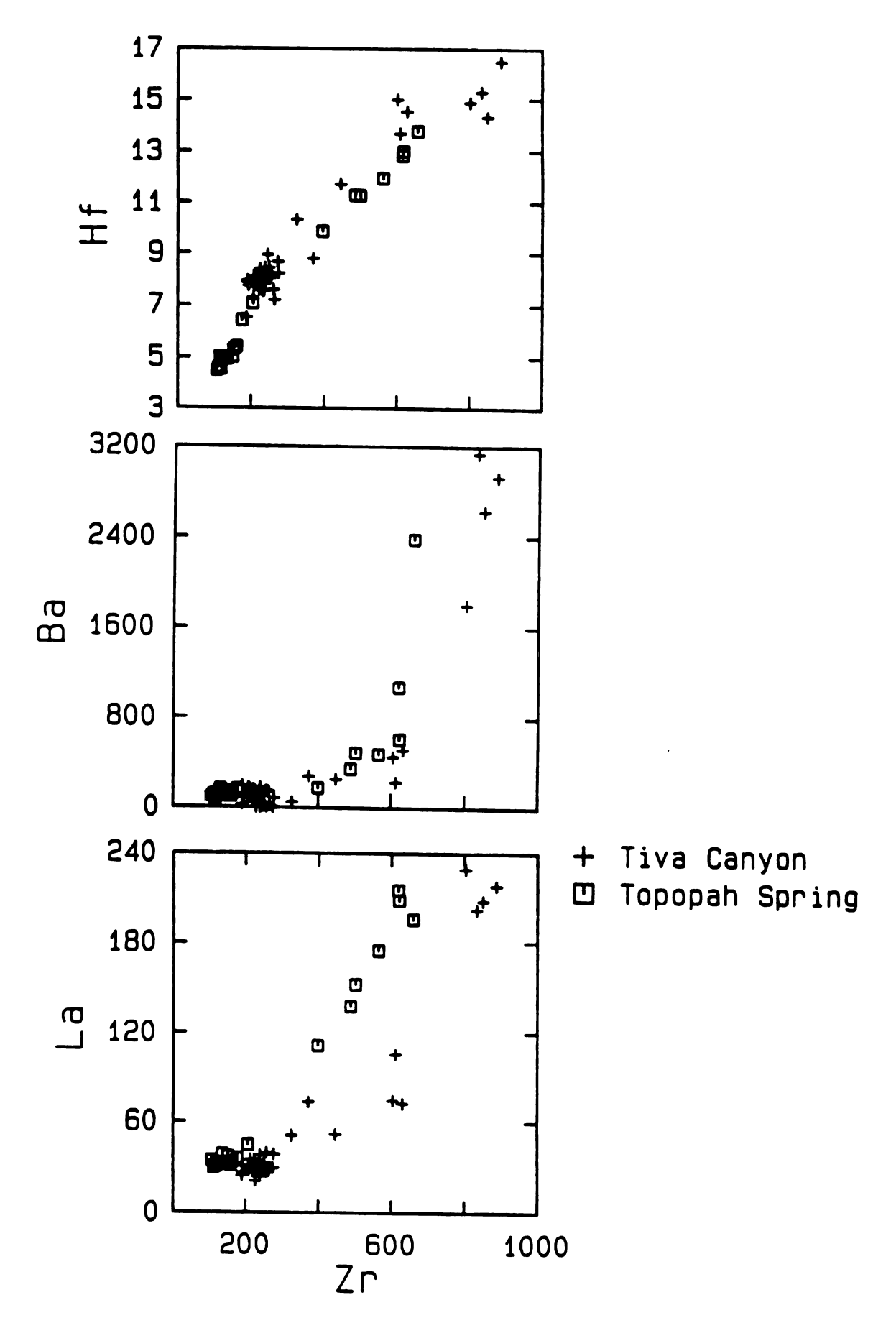


Figure 5. Plots of La, Hf and Ba against Zr for the Topopah Spring and Tiva Canyon Members.

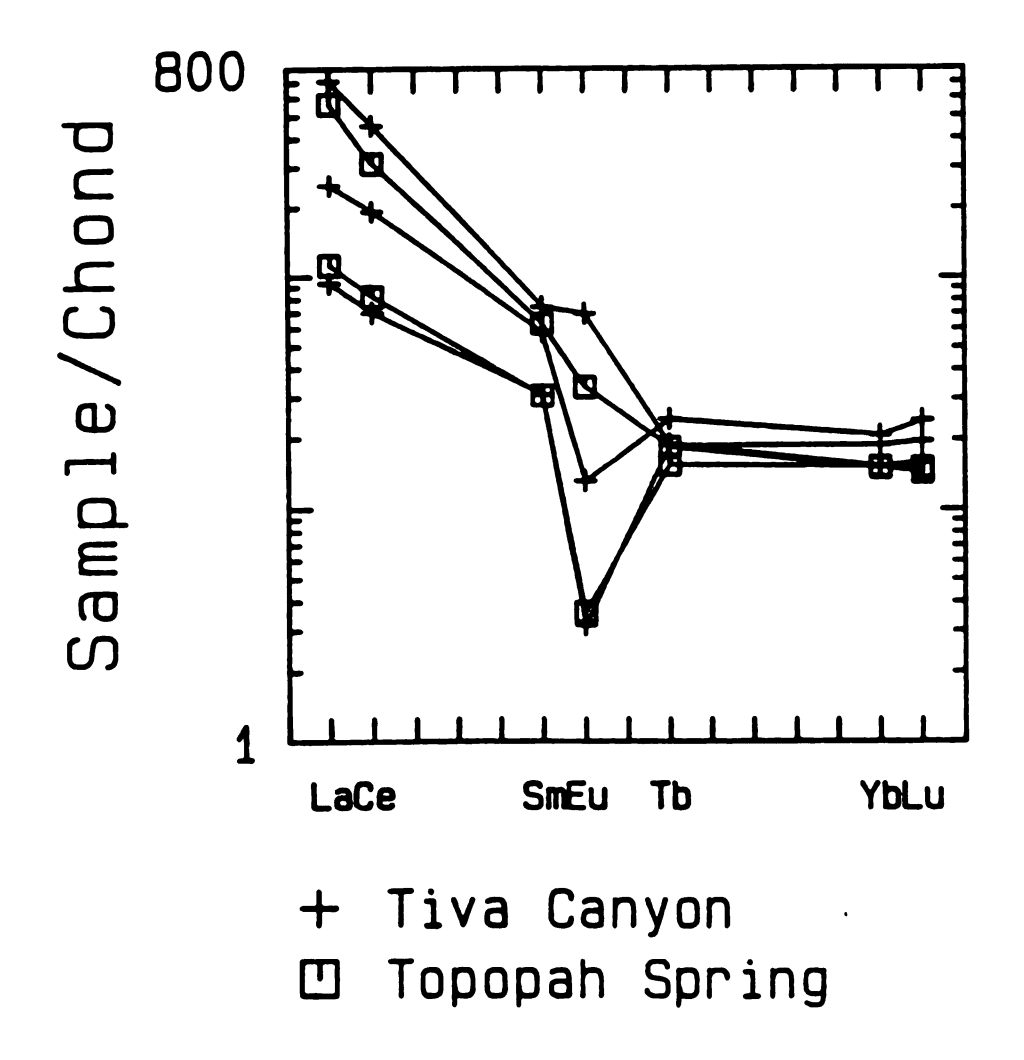


Figure 6. Average chondrite-normalized rare-earth element profiles of the Topopah Spring and Tiva Canyon Members.

Canyon Member is more primitive than the quartz latite of the Topopah Spring Member (Tables 1 and 4; Figs. 4 and 5). Certain elements highlight the chemical differences between the two units. For example the quartz latite of the Topopah Spring Member varies in SiO2 from 68.7% to 71.3%, Hf varies from 10 ppm to 15 ppm, and Zr varies from 397 to 659. For the quartz latite of the Tiva Canyon Member, SiO2 varies from 65.9% to 67.3%, Hf varies from 14 ppm to 16 ppm, and Zr varies from 802 ppm to 887 ppm. Ba values also indicate that the quartz latite of the Tiva Canyon is more primitive than the quartz latite if the Topopah Spring (Fig 4). The highest Ba concentration is 3100 ppm found in the Tiva Canyon Member, compared to a maximum Ba value in the Topopah Spring Member of 2380 ppm. The LREE of the Tiva Canyon Member are also more primitive than the LREE of the Topopah Spring Member (Fig. 6). The HREE concentrations of the quartz latite of the two members is very similar.

The significant difference between the Topopah Spring
Member and the Tiva Canyon Member is the existence of an
intermediate rhyolite in the Tiva Canyon Member. The
significance of this intermediate rhyolite will be discussed
in a later section.

EVOLUTION OF THE MAGMATIC SYSTEM

ORIGIN OF THE PAH CANYON

The Pah Canyon Member represents a significant step in the evolution of the Paintbrush Tuff magmatic system. The Pah Canyon ash-flow sheet was erupted after the Topopah Spring ash-flow sheet and is intermediate between the high-silica rhyolite and quartz latite of the Topopah Spring Member. Because the Pah Canyon Member and the Topopah Spring Member were part of the same magmatic system, the Pah Canyon Magma must have evolved by some process from the Topopah Spring Magma. The chemical and mineralogical data from the Pah Canyon Member is consistent with magma mixing of the high-silica rhyolite and quartz latite of the Topopah Spring magma to form the intermediate Pah Canyon magma.

Magma Mixing

Various quantitative tests can be applied to the proposal that the magma represented by the Pah Canyon ash-flow sheet formed by mixing of Topopah Spring high-silica rhyolite and lower-silica quartz latite. Linear trends on chemical variation diagrams would support magma mixing. Mixing can also be independently evaluated using ratio-ratio plots (Langmuir et al., 1977), and least squares multiple regression analysis (Wright and Doherty, 1970).

Variation diagrams of La, Zr, and Hf versus SiO2; and La, Sc, and Hf versus Zr for the Topopah Spring and Pah

Canyon Members are shown in Figures 7 and 8, respectively. The chemical compositions of pumices from the Pah Canyon ash-flow sheet fall intermediate and along a straight line between the chemical compositions of the more evolved high-silica rhyolite and the less evolved quartz latite of the Topopah Spring ash-flow sheet. This is consistent with the interpretation that the magma represented by the Pah Canyon Member formed by mixing of the contrasting magmas of the Topopah Spring Member.

Ratio-ratio plots in conjunction with companion plots are a powerful test of magma mixing (Langmuir et al., 1977; Cox et al., 1979). For this test of magma mixing, the ratios of the mixed magma should fall along the calculated hyperbola. A further test is that the corresponding companion plot, consisting of the ratio of the denominators plotted against one of the original ratios, must plot as a straight line (Langmuir et al., 1977). The hyperbola can be calculated by taking two well-separated points and applying a general mixing equation (Langmuir et al, 1977). The predicted hyperbola specific to the Pah Canyon ash-flow sheet was calculated by applying the mixing equation to a high-silica rhyolite and a quartz latite from the Topopah Spring Member and using the trace elements Zr, Ta, Rb and La. A plot of Zr/Ta versus Rb/La and an associated companion plot of Zr/Ta versus La/Ta, with a best fit line superimposed, are shown in Figures 9a and 9b respectively. The Pah Canyon data fit the hyperbola constructed from the Topopah Spring

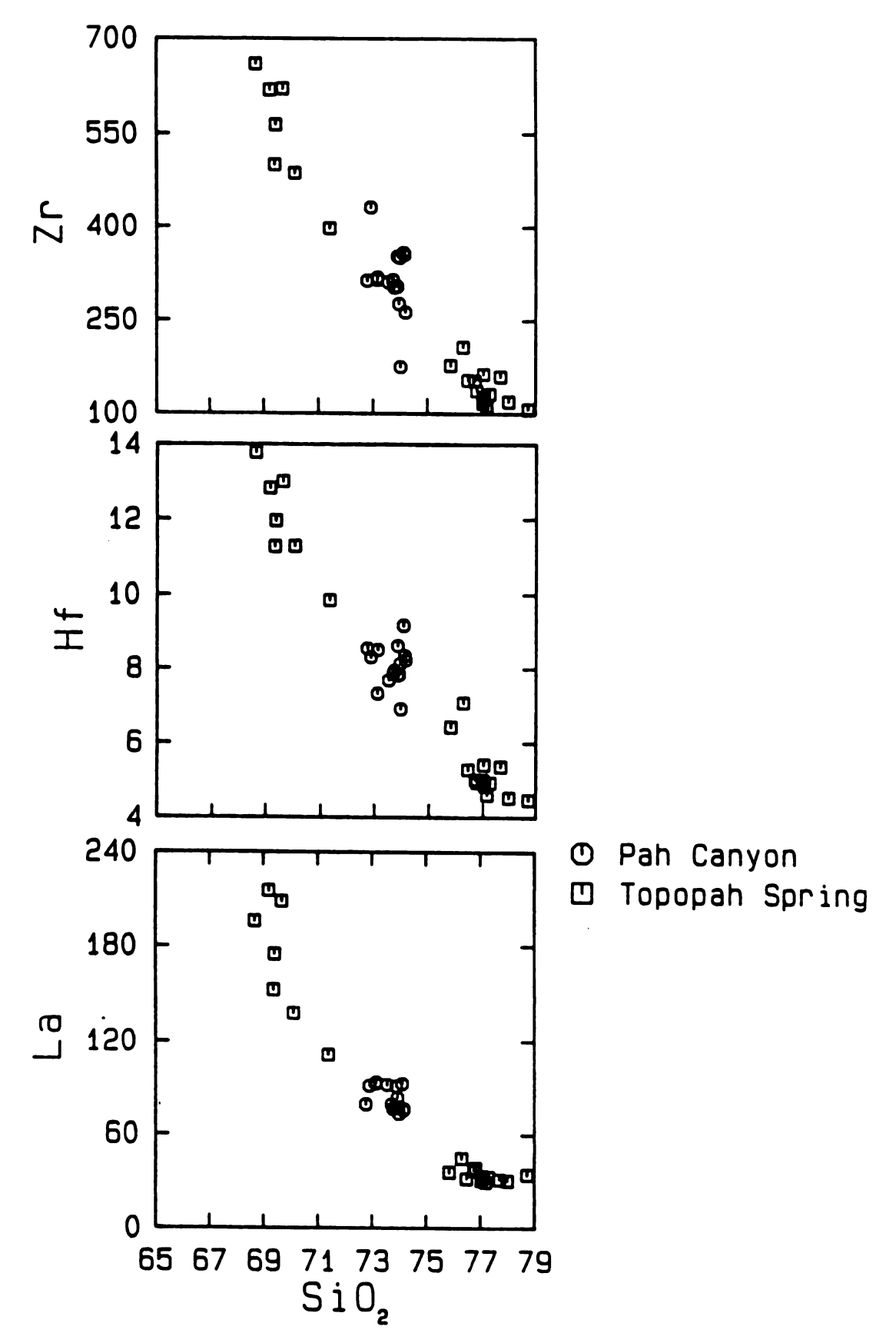


Figure 7. Plots of La, Zr, and Hf against SiO2 for the Topopah Spring and Pah Canyon Members.

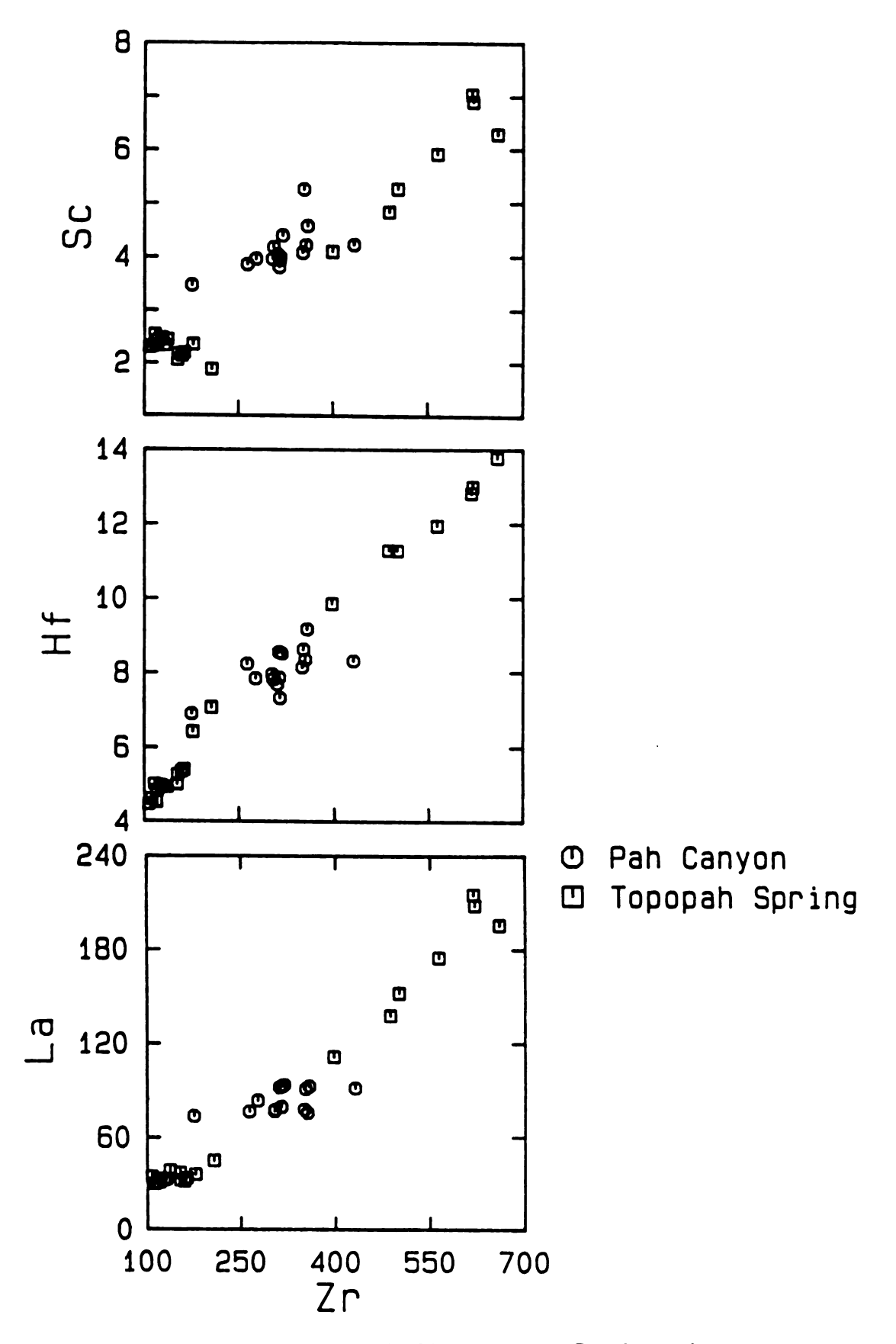


Figure 8. Plots of La, Sc, and Hf against Zr for the Topopah Spring and Pah Canyon Members.

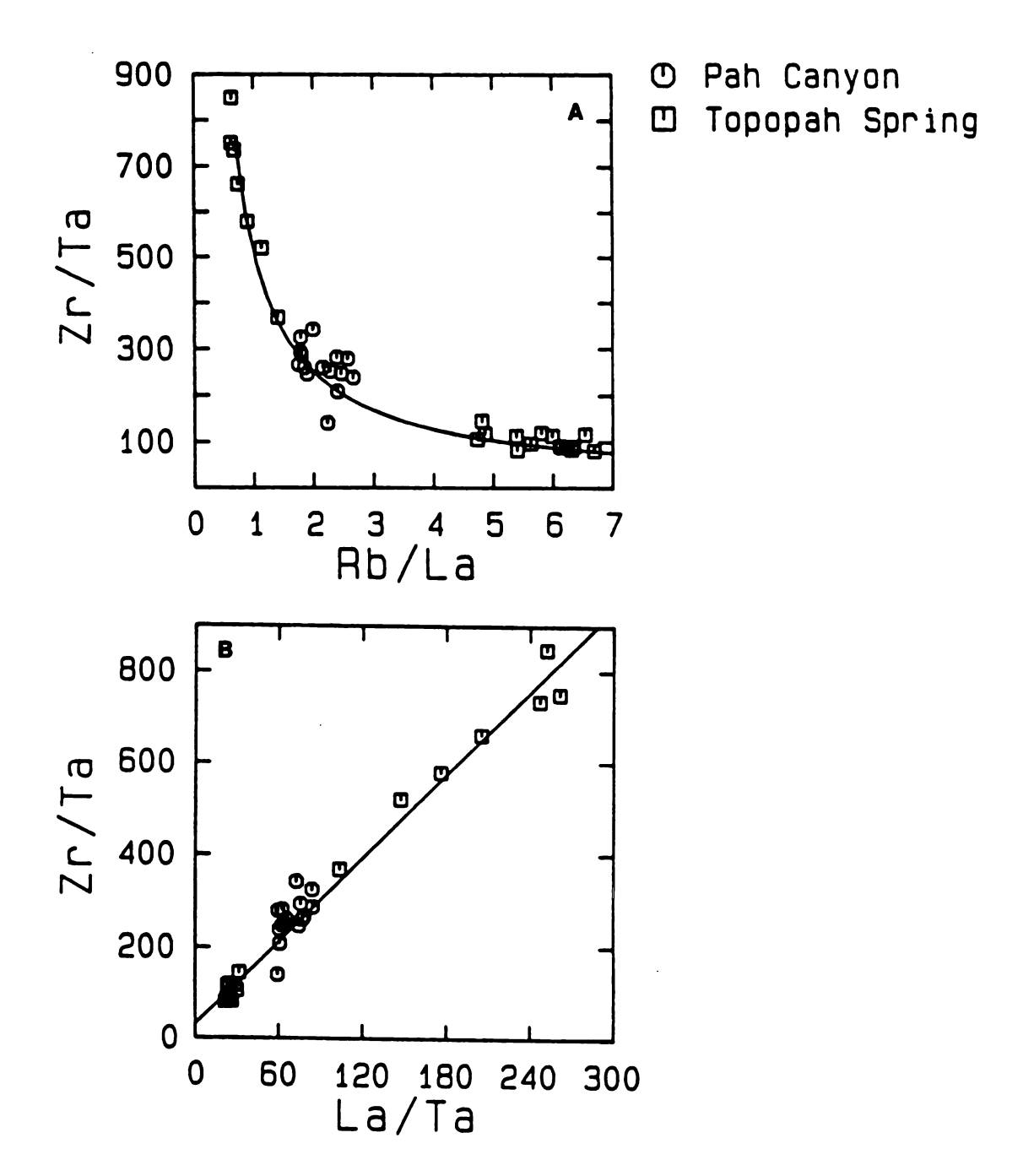


Figure 9. Ratio-ratio plots to evaluate magma mixing. A) Zr/Ta against Rb/La. B) Zr/Ta against La/Ta. Hyperbolic line in (A) was constructed from two endmember points. Line in (B) is best fit line. See text for discussion.

end-members remarkably well (Fig. 9a) and is consistent with magma mixing. It should be kept in mind that the equation for the hyperbola is calculated using the two Topopah Spring end-members only, and is independent of the data from the Pah Canyon Member. The goodness of fit of the straight line for the companion plot (Fig. 9b) is 0.97 and the correlation coefficient is 0.99. Both values are very good and support the hypothesis of magma mixing.

The rare earth element (REE) compositions of pumice from the Topopah Spring and Pah Canyon ash-flow sheets are presented in Figures 10a and 10b. Figure 10a illustrates the intermediate nature of the erupted Pah Canyon Member relative to the quartz latite (high La) and high-silica rhyolite (low La) of the Topopah Spring Member. Figure 10b are the means of the REE data seen in Figure 10a. This diagram is used only to highlight the intermediate nature of the Pah Canyon Member relative to the contrasting magmas of the Topopah Spring Member.

The mineralogical data also support the interpretation of magma mixing. The modal phenocryst abundance for the Pah Canyon Member (Table 6) reflects chemical trends and is intermediate between the high-silica rhyolite and the quartz latite of the Topopah Spring Member. The high-silica rhyolite contains as much as 5% total phenocrysts, the quartz latite contains approximately 10% to 20% total phenocrysts, and the Pah Canyon Member contains approximately 8% to 12% total phenocrysts. Temperatures,

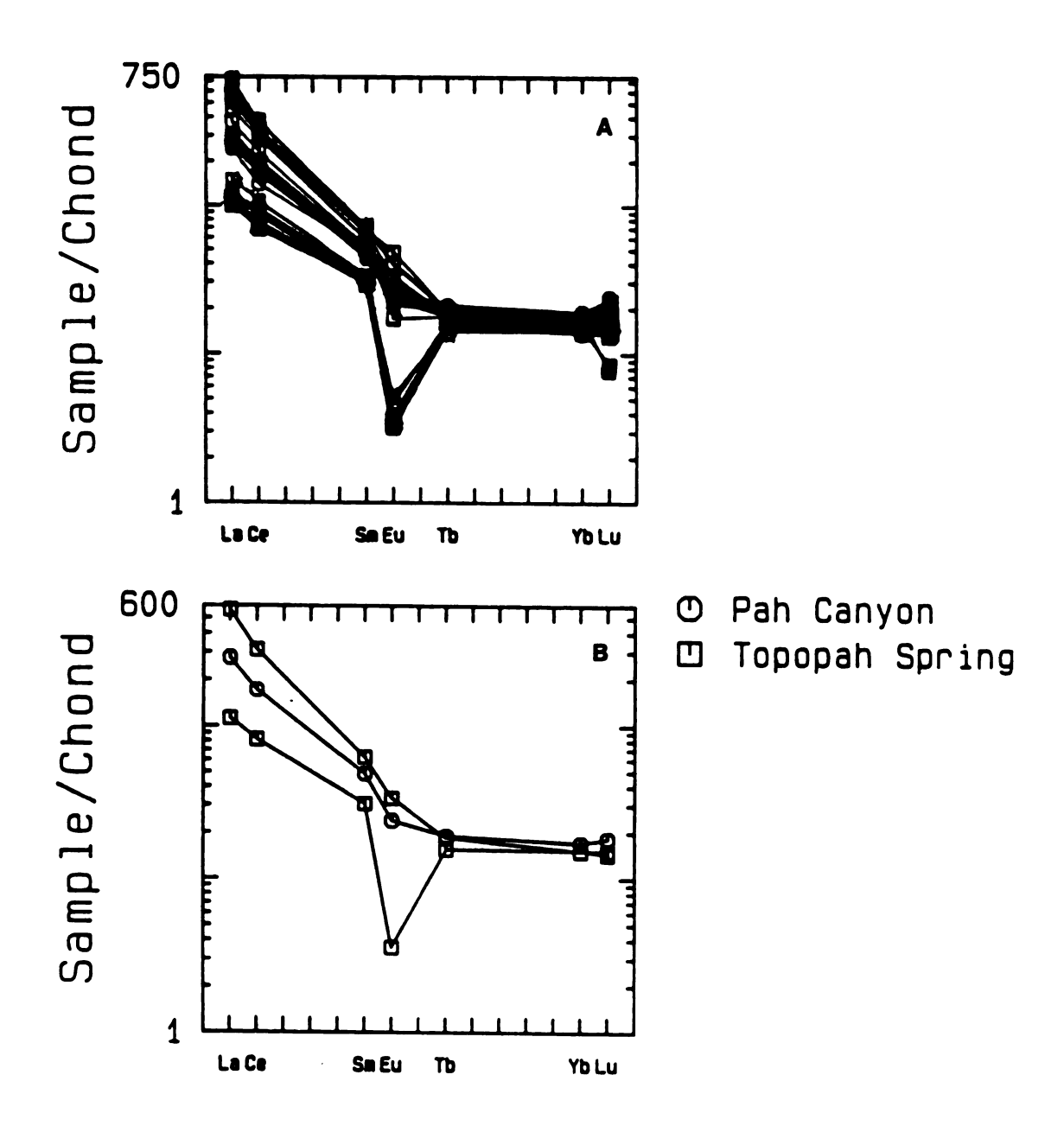


Figure 10. Chondrite normalized rare-earth element profiles of the Topopah Spring and Pah Canyon Members. A. All data. B. Average of separate members.

Table 6. Modal phenocryst abundances in the ash-flow sheets of the Paintbrush Tuff (from Byers et al. 1976b). Column abbreviations are: PHENS = phenocrysts recorded as percentage of total rock; The remaining abbreviations are recorded as percentage of total phenocrysts, with Pl = plagioclase, SAN = alkali feldspar, MF = mafics, BT = biotite, AMPH = amphibole, and CPX = clinopyroxene.

	PHENS	PL	SAN	MF	вт	AMPH	CPX
Tiva Canyon Member							
Quartz latite	8-25	10-20	75-87	3-9	2-6		13
Rhyolite	. 1-8	0-15	82-95	3-10	0-7	<1	2-4
Higher-silica rhyolite	1-4	0-8	90-99	2-7	0-2	1-3	<1
Yucca Mountain Member	<1	0-10	9-100				
Pah Canyon Member	8-12	35-55	35-55	6-13	6-10		1-2
Topopah Spring Member							
Quartz latite	9-20	20-40	55-70	7-12	4-6	<1	1-4
High-silica rhyolite	1-6	35-85	15-65	2-5	0-2		

determined by magnetite/ilmenite geothermometry, of the Pah Canyon Member are intermediate (Fig. 3), to the temperatures of the high-silica rhyolite and quartz latite of the Topopah Spring Member. This is consistent with magma mixing, but implies that enough time existed between mixing and eruption to equilibrate the magnetites and ilmenites to the new temperature regime imposed by mixing. Sphene is found as a phenocryst phase in the Pah Canyon Member, but is lacking in the Topopah Spring Member. This would seem to exclude simple magma mixing as an origin for the Pah Canyon Member. However, sphene has been noted in rocks formed by magma mixing where neither parent contains sphene (Vogel, 1986; pers. commun.).

Two independent tests of magma mixing based on multiple linear regression were performed. In the first, two pumice samples were chosen from the Topopah Spring Member, a high-silica rhyolite and a quartz latite. These represent some of the most evolved and least evolved magmas. The samples were regressed against a representative sample from the Pah Canyon Member. The regression equation was set up for ten of the major elements. The calculated best fit regression equation to evaluate mixing is:

1.00 A = 0.47 B + 0.53 C sum of squares of residuals = 0.41 $R^2 = 1.00$ (1)

where A is a representative Pah Canyon magma (P5B), B is a

quartz latite (LW4-15C) from the Topopah Spring Member, and C is a high-silica rhyolite (BB8-2) from the Topopah Spring Member.

For a good correlative regression: (1) The sum of the squares of the residuals should be low, generally less than 1.00; (2) The R² value should be near unity; and, (3) The mixing proportions should be geologically reasonable.

The major element multiple linear regression is consistent with magma mixing (Eq. 1). The sum of the squares of the residuals is 0.41, and the R² value is 1.00. The mixing proportions are 47 percent quartz latite and 53 percent high-silica rhyolite. An independent test involving the trace elements was performed using the same pumice samples. The mixing proportions, as determined from the major element regression (Eq. 1), were used to calculate a predicted value for the trace elements. The predicted values were then compared to the observed values (Table 7). The trace element concentrations in the Pah Canyon Member can be satisfactorily accounted for by mixing of quartz latite and high silica-rhyolite magma in the proportions predicted from the major element regression.

Fractional Crystallization

Fractional crystallization of the quartz latite to produce the Pah Canyon Member can also be evaluated using major element multiple linear regression. Fractional crystallization can be further evaluated by calculating

Table 7. Predicted and actual trace element abundances in the Pah Canyon Member.

	TOPOPAH	SPRING	PAH CA	NYON	
	QUARTZ LATITE	HIGH-SILICA RHYOLITE	PREDICTED	OBSERVED	PERCENT DIFFERENCE
SIO2	68.7	78.7	74 .0	74.1	2
Sc	6.3	2.3	4.2	4.0	10
Rb	123.3	186.5	156.8	164.5	26
Zr	659.4	107.5	366.9	358.0	3.0
Cs	2.7	5.1	3.9	3.7	18.0
Hf	13.8	4.5	8.9	9.2	6.3
Ta	0.8	1.3	1.1	1.1	0
Th	18.4	2.0	20.3	20.2	5.8
Ba	2380	100	1172	1170	0.1
La	195.7	34.6	110.3	92.4	24.6
Ce	291.2	82.1	180.4	173.8	5.7
Sm	12.3	5.9	8.9	9.0	3.0
Eu	3.30	0.25	1.67	1.8	11.7

trends of selected trace elements based on this major element multiple linear regression. The predicted chemical trends of both fractional crystallization and magma mixing can then be compared to the observed chemical trends of the Pah Canyon Member (Figs. 11 and 12).

A major element multiple linear regression was set up by selecting the most primitive quartz latite from the Topopah Spring Member (68.7% SiO2, 195.7 ppm La) and regressing it against the Pah Canyon Member and all combinations of the major mineral phases that occur in the system: alkali feldspar, plagioclase, biotite, magnetite, ilmenite, clinopyroxene, and orthopyroxene. The chemistry of the minerals used in the regression were obtained by electron microprobe analyses of phenocrysts found in the Topopah Spring and Pah Canyon Members. Where individual phase chemistries had a range in composition, a variety of compositions were used in the regression. For example, plagioclase compositions varied from An18 to An48, so for the regression, plagioclase values of An18, An27, An37, and An47 were employed. The equations that give the best results are:

1.0 B = .55 A + .32 San + .09 Pl + .03 Cpx + .01 Mt sum of squares of residuals = .062 $R^2 = 1.00$ (2)

1.0 B = .61 A + .25 San + .12 Pl +.01 Mt sum of squares of residuals =0.28 $R^2 = 1.00$ (3)

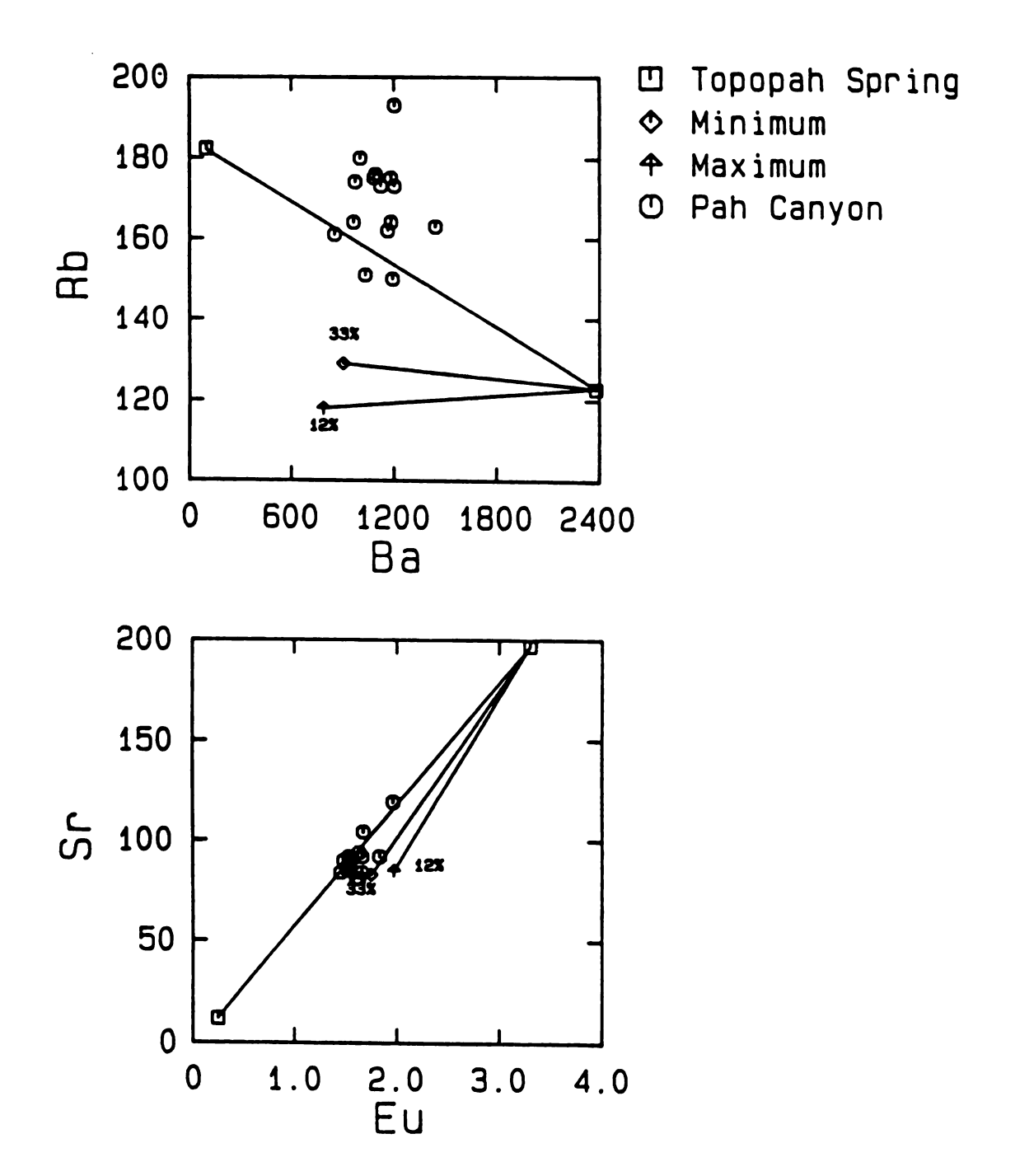


Figure 11. Comparison of magma mixing and fractional crystallization. A. Ba against Rb. B. Eu against Sr. Line connecting Topopah Spring data points is mixing line. Lines connecting a Topopah Spring data point to a predicted point is predicted fractional crystallization line. Percentage numbers indicate amount of fractionation from the Topopah Spring necessary to produce these values based on minimum and maximum distribution coefficients.

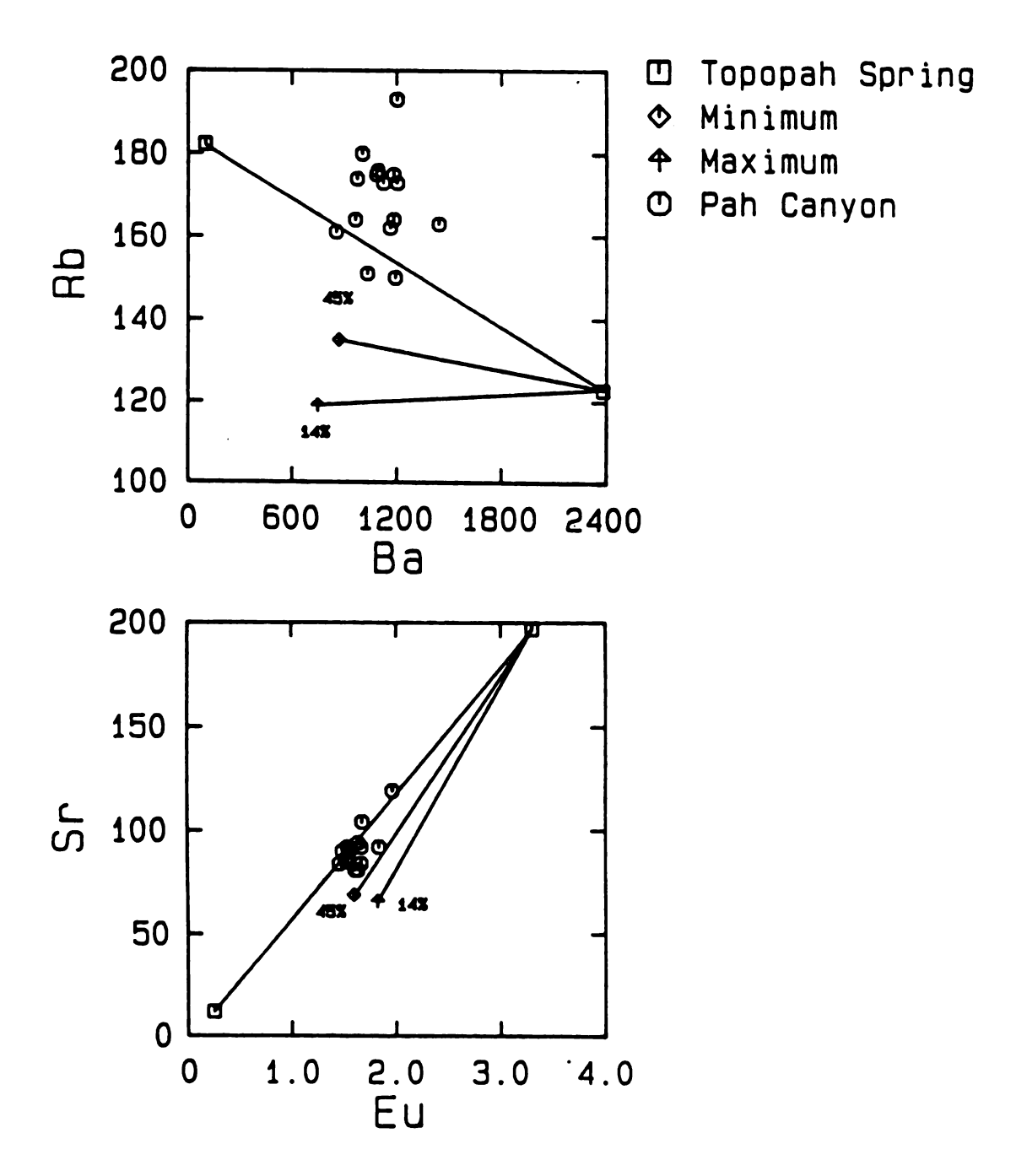


Figure 12. Comparison of magma mixing and fractional crystallization. A. Ba against Rb. B. Eu against Sr. Line connecting Topopah Spring data points is mixing line. Lines connecting a Topopah Spring data point to a predicted point is predicted fractional crystallization line. Percentage numbers indicate amount of fractionation from the Topopah Spring necessary to produce these values based on minimum and maximum distribution coefficients.

where A and B are the same as in equation 1, San represents alkali feldspar, Pl represents plagioclase, Cpx represents clinopyroxene, and Mt represents magnetite.

Trace element modeling was performed based on the results of the major element regression (Eqs. 2 and 3). elements were chosen that had a large variation in this system and that were not a major component of a trace phase. For example, Zr could not be used because it is a major component of the trace phase zircon and the REE could not be used because of the occurrence of REE-rich phases such as allanite and perrierite/chevkinite. Measured minimum and maximum distribution coefficients for silicic systems (Table 8 as compiled from; Nash and Crecraft, 1985 and Mahood and Hildreth, 1983) were selected for various degrees of batch fractional crystallization, and trace element concentrations were predicted. Minimum and maximum fractionation trends are shown for the respective major element linear regression equations for: Rb versus Ba; and Sr versus Eu (Eqs. 2 and 3, and Figs. 11 and 12). The amount of crystallization necessary to produce the respective elemental concentration is also shown for two points on each trend.

Magma Mixing and Fractional Crystallization

Fractional crystallization and magma mixing is compared to the observed Pah Canyon chemistry on Figures 11 and 12. The minimum and maximum fractionation trends originate at

Table 8. Distribution coefficients used for fractional crystallization modeling. Distribution coefficients of selected trace elements in major phases. Data compiled from Nash and Crecraft (1985), and Mahood and 'Hildreth (1983).

	ALKALI	FELDSPAR	PLAGIO	CLASE	BIOTI	TE .	CLINOPY	ROXENE	MAGNE	TITE
	Min	Max	Min	Max	Min	Max	Min	Max	Min	Max
Ba	7.2	24	0.6	3.3	5.6	36	0.1	0.1	-	-
Rb	1.2	1.8	0.1	0.1	2.3	4.1	-	-	-	-
Sr	4.5	7.3	6.8	33	0.3	0.5	0.5	0.5	-	-
Eu	3.3	6.5	3.8	7.9	0.6	4.7	3.2	5.8	0.5	2.1

the most primitive Topopah Spring quartz latite. The area between these two curves represents the allowable predicted trends. A mixing line connects the most primitive and most evolved Topopah Spring magmas. On both plots of Ba versus Rb (Figs. 11 and 12), the observed Pah Canyon data are on or close to the predicted mixing lines while none of the data fall within the fractionation window. On both plots of Eu versus Sr (Figs. 11 and 12), the predicted fractionation trends and the mixing trend are very similar. However, most of the Pah Canyon data lies directly on the predicted mixing line, or very close to it. None of the Pah Canyon data fall within the fractionation window, although some is very close.

A major element regression was done to evaluate the combined effects of magma mixing and fractional crystallization (Eq. 4).

The best result obtained is:

1.0 A = .58 C + .33 B + .06 San + .03 Pl + .00 Mt
sum of squares of residuals = 0.11
$$R^2 = 1.00$$
 (4)

where the symbols are as previously defined.

The above equation is consistent with the interpretation that the Pah Canyon magma may have formed by a combination of magma mixing and fractional crystallization.

Summary

Magma mixing and fractional crystallization can be evaluated, individually or in conjunction, for the origin of the Pah Canyon magma. The favored interpretation is that the dominant process that formed the Pah Canyon Magma was magma mixing. This interpretation is supported for the following reasons:

- 1) The two magmas that mixed to form the Pah Canyon magma, a quartz latite and a high-silica rhyolite, are represented as discreet pumice types at the top of the Topopah Spring ash-flow sheet. These two magmas were erupted at the same time and most likely existed in the magma chamber separated by a compositional interface. Neither the quartz latite nor the high-silica rhyolite was completely exhausted during the eruption of the Topopah Spring ash-flow sheet as demonstrated by the occurrence of both pumice types at the very top of the ash-flow sheet (Schuraytz, 1986). Therefore, we know that both end-member magmas involved in the proposed mixing existed as separate magmas at the same time, were in close proximity, and were not totally erupted. The proposed mechanism that mixed the two magmas was the disruption of the compositional interface due to eruption of the Topopah Spring magma.
- 2) The ratio plots (Figs. 9a and 9b) are a very rigorous test of mixing. The fact that chemical analyses of pumices from the Pah Canyon Member fall on the predicted hyperbola calculated from the end-members in the Topopah Spring Member

is consistent with mixing as a dominant process. Cox et al. (1979) state that very few mixing models have been established based on trace element data using this test.

- 3) Trace element modeling of magma mixing based on multiple linear regression can reasonably account for the variation of both compatible and incompatible trace elements (Table 7). It would be remarkably fortuitous if fractional crystallization produced the exact same trends.
- 4) Modal phenocryst abundances and calculated temperatures of the Pah Canyon Member are intermediate to the high-silica rhyolite and quartz latite of the Topopah Spring Member, and are proportional to what would be predicted for the mixing percentages (approximatley 50/50) calculated by the least squares multiple linear regression.

All the above tests yield necessary but not sufficient conditions for magma mixing. This is true for any inferred geological process that can not be observed directly (Hofmann and Feigenson, 1983).

Lavas which are less evolved than the Pah Canyon Member are found between the Topopah Spring ash-flow sheet and the Pah Canyon ash-flow sheet (Byers et al., 1976b). These lavas also may have formed by magma mixing of the contrasting magmas represented in the Topopah Spring ash-flow sheet, as they generally conform to the same rigid mixing tests as the Pah Canyon magma (Warren, pers. commun., 1986). A systematic variation in certain phenocryst compositions, for example Cn in sanidines and Or values of

sanidines, seems to exist starting with the Topopah Spring Member and continuing through the Tiva Canyon Member, including these lavas and the Pah Canyon magma. This has been attributed to a systematic fractionation mechanism (Broxton et al., 1985; Warren and Byers, 1985).

Irrespective of the amount or type of chemical evolution, the dominant chemical signature on the pre-Pah lavas and the Pah Canyon Member is magma mixing.

ORIGIN OF THE YUCCA MOUNTAIN MEMBER

The Yucca Mountain Member is a simple cooling unit with a volume of <20 km³, and was the third major ash-flow sheet of the Paintbrush Tuff to be erupted (Fig. 2).

The change in composition from the Pah Canyon Member to the Yucca Mountain Member represents the reestablishment of a high-silica rhyolite within the system. This transition is an essential component in understanding the evolution of the Paintbrush Tuff. Assuming that the transition between the Pah Canyon Member and the Yucca Mountain Member represents the evolution of the same magmatic system, then the high-silica rhyolite of the Yucca Mountain Member must have formed by some fractionation process from the magma of the Pah Canyon Member. This is significant because it implies a starting point from which to model fractionation mechanisms. Such is not the case for the high-silica rhyolite of the Topopah Spring Member. The Topopah Spring Member consists of a high-silica rhyolite separated from an underlying quartz latite by a sharp compositional interface (Schuraytz et al., 1985, 1986). The origin of this high-silica rhyolite is not known. For example, it has not been determined if the high-silica rhyolite evolved from the quartz latite, or if it evolved from a magma of some other composition. It may have formed by some other process or processes such as partial melting or assimilation.

The magmas of the Pah Canyon Member and the Yucca Mountain Member are both chemically very homogenous.

Pumices from the Pah Canyon Member have a very small compositional range: for example, SiO2 varies from only 72.8% to 74.2%; La from only 73 ppm to 93 ppm; and Hf from only 7 ppm to 9 ppm (Table 2). Similarly, pumices from the Yucca Mountain Member have a very small compositional range: for example, SiO2 varies from only 75.8% to 77.4 %; La from only 28 ppm to 33 ppm; and Hf from only 7 ppm to 9 ppm (Table 3). Variation diagrams of La, Sc, and Hf versus SiO2, and Zr for the Pah Canyon and Yucca Mountain Members are shown in Figures 13 and 14 respectively. The average REE compositions of the two units are shown in Figure 15. The homogenous nature of these two units is illustrated by the clustering of points on the chemical variation diagrams (Figs. 13 and 14).

Certain elements are enriched, and certain elements are depleted between the Pah Canyon Member and the Yucca Mountain Member. Those distinctly depleted elements are; Ba, Ti, HREE, and Zr. Those distinctly enriched elements are Si, Ta, Th, and, Rb. Any proposed fractionation mechanism must account for the variation of these different elements.

Rejection of Magma Mixing and Assimilation

Magma mixing and assimilation can be dismissed as possible fractionation mechanisms for the origin of the Yucca Mountain magma because the required component needed to mix with the Pah Canyon magma to form the Yucca Mountain

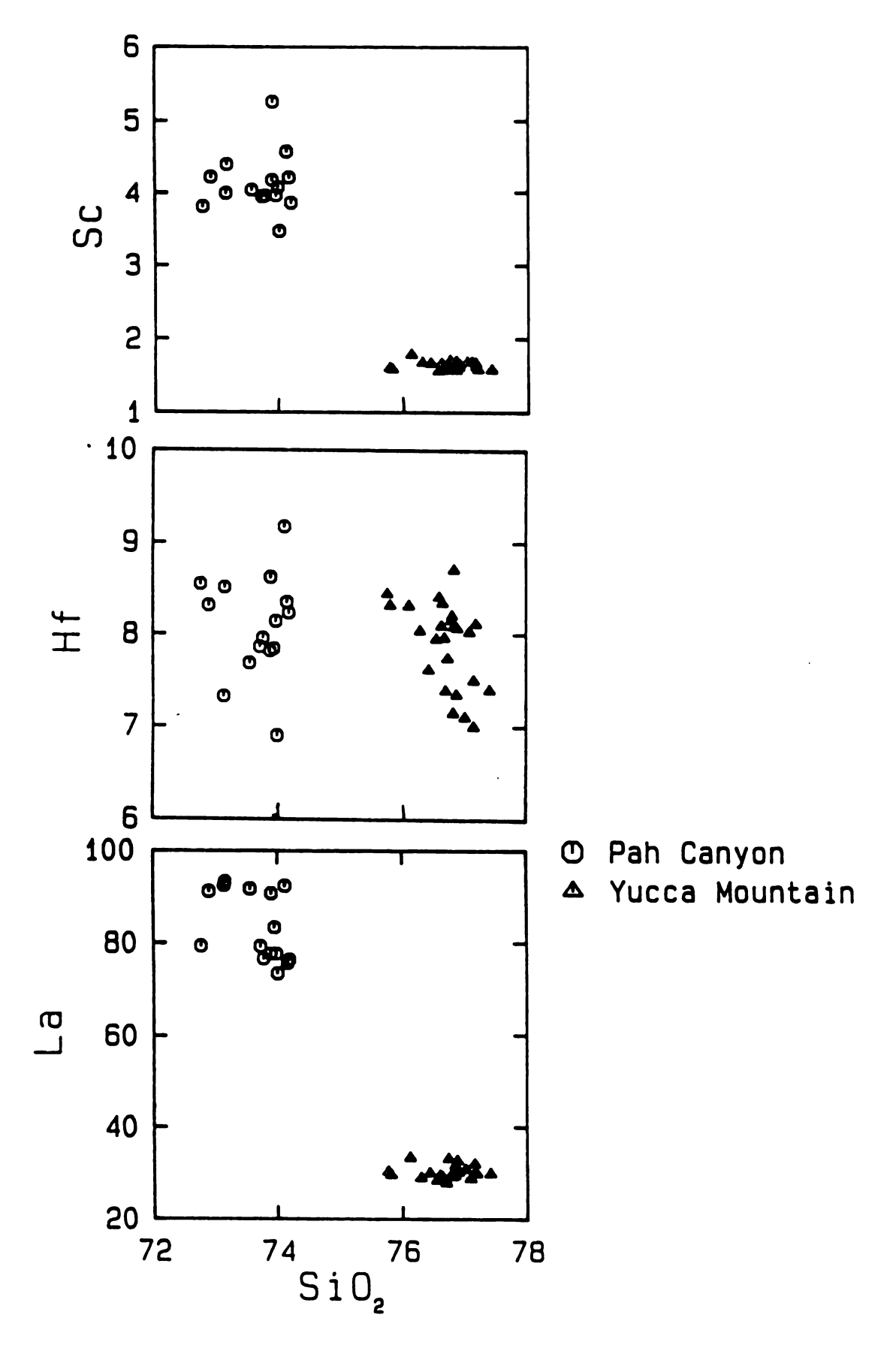


Figure 13. Plots of La, Sc, and Hf against SiO2 for the Pah Canyon and Yucca Mountain Members.

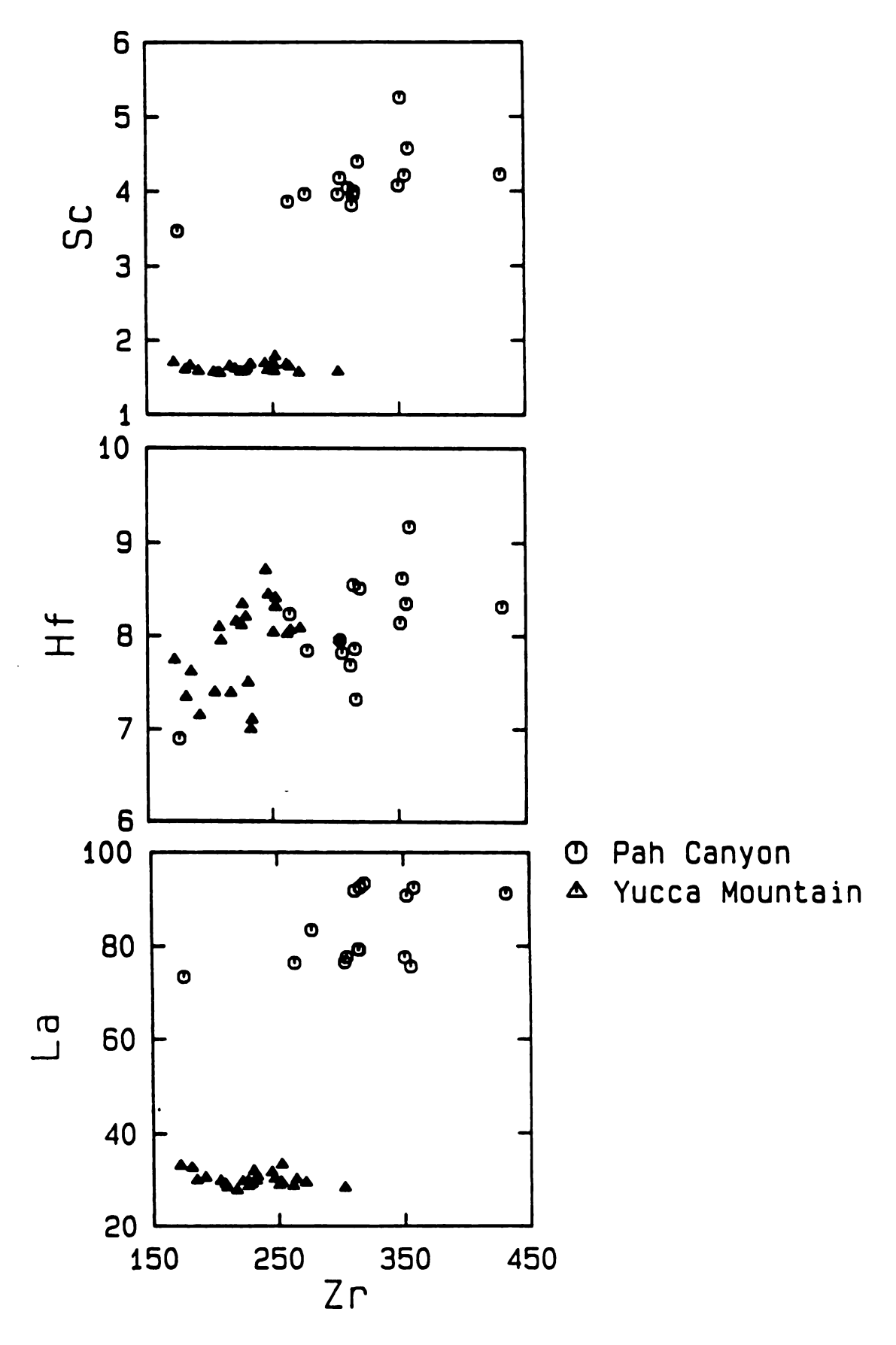
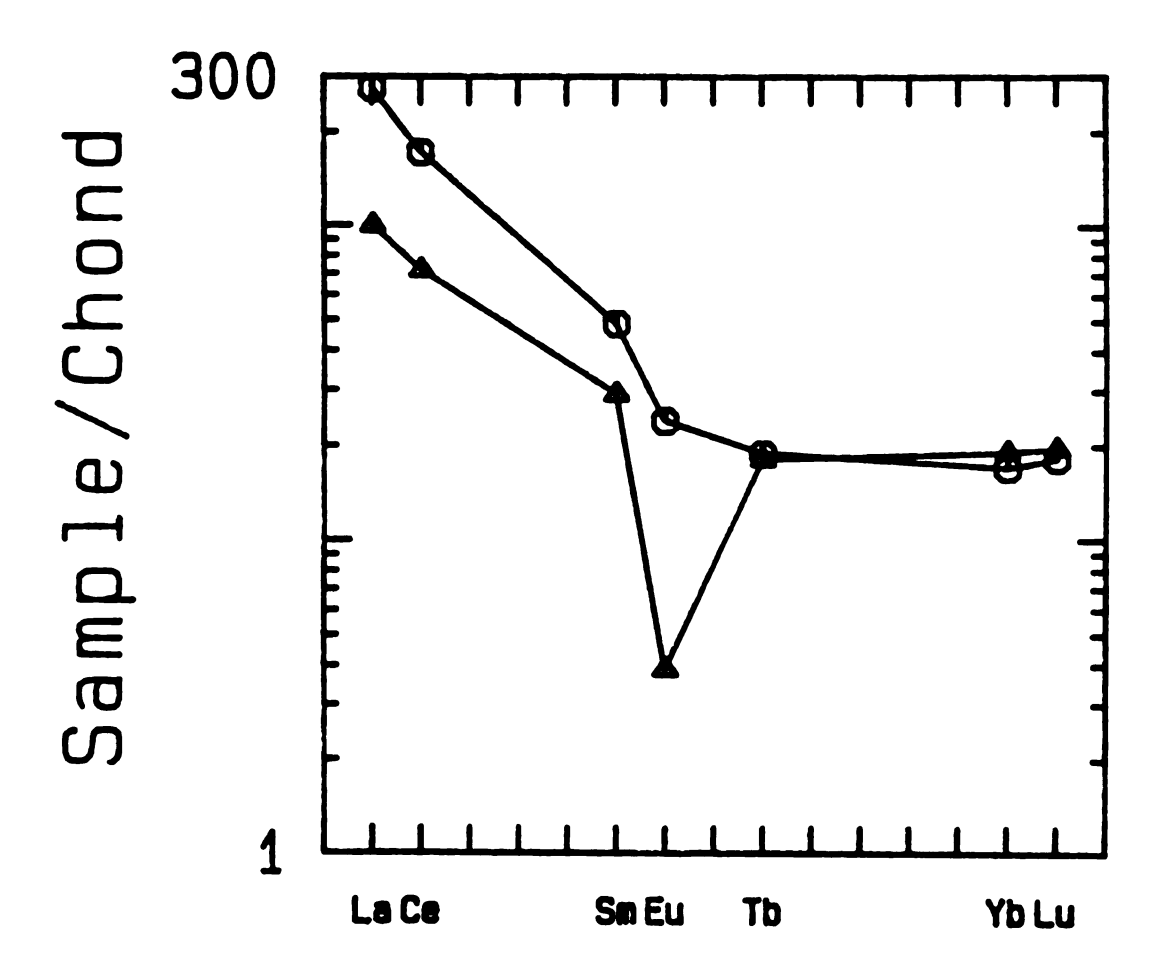


Figure 14. Plots of La, Sc, and Hf against Zr for the Pah Canyon and Yucca Mountain Members.



○ Pah Canyon
△ Yucca Mountain

Figure 15. Average chondrite-normalized rare-earth element profiles of the Pah Canyon and Yucca Mountain Members.

Member would have to have a bulk chemical composition which exceeds 80% SiO2. This would exceed the theoretical SiO2 limit for an igneous rock (Tuttle and Bowen, 1958), therefore magma mixing is ruled out. Rocks which have the necessary SiO2 content, such as sandstone or quartzite, are not found in the near vicinity and are similarly dismissed.

Fractional Crystallization

Major element fractional crystallization from the Pah Canyon Member to the Yucca Mountain Member can be evaluated using least squares multiple linear regression. The regression was set up by choosing a representative sample from the Pah Canyon Member and regressing it against the Yucca Mountain Member, and all combinations of the major minerals that are found in the Pah Canyon Member: plagioclase, alkali feldspar, clinopyroxene, biotite, magnetite and ilmenite. Where individual phase chemistries varied, different compositions were used in the regressions. For example, plagioclase compositions varied from Ania to Ania, so for the regression, plagioclase values of Ania, Ania, and Ania were used. The regression equation was set up for ten of the major elements.

Reasonable results were obtained from many equations.

The equations that gave the best results are:

1.0 D = .84 G + .09 San + .04 Pl + .02 Bt + .01 Cpx sum of squares of residuals = 0.20 $R^2 = 1.00$ (5)

1.0 D = .85 E + .07 San + .05 Pl + .02 Bt + .01 Cpx sum of squares of residuals = 0.28 $R^2 = 1.00$ (6)

1.0 F = .76 G + .17 San + .02 Pl + .03 Bt + .02 Cpx sum of squares of residuals = 0.26 $R^2 = 1.00$ (7)

1.0 D = .83 G + .11 San + .04 Pl + .01 Bt + .01 Cpx + .004 Mt

sum of squares of residuals = 0.14 R² = 1.00 (8)

where D and F are representative Pah Canyon magmas P5B and P2C respectively, E and G are representative Yucca Mountain magmas Y-1B-E and Y-3b respectively, San represents alkali feldspar, Pl represents plagioclase with a value of An27, Bt represents biotite, and Cpx represents clinopyroxene.

The interpretation of the major element multiple linear regression is consistent with a fractional crystallization origin of the Yucca Mountain magma from the Pah Canyon magma. All reasonable major element multiple linear regressions have low residuals and R² values near unity. Four of the best results are shown in Equations 5 through 8. The best regression shown, Eq. 8, requires 17% crystallization of the phases alkali feldspar (11%),

plagioclase (4%), biotite (6%), clinopyroxene (6%), and magnetite (.4%). When the crystallizing phases are normalized to one hundred percent, this corresponds to 63% alkali feldspar, 23% plagioclase, 6% biotite, 6% clinopyroxene, and 2% magnetite. Modal phenocryst analysis of the Pah Canyon Member (Table 6) is in rough agreement with predicted relative amounts of crystallization from the linear regression. For example, the relative percentages of phenocrysts in the Pah Canyon Member are: 32% to 55% alkali feldspar; 36% to 56% plagioclase; 4% to 10% biotite; 1% to 2% clinopyroxene; and less than 1% magnetite. This corresponds roughly to the relative phenocryst percentages of Eq. 8, but even better to the relative phenocryst percentages of Eq. 6 which are; 47% alkali feldspar, 33% plagioclase, 13% biotite, and 7% clinopyroxene.

Using the results of the major element regression, a test of fractional crystallization was performed with selected trace elements. The trace elements were chosen based on their large variation in the system and the assumption that they are not the major components of any trace mineral that occurs. For example, Zr was not chosen as a trace element for this test because it is the dominant component of the trace phase zircon. The known maximum and minimum distribution coefficients for silicic systems (Table 8, Nash and Crecraft, 1985; Mahood and Hildreth, 1983) were used for various degrees of batch crystallization, and trace element concentrations were predicted. Maximum and minimum

predicted fractionation trends for; Ba versus Rb; and Eu versus Sr, are shown for the respective major element regression equations (Eqs. 5-8, and Figs. 16-19). The origins of the fractionation trends are at typical Pah Canyon magma (P5B) concentrations for the respective elements.

Trace element analyses also support the interpretation that the Yucca Mountain Member formed from the Pah Canyon Member by fractional crystallization. Figures 16 through 19 show minimum and maximum fractionation trends for; Ba versus Rb; and Eu versus Sr; based on the major element regression Equations 5 through 8, respectively. Assuming the published minimum and maximum distribution coefficients reflect a real range, the area between the curves are the predicted allowable trends, a fractionation window. On both plots of Ba versus Rb, the Yucca Mountain Member has elevated measured Rb values compared to predicted Rb values. However, Figs. 17 and 19 have Rb values which are only 2% to 13% higher the predicted range. These two regressions also have modal phenocryst percentages that are close to those predicted by major element multiple linear regression. On all plots of Eu versus Sr (Figs. 16 through 19), the measured values of the Yucca Mountain all fall within or very close to the predicted fractionation window.

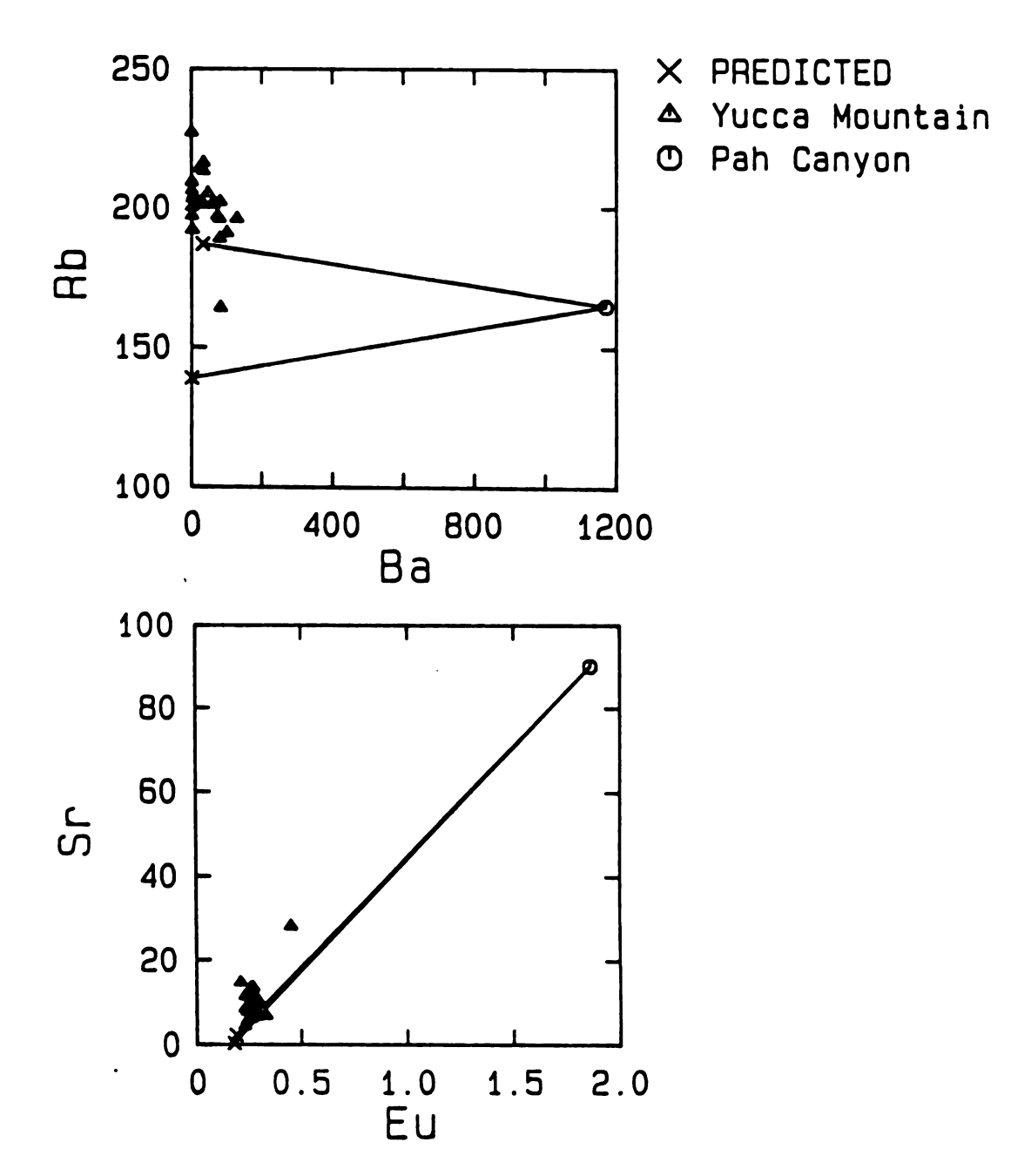


Figure 16. Fractional crystallization: Predicted and actual values for A) Ba against Rb, and B) Eu against Sr. Lines connecting Pah Canyon data point to predicted data points is allowable fractionation line based on minimum and maximum distribution coefficients as modeled by equation 5. See text for further explanation.

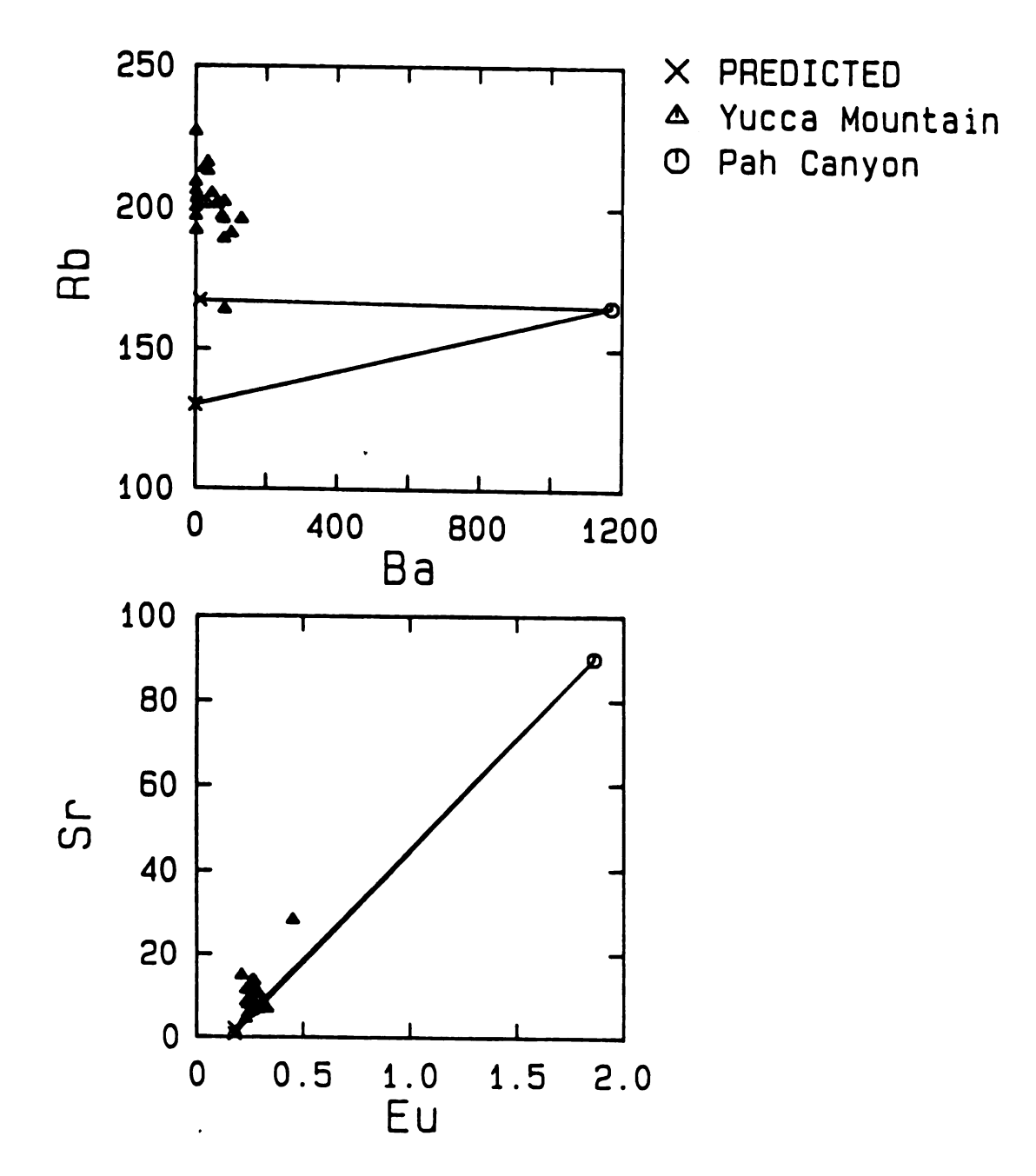


Figure 17. Fractional crystallization: Predicted and actual values for A) Ba against Rb, and B) Eu against Sr. Lines connecting Pah Canyon data point to predicted data points is allowable fractionation line based on minimum and maximum distribution coefficients as modeled by equation 6. See text for further explanation.

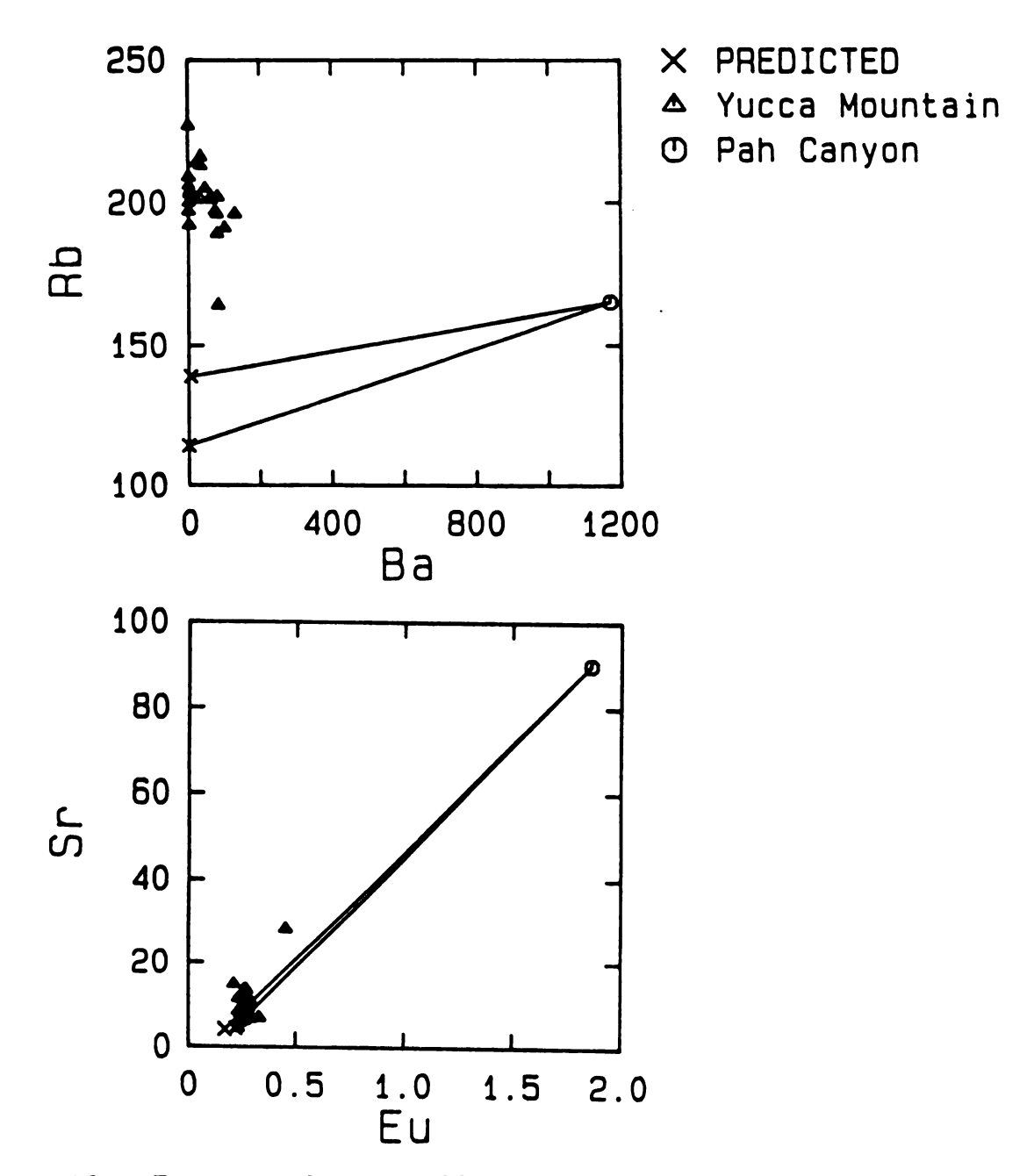


Figure 18. Fractional crystallization: Predicted and actual values for A) Ba against Rb, and B) Eu against Sr. Lines connecting Pah Canyon data point to predicted data points is allowable fractionation line based on minimum and maximum distribution coefficients as modeled by equation 7. See text for further explanation.

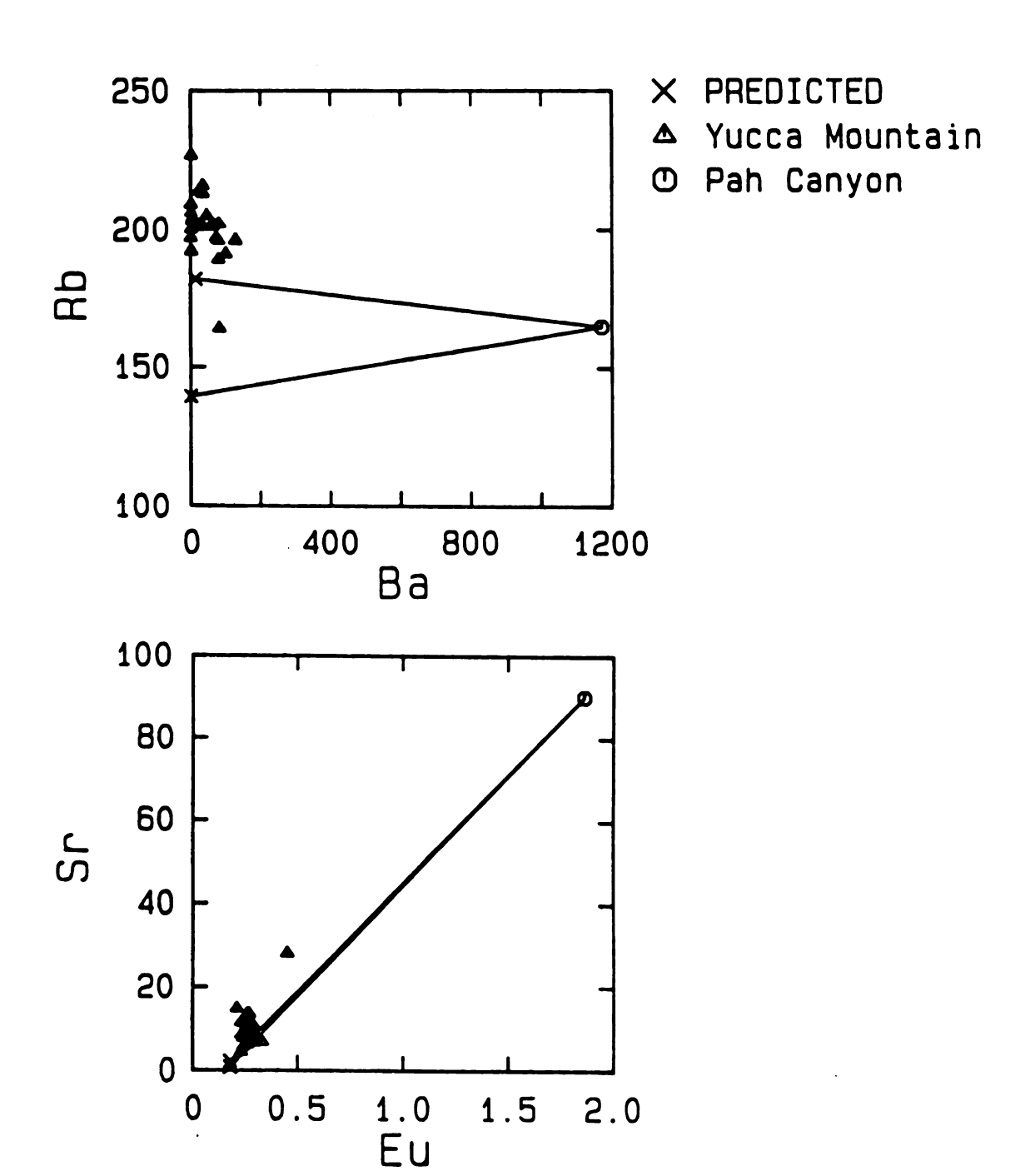


Figure 19. Fractional crystallization: Predicted and actual values for A) Ba against Rb, and Eu against Sr. Lines connecting Pah Canyon data point to predicted data points is allowable fractionation line based on minimum and maximum ditribution coefficients as modeled by equation 8. See text for further explanation.

Summary

The results of an evaluation of the major elements and selected trace elements are consistent with the interpretation that the Yucca Mountain Member was derived from the Pah Canyon Member by fractional crystallization.

Based on major element regression, the Yucca Mountain Member could be formed by 15% to 24% fractional crystallization of a typical Pah Canyon magma. Alkali feldspar is the dominating crystallizing phase, plagioclase is subordinate, biotite and clinopyroxene are relatively minor, and magnetite is a trace to absent phase. This fractionating scheme is consistent with reported modal phenocryst abundances in the Pah Canyon Member (Byers et al., 1976b).

The trace elements are also consistent with this interpretation, although some deviation occurs. The variation of some of the measured trace element data from the predicted data, particularly Rb, could be due to: 1) Distribution coefficients that are not correct for this system. Nash and Crecraft (1985) warn against using distribution coefficients that were not determined specifically for the system in question. 2) Measured trace elements concentration in the pumices are not the same as those in the magma. Post eruptive processes, such as hydrothermal leaching and reprecipitation, may have redistributed some elements. Rb is a particularly mobile element, and may have been affected in this manner. 3) Fractional crystallization may not have operated

independently and some other process and/or processes affected the distribution of certain elements. Such processes could include diffusional liquid/liquid processes, some magma mixing, or some type of assimilation.

ORIGIN OF THE TIVA CANYON MEMBER Introduction

The Tiva Canyon Member represents the final major (12.7 m.y.) eruption (>1000 km³) from the same magmatic system that produced the Topopah Spring, Pah Canyon, and Yucca Mountain Members (Fig. 2). A petrographic and field description of the Tiva Canyon Member has been summarized by Byers et al. (1976b). Three compositional zones have been recognized in the Tiva Canyon Member (Byers et al., 1976b). The lowermost zone is crystal-poor sanidine- and hornblende-bearing higher-silica rhyolite. This grades upward into a middle crystal-poor rhyolite with biotite. This middle zone is in turn overlain by an upper crystal-rich quartz latite hornblende-absent (caprock). Individual glassy pumices, that are characteristic of each of these three zones, occur at the top of the ash-flow sheet.

The intention of this segment of the study is to determine the origin of, and the relationship between, the three distinct compositional zones recognized in the Tiva Canyon Member. Important questions to be addressed are:

1) Did all three zones exist as distinct liquids in the magma chamber? 2) If all three zones existed as distinct liquids within the magma chamber, what was the nature of the boundary between these layers (ie. sharp or gradational)?

3) What is the origin of the rhyolite, that has a major element chemistry intermediate between the quartz latite and the higher-silica rhyolite? 4) What is the origin of the higher-silica rhyolite? These questions will be discussed below using various quantitative tests.

Comparison of the Yucca Mountain Member and Higher-Silica Rhyolite of the Tiva Canyon Member

The Yucca Mountain Member is chemically and petrographically very similar to the higher-silica rhyolitic portion of the Tiva Canyon Member. Byers et al. (1976b) has suggested that the Yucca Mountain Member represents an early eruptive phase of the Tiva Canyon Member because of a close stratigraghic association between the two units, and a petrochemical trend towards increasing phenocrysts and decreasing silica content. Moreover, the Tiva Canyon Member was erupted shortly after the eruption of the Yucca Mountain Member, probably measurable in tens of years (Byers et al., 1976b).

This study provides additional data that shows that the Yucca Mountain Member and the higher-silica rhyolite of the Tiva Canyon Member are chemically very similar (Figs. 20 and 21). Pumices from the Yucca Mountain Member, as previously

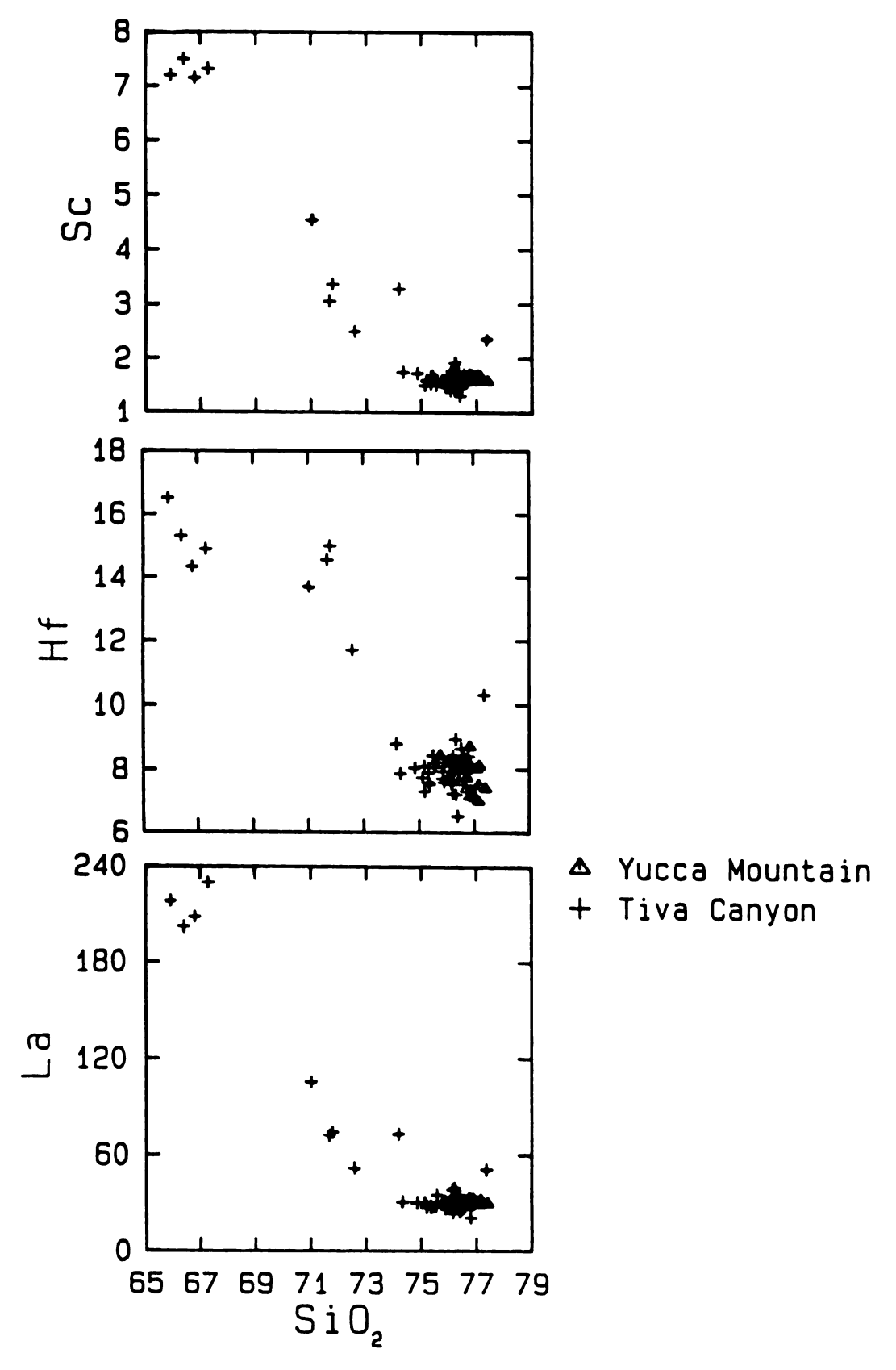


Figure 20. Plots of La, Sc, and Hf against SiO2 for the Young Mountain and Tiva Canyon Members.

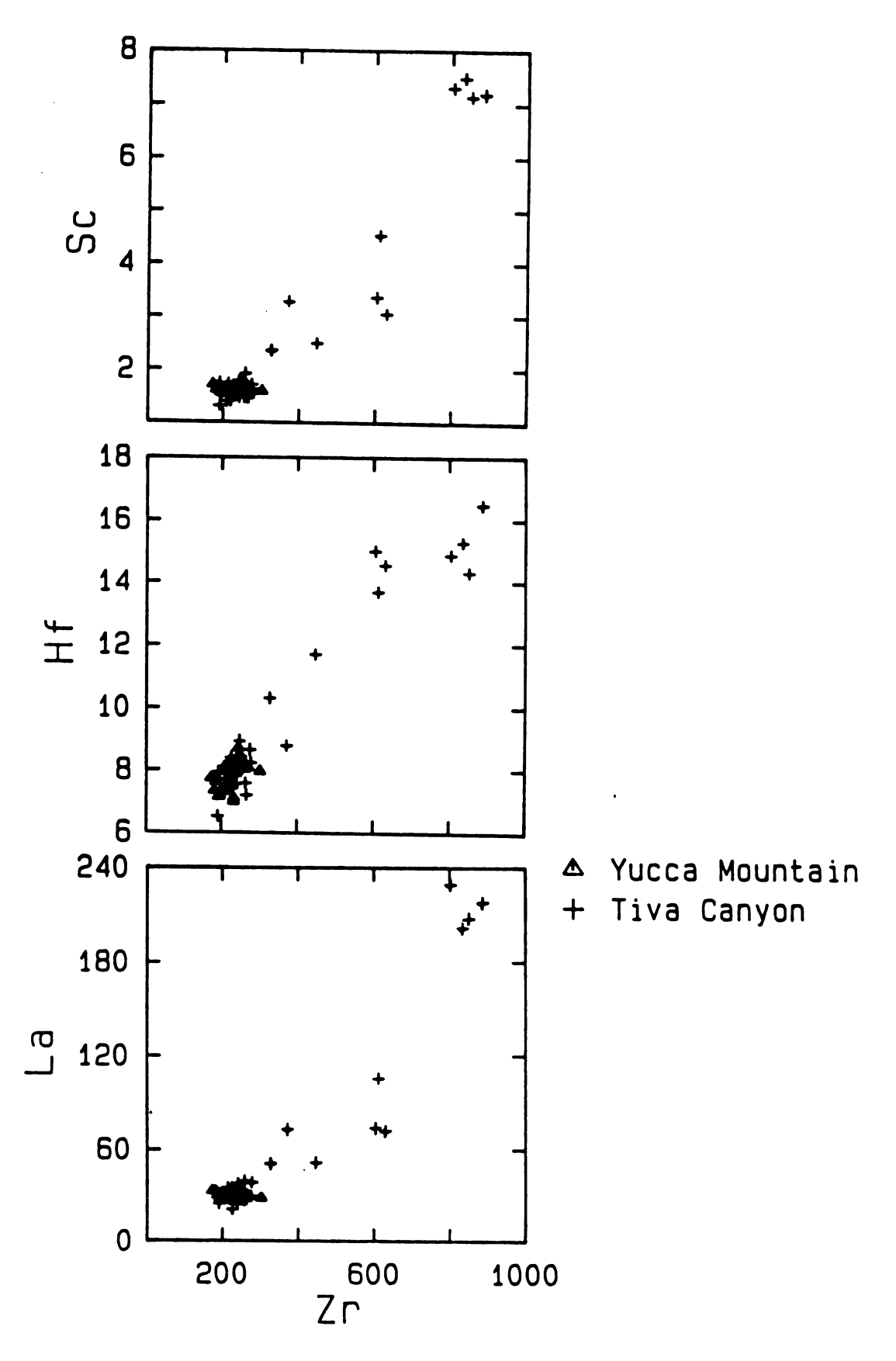


Figure 21. Plots of La, Sc, and Hf against Zr for the Yucca Mountain and Tiva Canyon Members.

discussed, range in SiO2 from only 75.8% to 77.4%; La varies from only 28 ppm to 33 ppm; and Hf varies from only 7 ppm to 9 ppm (Table 3). Pumices of the higher-silica rhyolite from the Tiva Canyon Member range in SiO2 from only 74.3% to 77.4%; La varies from only 21 ppm to 40 ppm; and, Hf varies from only 7 ppm to 10 ppm (Table 4). It is emphasized that pumices of the higher-silica rhyolite of the Tiva Canyon Member are found at both the top and the bottom of the ash-flow sheet.

The chemical similarity of the Yucca Mountain Member and the higher-silica rhyolite of the Tiva Canyon Member is evident on chemical variation diagrams (Figs. 20 to 21). The two units cluster together on plots of SiO2 versus various trace elements (Fig. 20), although the Yucca Mountain Member tends towards slightly higher SiO2 contents. On plots of various trace elements versus other trace elements (Fig. 21), there is an even tighter clustering of the two units, indicating very similar chemical characteristics.

The chemistry of the Yucca Mountain Member and the higher-silica rhyolite of the Tiva Canyon Member can also be compared quantitatively using a two sample T-test. In this type of test, two populations are compared against one another at a specified confidence interval to determine the uniqueness of each population. The Yucca Mountain Member was compared to the higher-silica rhyolite of the Tiva Canyon Member at a 95% confidence interval. The mean, the

standard deviation, and the significance of the test is shown for several elements in Table 9. The test was significant for all trace elements. This means that for the element in question, there is no statistical difference between the two units at a 95% confidence interval. The test was not significant for SiO2, but a check of means and the standard deviations (Table 9) for the two units indicates that it approached significance. This pattern is reflected on the variation diagrams (Figs. 20 and 21) where the overlap on the trace element versus trace element plots is much greater than on the plots of SiO2 versus the trace elements.

The modal mineralogy of the Yucca Mountain Member and the higher-silica rhyolite of the Tiva Canyon Member is very similar (Table 6), as noted by Byers et al. (1976b). Alkali feldspar and plagioclase are the dominant mineral phases and comprise as much as 95% of the mineral phases in both groups, with alkali feldspar dominating over plagioclase. The mafic phenocrysts comprise as much as 10% of the mineral phases in both groups, with biotite being the main mafic mineral phase. The Yucca Mountain Member has less than 1% total phenocrysts, while the higher-silica rhyolite of the Tiva Canyon Member has less than 4% total phenocrysts.

The compositional range of the various phases found in the Yucca Mountain Member and the higher-silica group of the Tiva Canyon Member are also very similar. For example, hornblende and clinopyroxene compositions, represented as

TABLE 9. Comparison of the Yucca Mountain Member and the higher-silica rhyolite of the Tiva Canyon Member using a statistical T-test.

	Mean	Standard	Significant at	Significance
		Deviation	95% Confidence	Level Attained
	(TPY-TPC)	(TPY-TPC)		
Sc	1.63-1.61	0.06-0.18	yes	0.42
Rb	201.19-213.33	11.1-38.9	yes	0.08
Zr	227.62-232.09	30.3-28.0	yes	0.55
Hf	7.85-7.96	0.47-0.59	yes	0.40
Ta	1.53-1.57	0.07-0.08	yes	0.12
La	30.08-30.32	1.47-5.20	yes	0.79
SiO2	76.72-75.92	0.39-0.66	no	

magnesium numbers (Appendix 3), and sanidine compositions, as represented by orthoclase content (Appendix 3), show little variation.

Summary

The data of this study are consistent with the interpretation that the Yucca Mountain Member represents an early eruptive phase of the higher-silica rhyolite of the Tiva Canyon Member (Byers et al. 1976b). A statistical T-test of the trace elements at a 95% confidence interval does not discriminate between the two populations. The modal phenotypes and abundances are comparable, and the chemical compositions of the minerals between the two groups are very similar.

If the Yucca Mountain Member is an early eruptive phase of the higher-silica rhyolite of the Tiva Canyon, then their origins must be the same. It is inferred that 15% to 24% fractional crystallization of the Pah Canyon magma produced the magma that was the source for both the Yucca Mountain ash-flow sheet and higher-silica rhyolite portion of the Tiva Canyon ash-flow sheet.

Origin of the Rhyolite

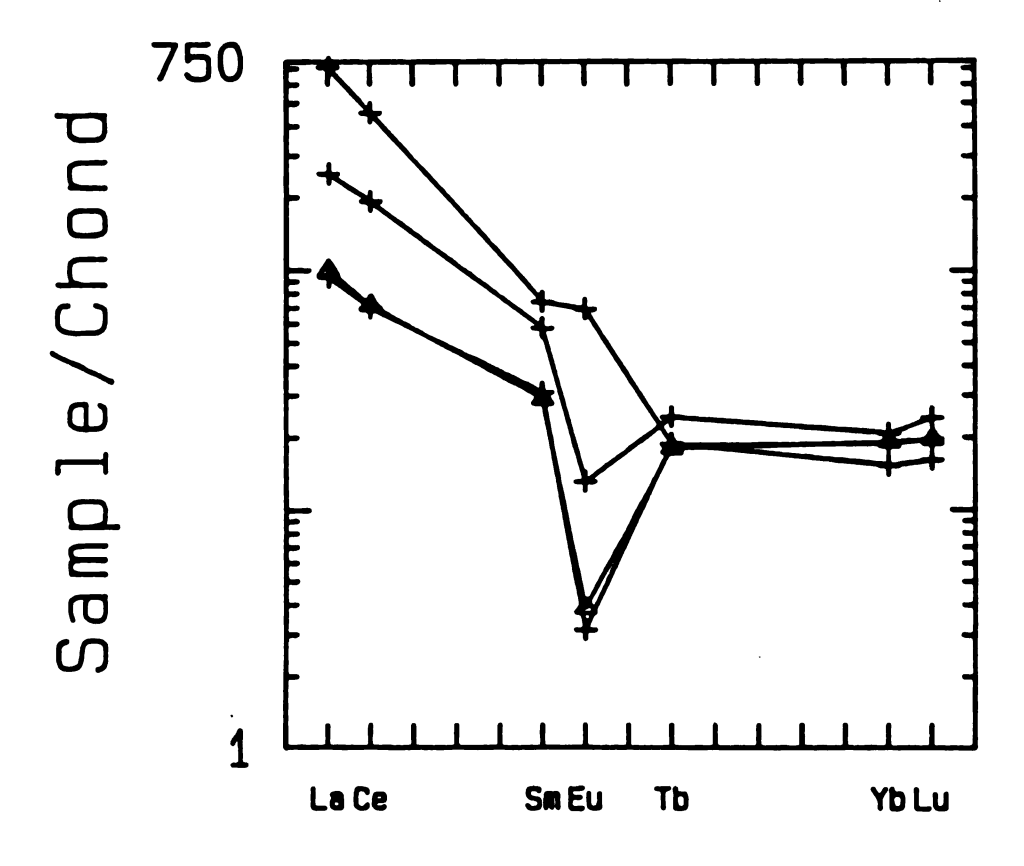
Rejection of magma mixing

The rhyolite pumices are intermediate in composition between the pumices of the quartz latite and the higher-silica rhyolite that also occur in the ash-flow sheet.

Magma mixing can be evaluated using various quantitative tests discussed previously, including; multiple linear regression of the major elements, and an independent test of the trace elements based on the major element linear regression.

If the rhyolite of the Tiva Canyon Member formed by magma mixing, then its chemistry should fall intermediate and along mixing lines on variation diagrams. Variation diagrams for La, Sc, and Hf versus SiO2 and Zr for the Tiva Canyon Member are shown in Figures 20 and 21, respectively. Generally, the rhyolite is intermediate, but does not fall along mixing lines between the quartz latite and the higher-silica rhyolite. The REE chemistry of the Tiva Canyon Member also does not conform to a simple magma mixing model. The LREE are intermediate between the between the quartz latite and the higher-silica rhyolite, as indicated on a plot of the means for each of the three zones of the Tiva Canyon Member (Fig. 22), however, a crossover occurs at Tb and the HREE of the rhyolite are enriched compared to both the higher-silica rhyolite and the quartz latite.

Magma mixing can also be rejected based on a quantitative evaluation of the major and trace elements. A pumice sample of the quartz latite and the higher-silica rhyolite was regressed against a pumice sample of the rhyolite. The regression was set up for ten of the major elements. Many regressions were performed using various combinations of



- △ Yucca Mountain
- + Tiva Canyon

Figure 22. Average chondrite-normalized rare-earth element profiles for the Yucca Mountain and Tiva Canyon Members.

samples from the quartz latite, the rhyolite, and the higher-silica rhyolite. The best regression obtained was:

1.00 A = 0.48 B + 0.52 C sum of squares of residuals = 0.06 $R^2 = 1.00$ (9)

where A is rhyolite sample C4AO, B is quartz latite sample C1AA, and C is higher-silica rhyolite sample C4AP.

Although magma mixing is consistent with the major element regression, it can be rejected based on the trace element analysis. The mixing proportions, as determined from the major element regressions, were used to calculate a predicted value for the trace elements. The predicted values were then compared to the observed values (Table 10). The trace element concentrations in the rhyolite cannot be accounted for mixing of the quartz latite and the higher-silica rhyolite in the proportions determined from the major element regression. For example, predicted Eu values should range from 0.80 ppm to 1.07 ppm, whereas observed values range from 1.9 ppm to 2.59 ppm, almost double what was predicted. Predicted Ba values range from 236 ppm to 458 ppm, whereas the observed values range from 906 ppm to 1444 ppm, more than double what was predicted. Many of the other trace elements also are not consistent with a mixing model, most notably; HREE, Rb, Hf, and La. The nonconformability of the trace elements to the major clement modeling makes it possible to reject simple magma

TABLE 10. Predicted and actual trace element abundances in the rhyolite of the Tiva Canyon Member.

TIVA CANYON MEMBER						
6	Quartz Latite	High-Silica	Rhy	Rhyolite		
		Rhyolite	Predicted	Observed		
SiO2	67.3	75.9	71.7	71.7		
Sc	7.3	1.5	4.6	3.4		
Rъ	181.7	165.0	173.0	**138.0		
Zr	802.4	221.2	500.0	603.0		
Hf	14.9	7.7	11.0	**15.0		
Ta	0.7	1.5	1.1	1.3		
Th	15.2	21.1	18.3	20.1		
La	229.5	31.5	126.5	*74.2		
Eu	4.11	0.29	2.1	*0.91		
Ba	1801	169	952	*458		

^{*} indicates significant variation

^{**} indicates cannot be produced by simple mixing

mixing as an origin for the rhyolite of the Tiva Canyon Member.

Significantly, if magma mixing can be rejected, then the rhyolite of the Tiva Canyon Member must have existed as a separate compositional layer or zone in the magma chamber, distinct from the quartz latite and the higher-silica rhyolite.

Fractional crystallization and magma mixing

The rhyolite of the Tiva Canyon Member may have formed by one of three possible mechanisms: 1) Fractional crystallization from the quartz latite of the Tiva Canyon Member; 2) Fractional crystallization and magma mixing involving mixing of Pah Canyon magma and the quartz latite of the Tiva Canyon Member; and, 3) Fractional crystallization and magma mixing involving mixing of the higher-silica rhyolite and quartz latite of the Tiva Canyon Member.

A quantitative evaluation of each of these three schemes was done for the major elements using multiple linear regression. The regressions were set up for ten of the major elements. Acceptable results (low residuals, R² near unity) were obtained from many equations for all three schemes.

The equations that gave the best results involving fractional crystallization from the quartz latite are:

1.0 D = 0.65 E + 0.12 Pl + 0.18 San + 0.04 Bt + 0.01 Mt sum of squares of residuals = 0.18 $R^2 = 1.00$ (10)

1.0 D = 0.64 F + 0.12 Pl + 0.20 San + 0.03 Bt + 0.01 Mt sum of squares of residuals = 0.13 R² = 1.00 (11)

The equations that produced the best results involving fractional crystallization and the mixing components Pah Canyon and quartz latite of the Tiva Canyon are:

$$1.0E = 1.33D + 0.21N - 0.20Pl - 0.26San - 0.06Bt - 0.01Mt$$

sum of squares of residuals = 0.13 R² = 1.00 (12)

$$1.0F = 1.00D + 0.28P - 0.13P1 - 0.13San - 0.02Bt - 0.01Mt$$

sum of squares of residuals = 0.23 R² = 1.00 (13)

The equations that produced the best results involving fractional crystallization and the mixing components higher-silica rhyolite and quartz latite of the Tiva Canyon are:

$$1.0E = 0.70D + 0.49Q - 0.08P1 - 0.07San - 0.03Bt - 0.01Mt$$

sum of squares of residuals = 0.06 R² = 1.00 (14)

$$1.0F = 0.45D + 0.49R - 0.01Pl - 0.06San - 0.01Bt - 0.001 Mt$$

sum of squares of residuals = 0.22 R² = 1.00 (15)

where D is quartz latite sample C1A7, E and F are rhyolite samples C1A6 and C3D respectively, N and P are Pah Canyon magmas P2C and P5B respectively, Q and R are Tiva Canyon higher-silica rhyolites C4AK and C3A3 respectively, and the mineral abbreviations are as previously defined. The chemistry of the minerals used in the regressions were obtained by electron probe analysis of phenocrysts found in pumices from the Pah Canyon ash-flow sheet and quartz latite portion of the Tiva Canyon.

An independent test involving selected trace elements was done based on the each of the major element regressions above (Equations 10-15). The results of the trace element evaluation was inconclusive. None of the three proposed fractionation schemes could be rejected.

The origin of the rhyolite of the Tiva Canyon Member may be modeled by fractional crystallization, or a combination of magma mixing and fractional crystallization. The best results involving fractional crystallization from the quartz latite of the Tiva Canyon Member are shown in Equations 10 and 11, and require approximately 35% fractional crystallization of phases; alkali feldspar (18%), plagioclase (12%), biotite (4%), and magnetite (1%). The best results involving the Pah Canyon magma as a mixing component are shown in Equations 12 and 13. The best regression (Eq. 12), when normalized to a summed mixing

ratio of one, requires mixing 0.86 parts of quartz latite (C1A7) and 0.14 parts of Pah Canyon magma (P2C) coupled with 35% fractional crystallization of the phases; alkali feldspar (17%), plagioclase (13%), biotite (4%), and magnetite (1%). The relative percentage of phenocrysts is; 49% alkali feldspar, 38% plagioclase, 11% biotite, and 2% magnetite. The best results of the multiple linear equations involving the higher-silica rhyolite of the Tiva Canyon as a mixing component are shown in Equations 14 and The best regression (Eq. 14), when normalized to to a summed mixing ratio of one, requires mixing of 0.59 parts of quartz latite (C1A7) and 0.41 parts of higher-silica rhyolite of the Tiva Canyon (C4AK) coupled with 15% fractional crystallization of the phases; alkali feldspar (6%), plagioclase (7%), biotite (2%), and magnetite (<1%). The relative percentage of phenocrysts is; 38% alkali feldspar, 44% plagioclase, 15% biotite, and 3% magnetite.

The major element multiple linear regression for fractional crystallization and magma mixing produced similar results for mixing involving the quartz latite of the Tiva Canyon with either the Pah Canyon magma or the higher-silica rhyolite of the Tiva Canyon. A greater amount of crystallization is required if the Pah Canyon magma is involved in mixing rather than the higher-silica rhyolite, 35% to 15%, respectively. The relative proportions of the crystallizing phases is similar, with slightly more alkali

feldspar than plagioclase removed if the Pah Canyon magma is used as the mixing component.

Summary

It is not surprising that the origin of the rhyolite of the Tiva Canyon Member can be modeled by fractional crystallization and magma mixing involving either the Pah Canyon magma or the higher-silica rhyolite of the Tiva Canyon Member, because the higher-silica rhyolite itself can be modeled as a derivative of the Pah Canyon magma by fractional crystallization. For quantitative modeling studies, the difference is simply an additional step in the equations. Relative to the magmatic system, however, the difference is significant.

The preferred interpretation is that the rhyolite of the Tiva Canyon Member formed as the result of fractional crystallization and mixing of the Pah Canyon magma and the quartz latite of the Tiva Canyon Member for the following reasons:

1) The rhyolite of the Tiva Canyon existed in the magma chamber as a separate layer separated by a compositional gap of approximately 4% SiO2 from the quartz latite and approximately 2% SiO2 from the higher-silica rhyolite.

Although volume estimates of this layer cannot be determined quantitatively, it was large enough in volume to be recognized as a distinct and laterally persistent compositional zone over much of the depositional area of the

Tiva Canyon ash-flow sheet (Byers et al., 1976b). It seems unlikely, considering the nature of the compositional gaps and the apparent large volume of this rhyolite layer, that it reflects a mixing zone or boundary zone between the quartz latite and the higher-silica rhyolite. Rather, it would seem a magmatic event would be needed to produce the necessary amount of magma interaction necessary to initiate this zone. One scenario would have the quartz latite intrude into the base of the Pah Canyon magma chamber. This could account for the eruption of the Pah Canyon ash-flow sheet and at the same time provide the mixing mechanism.

2) Experimental studies (Kouchi and Sunagawa, 1983, 1985) have shown that it is easier to mix a small amount of a high viscosity magma into a lower viscosity magma than vise The lower viscosity magma is therefore involved to a greater degree in the mixing process than the higher viscosity magma. From Equations 12 and 13, the mixing proportions would be 78%-87% of the quartz latite to 13%-22% of the Pah Canyon magma. This is consistent with the experimental work of Kouchi and Sunagawa (1983, 1985) and the theoretical modeling of Sparks and Marshall (1986). Conversely, from Equations 14 and 15, the mixing proportions would be 48%-59% quartz latite to 41%-52% higher-silica rhyolite. This proposed mixture is almost 50/50, and due to the limitations imposed on magma mixing due to viscosity differences, is difficult to reconcile without a major mixing mechanism.

A schematic outline of this scenario is illustrated in Figure 23. The Pah Canyon magma existed in the magma chamber as a discreet body (Fig. 23A). This magma was intruded by a quartz latite magma similar to the quartz latite found in pumice from the Tiva Canyon ash-flow sheet. This intrusion may have triggered the eruption of the Pah Canyon ash-flow sheet, and caused mixing of the quartz latite magma and the Pah Canyon magma (Fig. 23B). mixing resulted in the establishment of three separate layers or zones in the magma chamber. The original Pah Canyon magma and the newly formed mixed layer evolved by fractional crystallization to form the higher-silica rhyolite and the rhyolite of the Tiva Canyon respectively (Fig. 23C). This scenario implies the establishment of three layers or zones early in the development of the Tiva Canyon magma types.

An alternative interpretation is that the rhyolite of the Tiva Canyon Member formed by fractional crystallization and magma mixing of the higher-silica rhyolite and the quartz latite portions of the Tiva Canyon Member. In this scenario (Fig. 24), the Pah Canyon magma (Fig. 24A) fractionated completely to form the high-silica rhyolite of the Tiva Canyon Member (Fig. 24B). The higher-silica rhyolite and the quartz latite mixed and fractionated, probably along a boundary zone, to form the rhyolite of the Tiva Canyon Member (Fig. 24C). This scenario implies that the three layers or zones of the Tiva Canyon could have formed latter

in the development of the Tiva Canyon magma types.

Another alternative interpretation is that the rhyolite of the Tiva Canyon Member formed by simple fractional crystallization from the quartz latite. In this scenario (Fig. 25), all of the Pah Canyon magma (Fig. 25A) fractionated to form the higher-silica rhyolite of the Tiva Canyon Member, while concurrently, the quartz latite fractionated to produce the rhyolite (Fig. 25B). This scenario implies that the Pah Canyon magma was underlain by quartz latite and that there was little to no interaction between the two magmas. The rhyolite zone could have been established early or late in the development of the Tiva Canyon magma types.

VOLUME RELATIONSHIPS

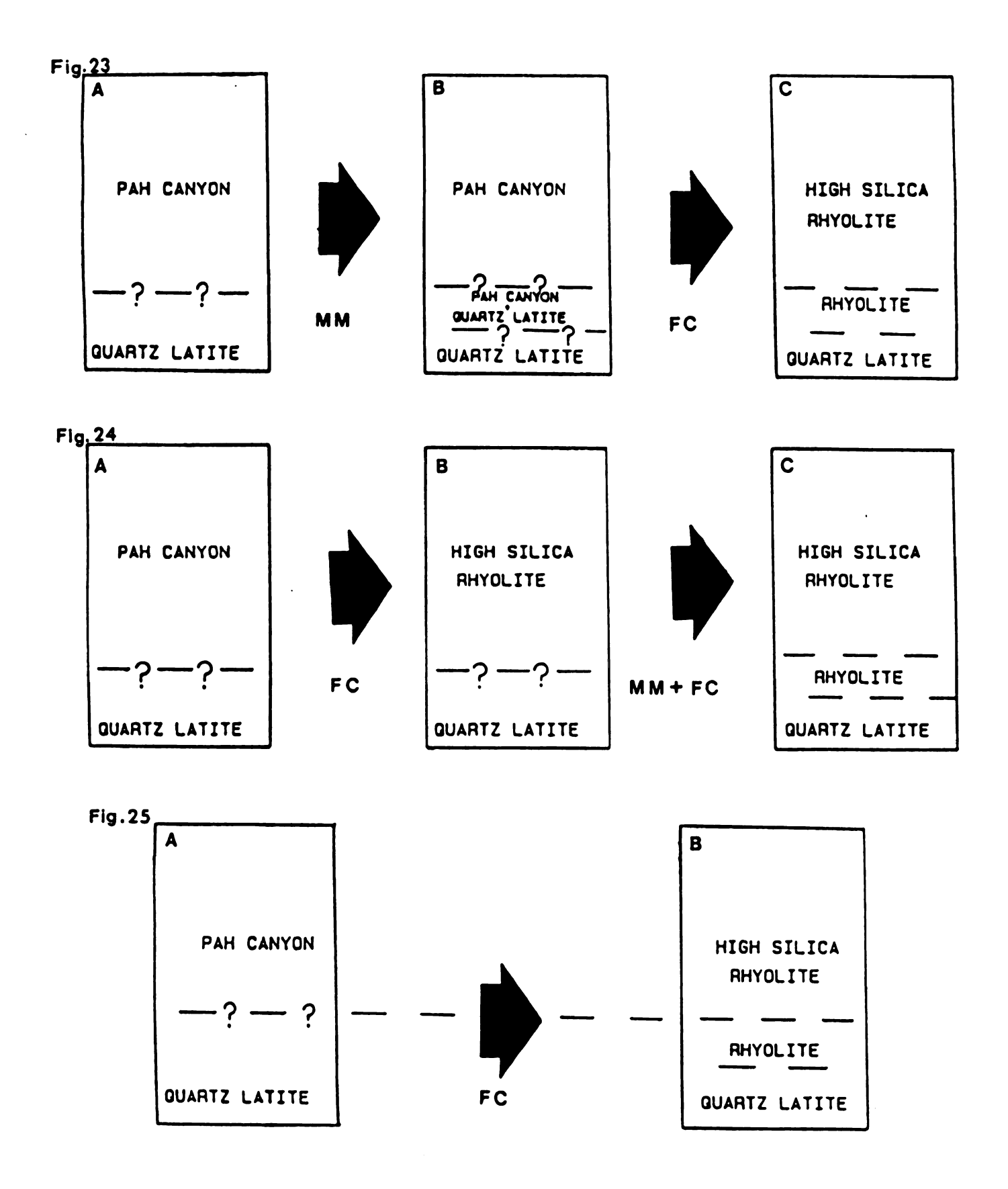
Volume relationships between the different Members of the Paintbrush Tuff can be inferred based on the interpretations of their origins. This is best accomplished by working backwards from the youngest unit, the Tiva Canyon Member, to the oldest unit, the Topopah Spring Member.

The Tiva Canyon Member is a large volume ash-flow sheet with an eruptive volume of greater than 1000 km³. A conservative estimate, based on aerial distribution of the zones of the Tiva Canyon Member, is that 50% of the ash-flow sheet is comprised of higher-silica rhyolite (F.M. Byers Jr., pers. commun., 1986). The Yucca Mountain Member has a volume of <20 km³. It is inferred that the high-silica

Figure 23. Schematic illustration depicting the origin of the rhyolite of the Tiva Canyon Member by magma mixing (MM) and fractional crystalization (FC) involving mixing of the Pah Canyon magma and the quartz latite.

Figure 24. Schematic illustration depicting an alternate origin of the rhyolite of the Tiva Canyon Member. The rhyolite formed by magma mixing (MM) and fractional crystallization (FC) involving mixing of the higher-silica rhyolite of the Tiva Canyon Member and the quartz latite.

Figure 25. Schematic illustration depicting the origin of the rhyolite of the Tiva Canyon Member by fractional crystallization (FC) from the quartz latite.



rhyolite of the Yucca Mountain ash-flow sheet had the same origin as the higher-silica rhyolite of the Tiva Canyon Member. This places a minimum estimate of 520 km³ of higher-silica rhyolite that formed by fractional crystallization from the Pah Canyon magma. From Equations 5 to 8, it was determined that 15% to 24% fractional crystallization of the Pah Canyon magma is necessary to produce the higher-silica rhyolite of the Yucca Mountain and Tiva Canyon Members. This places the minimum volume of the Pah Canyon magma at approximately 610 km3 to 680 km3. The Topopah Spring Member is another large volume ash-flow sheet with an eruptive volume of greater than 1200 km3. If the Pah Canyon Member formed by a mixture of approximately 50% quartz latite and 50% higher-silica rhyolite of the Topopah Spring Member, this implies that at least 610 km3 to 680 km3 of Topopah Spring magma was not erupted. The total volume of the Topopah Spring magma chamber therefore must have a minimum approximated volume of 1810 km^3 to 1880 km^3 .

Several interesting implications can be made from these volume estimates:

1) Small volume ash-flow sheets do not necessarily reflect small volume reservoirs. The Pah Canyon and Yucca Mountain Members were relatively small volume eruptions relative to this system, $<40~\rm km^3$ and $<20~\rm km^3$, respectively. Yet, minimum estimates of the reservoirs that produced these small eruptions are approximately $650~\rm km^3$ and $1000~\rm km^3$,

respectively.

2) A large volume of upper, more evolved magma may be left in the reservoir even after a large eruption. The minimum amount of high-silica rhyolite (50%) needed to mix with quartz latite (50%) to produce the approximately 650 km³ of magma in the Pah Canyon reservoir is 325 km³. A conservative estimate is that 60% of the 1200 km³ of erupted Topopah Spring material is high-silica rhyolite. The total minimum amount of high-silica rhyolite in the Topopah Spring reservoir before eruption was therefore greater than 1045 km³. After eruption of the Topopah Spring ash-flow sheet, more than 325 km³ or 31% must have remained in the chamber.

DISCUSSION

Models for the evolution of the Paintbrush Tuff magmatic system can be evaluated and constrained by careful use of chemical and thermal data obtained from individual whole-pumices and phenocrysts included therein. Pumices from ash-flow sheets represent an instantaneous sampling and best approximation to the primary magma (liquid + phenocrysts) from the magma reservoir. Pumices from successive ash-flow sheets belonging to the same magmatic system provide periodic samplings of the conditions of the system, at a particular instant in time, and can be used to model and constrain the evolution of the entire system. The evolution of the four members of the Paintbrush Tuff have been modeled in this progressive manner and hence the evolution of the entire magmatic system has been evaluated and constrained.

The Topopah Spring Member was the first ash-flow sheet of the Paintbrush Tuff to be erupted. Schuraytz et al. (1986) has determined that prior to the eruption of this member, a sharp compositional interface existed in the magma chamber between a quartz latite and a high-silica rhyolite. The sharp compositional gap is inferred due to the existence of corresponding major and trace element gaps, a paucity of temperature data which corresponds to the compositional gaps, and a distinct change in temperature gradients for each of the magma types.

The Topopah Spring Member is a large ash-flow sheet of greater than 1200 km³ of erupted material (Scott et al., 1984). The size of the magma reservoir must have been considerably larger. The reservoir for the Pah Canyon Member, which formed by approximately a 50/50 mixing of high-silica rhyolite and quartz latite from the Topopah Spring Member, was calculated to have a minimum volume of 610 km³. High-silica rhyolite forms greater than 60% or 720 km³ of the erupted volume of the Topopah Spring Member (F.M. Byers Jr., pers. commun., 1986). Therefore, a minimum estimate of the volume of the Topopah Spring reservoir is 1810 km³, with an approximate minimum value of high-silica rhyolite of 1045 km³. After eruption of the Topopah Spring Member, 325 km³ or 31% of the high-silica rhyolite remained in the chamber.

The Pah Canyon Member was the second ash-flow sheet erupted from the same magmatic system. It is inferred that the Pah Canyon magma formed by magma mixing of approximately 50% high-silica rhyolite and 50% quartz latite from magmas represented in the Topopah Spring Member. Eruption of the Pah Canyon Member must have occurred sometime later than the mixing event because: 1) Temperatures for the Pah Canyon are intermediate to those of the high-silica rhyolite and the quartz latite of the Topopah Spring Member. This is consistent with magma mixing, but only if the magnetites and ilmenites used for the temperature determinations had time to equilibrate at a lower, intermediate temperature.

2) Sphene is found as a phenocryst in the Pah Canyon Member, but is absent in the Topopah Spring Member, and therefore a minimum amount of time was needed to nucleate and grow this new phase.

The Pah Canyon Member was a relatively small ash-flow with <40 km³ of erupted material. However, as already noted, the size of the magma reservoir must have been considerably larger. The Yucca Mountain Member and higher-silica rhyolite of the Tiva Canyon Member total 520 km³ of higher-silica rhyolite and are inferred to have formed by 15% to 24% fractional crystallization from the Pah Canyon Member. This would imply that the minimum volume of the Pah Canyon reservoir was on the order of 610 km³ and only 7% (40 km³) was erupted.

The reservoir for the Pah Canyon magma was shallow.

Pressure determinations from coexisting magnetite, ilmenite, plagioclase and sanidine indicate that these minerals equilibrated at approximately one kilobar pressure, or a depth of less than three kilometers. Presumably, the mixing event also occurred in this shallow region.

The Yucca Mountain Member was the third ash-flow sheet erupted from the Paintbrush Tuff, and significantly, represents the reestablishment of high-silica rhyolite in the system. It represents an early eruptive phase of the higher-silica rhyolite portion of the Tiva Canyon Member. The Yucca Mountain Member and the higher-silica rhyolite of the Tiva Canyon Member is interpreted to have formed by 15%

to 24% fractional crystallization from the Pah Canyon Member. The dominant crystallizing phases were alkali feldspar and plagioclase, with minor biotite and clinopyroxene.

The Yucca Mountain Member was a relatively small ash-flow with an erupted volume of <20 km³. The size of the reservoir is calculated to be considerably larger. If the Yucca Mountain Member represents an early erupted leakage of the Tiva Canyon Member, then the reservoir for the Yucca Mountain Member is at least as large as the erupted volume of the Tiva Canyon ash-flow sheet, >1000 km³. The Yucca Mountain ash-flow sheet (<20 km³) would represent the eruption of less than 2% of the magma reservoir.

Temperature estimates are limited and pressure determinations not possible for the Yucca Mountain Member. Two acceptable temperature determinations place the temperature in the range of 691°C to 721°C. Although no pressure or depth determinations were able to be calculated, it is inferred that the higher-silica rhyolite of both the Yucca Mountain and Tiva Canyon Members originated at shallow depths. The Pah Canyon reservoir existed at shallow depths, <3 kilometers. If higher-silica rhyolite of the Yucca Mountain and the Tiva Canyon Members formed by fractional crystallization from the Pah Canyon Member, then it seems likely that this higher-silica rhyolite also formed at shallow depths.

The Tiva Canyon Member was the fourth ash-flow erupted

from the Paintbrush Tuff magmatic system. Three distinct compositional zones are recognized, a higher-silica rhyolite, a rhyolite and a quartz latite. Schuraytz et al., (1985, 1986) determined that a sharp compositional interface existed in the magma chamber prior to eruption of the Topopah Spring Member. Many similarities exist between the Topopah Spring Member and the Tiva Canyon Member relative to chemical composition and compositional gaps, however, the nature of the boundaries between the compositional zones of the Tiva Canyon Member have not been determined due to a lack of mineralogical data, particularly magnetite and ilmenite phenocryst data used for temperature determinations.

Higher-silica rhyolite was the first magma of the Tiva Canyon ash-flow sheet to be erupted. It is similar to the Yucca Mountain Member and is interpreted to represent a later phase of it. This higher-silica rhyolite is interpreted to have formed by fractional crystallization from the Pah Canyon Member. Only one temperature estimate was determined, 734°C. Byers (personal commun., 1986) has estimated that 50% of the total erupted volume of the Tiva Canyon ash-flow sheet was higher-silica rhyolite. This would place a volume estimate of >500 km² on the higher-silica rhyolite.

A small chemical zonation is inferred for the higher-silica rhyolite from the Yucca Mountain Member to the Tiva Canyon Member. If the Yucca Mountain magma represents

an early eruptive phase of the higher-silica portion of the Tiva Canyon magma, then they existed as part of the same magmatic reservoir before eruption. Although the two magmas were similar, the Yucca Mountain was slightly more evolved as indicated by slightly higher silica values, lower total phenocryst content, and lower temperature range. By inference, a zonation must have existed in the magma chamber prior to the eruption of the Yucca Mountain Member.

The rhyolite of the Tiva Canyon Member was erupted in the same ash-flow, but later than the higher-silica rhyolite. It is recognized as a distinct compositional zone in the ash-flow sheet (Byers et al., 1976b) and as individual pumices at the top of the ash-flow sheet. The origin of the rhyolite is best modeled by a combination of fractional crystallization and magma mixing of the quartz latite of the Tiva Canyon, and either the Pah Canyon Magma or the higher-silica rhyolite of the Tiva Canyon Member. preferred interpretation is that the rhyolite formed by magma mixing of the Pah Canyon Magma and the quartz latite in conjunction with fractional crystallization. interpretation is preferred for several reasons: 1) Experimental work (Kouchi and Sunagawa, 1983, 1985) has shown that for magmas of contrasting viscosities, the more viscous magma (higher-silica rhyolite) will be incorporated more readily into the less viscous magma (quartz latite) than vice versa. Predicted mixing ratios involving the Pah Canyon Member are on the order of 85% quartz latite to 15%

Pah Canyon, while for the higher-silica rhyolite the mixing ratios are on the order of 50% quartz latite to 50% higher-silica rhyolite. The ratios involving the Pah Canyon magma conform much better to experimental work and theoretical considerations (Sparks and Marshall, 1986). 2) The volume of the rhyolite zone is unknown, but large enough to be recognized as a distinct compositional zone in the field (Byers et al., 1976b). If the mixing occurred as a boundary zone phenomena, it seems unlikely that such a large volume would be produced. Further, to develop such a large volume of mixed magma would seem to require a mechanism to first mechanically mix the two magmas (Sparks and Marshall, If the eruption of the Pah Canyon Magma was 1986). triggered by an input of more primitive magma, this could also be the same mechanism which perturbed the magma chamber and caused mixing at the base between the Pah Canyon magma and quartz latite. This same argument only pertaining to the eruption of the Yucca Mountain magma can be rejected because, recalling that the rhyolite could not have formed by a simple mixture of higher-silica rhyolite and quartz latite, the time interval between the eruption of the Yucca Mountain ash-flow sheet and the Tiva Canyon ash-flow sheet is too short, tens of years (Byers et al., 1976b), to allow the required amount of fractional crystallization to occur.

The temperature of the rhyolite of the Tiva Canyon Member is intermediate to that of the higher-silica rhyolite and the quartz latite. The rhyolite is represented by only

three acceptable temperature determinations. The range is narrow and varies from 755°C to 773°C.

The quartz latite of the Tiva Canyon Member is found only in the latter stages of eruption of the ash-flow sheet. The origin of the quartz latite is unknown. The quartz latite compares very favorably to the quart latite of the Topopah Spring Member, only being slightly more mafic. Temperatures in the quartz latite are represented by only 2 samples and range from 845°C to 863°C.

CONCLUSIONS

The purpose of this investigation was to obtain chemical and thermal data from pumices of a series of four ash-flow sheets erupted from the same magmatic system, the Paintbrush Tuff, and use this data to constrain fractionation mechanisms for the evolution of the system. The significant conclusions that resulted from this study are:

- 1) The processes of fractional crystallization and magma mixing alone, and/or in combination, can account for the chemical evolution of the system. No other processes including liquid/liquid type processes need be invoked.
- 2) The Pah Canyon Member originated by magma mixing of the two contrasting magma types of the Topopah Spring Magma, quartz latite and high-silica rhyolite in a large shallow reservoir. The mixing proportions were approximately 50/50. Magma mixing most likely occurred due to disruption of the sharp compositional interface that existed in the the

Topopah Spring magma chamber because of eruption of the Topopah Spring Member.

- 3) The Yucca Mountain Member is an early eruptive phase of the higher-silica rhyolite of the Tiva Canyon Member (Byers et al., 1976b).
- 4) The higher-silica rhyolite of the Yucca Mountain Member and the Tiva Canyon Member formed by 15% to 24% fractional crystallization from the Pah Canyon Member. The dominant crystallizing phases were alkali feldspar and plagioclase, with minor biotite and clinopyroxene.
- 5) The rhyolite of the Tiva Canyon Member existed as a distinct layer or zone in the magma chamber. The preferred interpretation is that it formed by a combination of fractional crystallization and magma mixing of the Pah Canyon magma and the quartz latite of the Tiva Canyon Member. The mixing mechanism may have been the intrusion of primitive magma, perhaps quartz latite, into the reservoir. This event may also have triggered the eruption of the Pah Canyon ash-flow. Alternatively, the rhyolite formed by fractional crystallization and magma mixing of the higher-silica rhyolite and the quartz latite of the Tiva Canyon Member.
- 7) The high-silica rhyolite of the Topopah Spring Member is more differentiated than the higher-silica rhyolite of the Tiva Canyon Member, whereas the quartz latite of the Tiva Canyon Member is more primitive than the quartz latite of the Topopah Spring Member.

8) The size of the ash-flow eruptions do not reflect the size of the associated resevoir. The Pah Canyon and Yucca Mountain ash-flow sheets are <40 km³ and <20 km³ in volume respectively, while the calculated minimum size of the reservoirs is 610 km³ and 1000 km³, respectively.

Future Considerations

A study of this nature and scope invariably raises many more questions than it answers. Some of the more intriguing questions are:

1) At what depth did the magma reservoirs exist before eruption? The source for voluminous ash-flow sheets was generally accepted to be shallow seated reservoirs, calderas representing the surficial expression of their drainage (Smith, 1979; Hildreth, 1981; McBirney, 1985). Recent workers (Stormer and Whitney, 1985; Whitney and Stormer, 1986) have suggested that perhaps the source for some voluminous ash-flow eruptions was a much deeper crustal source. These estimates are based on temperatures determined from magnetite and ilmenite and the nature of the coexisting feldspars. The depth of the magma reservoir for the Yucca Mountain and Tiva Canyon Members would have implications regarding genesis of these units. If the pressure calculations reflect real depths to magma reservoirs, a comparison of depths of the reservoirs could be used as an independent check on proposed fractionation mechanisms. For example, the magma reservoir for the Pah

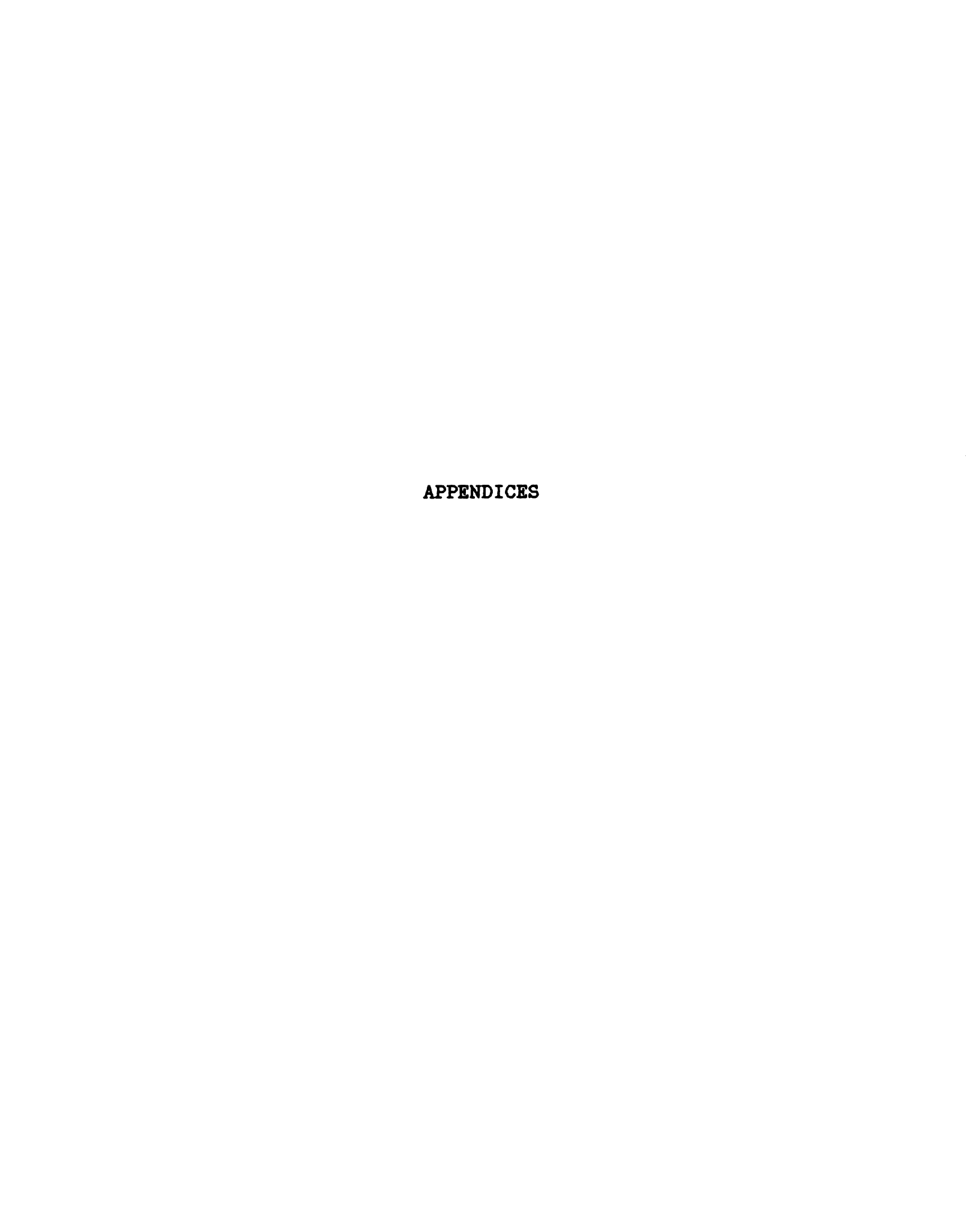
Canyon Member was determined to be shallow, on the order of one kilobar in pressure. The higher-silica portion of the Tiva Canyon Member is inferred to have formed by fractional crystallization from the Pah Canyon Member. Therefore, the reservoir for the Tiva Canyon Member should also be shallow. If the phenocrysts equilibrated at depth, this would not be consistent with fractional crystallization of the Pah Canyon magma to produce the Tiva Canyon Member, unless one could envision high-viscosity magma moving up and down the conduit considerable distances.

- 2) What is the origin of the high-silica rhyolite of the Topopah Spring Member? An initial estimated volume of >900 km³ of high-silica rhyolite has been proposed for the Topopah Spring magma reservoir. Did it form by fractional crystallization from the quartz latite, from partial melting of crustal rocks, a combination of these processes, or some other process?
- 3) What is the origin of the quartz latite that is found as the most primitive magma in both the Topopah Spring and Tiva Canyon ash-flow sheets and in later Timber Mountain Tuffs? Does it represent a partial melt of the lower crust or upper mantle, or a fractionation product from a magma more primitive in composition.
- 4) Why is there an absence or paucity of chemically banded pumice when great volumes of contrasting magma types are erupted simultaneously? Higher-silica rhyolite and quartz latite are found as pumice types at the top of the

Topopah Spring and Tiva Canyon ash-flow sheets. No chemically banded pumice has been identified for either unit. If the contrasting magma types were commingled by shearing on a small scale during eruptive transport, then the banding could be obscured. If this is the case however, then magmas intermediate in composition between the end members should be able to be identified. A hint of this fine-scale commingling of contrasting magma types can be seen on ratio/ratio plots involving the Topopah Spring Member.

- 5) What is the nature of conspicuous color banding in chemically homogenous pumice taken from the base of the Tiva Canyon ash-flow sheet? The pumice is color banded from light pink to black. Transmitted electron microscopy reveals that the boundaries of the bands are diffuse to sharp. Differential shearing can explain color banding in rhyolitic lava flows. However, it is difficult to reconcile how differential shearing could occur in pumice given the nature of pumice formation. In addition, no difference in texture or vesicularity was observed in thin section. Differences in oxidation states of certain elements can result in color differences. The color banding may be the result of different oxidation states of elements such as Fe or Mn.
- 6) What happened to the large volume of cumulates that must have formed if the higher-silica rhyolite of the Yucca

Mountain and Tiva Canyon Members formed by fractional crystallization from the Pah Canyon Member? Allowing for volume differences, greater than 100km³ of cumulates must have been removed from the Pah Canyon magma to form the Yucca Mountain and Tiva Canyon magmas. Few plutonic rock fragments are found in either the Yucca Mountain or Tiva Canyon Members.



Appendix 1. Sample locations

Samples	Numbering Sequence	Location Description
P1A-P1F	22-27	S1/2, SE1/4, NE1/4, Topopah Spring NW 7.5 Min. Quad. Mercator coordinates 566E, 4089N. West of Shoshone Mountain.
P2AA P5B-P2H	28 29-34	N1/2, SW1/4, SW1/4, Topopah Spring NW 7.5 Min. Quad. Mercator coordinates 546E, 4084N. Prow Pass Area.
P5B-P5E	35-37	S1/2, SE1/4, SW1/4, Topopah Spring NW 7.5 Min. Quad. Mecator coordinates 548.5E, 4084N.
Y3B-Y3I	37-42	Prow Pass Area. See above.
Y1B-Y1D	43-45	N1/2, SE1/4, SW1/4, Topopah Spring NW 7.5 Min. Quad. Mercator coordinates 548.5E, 4083N.
Y1BA-Y1BH	46-53	S1/2, SW1/4, SW1/4, Topopah Spring NW 7.5 Min. Quad. Mercator coordinates 546E, 4083N.
Y4AA-Y4AB Y4BB-Y4BH		Prow Pass Area. See above.
C2BA-C2BD C2EA-C2ED		NW1/4, SE1/4, Topopah Spring SW 7.5 Min. Quad. Mecator coordinates 552E, 4071N. East side Busted Butte Area.
C4B2-C4H2	70-76	N1/2, NW1/4, SE1/4, Topopah Spring SW 7.5 Min. Quad. Mercator coordinates 552E, 4071N. West side Busted Butte Area.
C5BI-C5BP	77-84	Prow Pass Area. See above.

Samples	Numbering Sequence	Location Description
C4AI-C4AP	85-91	S1/2, SW1/4, NW1/4, Topopah Spring SW 7.5 Min. Quad. Mercator Coordinates 548E, 4074N.
C1A6-C1A7	92-93	S1/2, SE1/4, SW1/4, Topopah Spring NW 7.5 Min. Quad. Mercator coordinates 548E, 4083N.
C1AA-C1AE	94-98	N1/2, NW1/4, NW1/4, Mine Mountain 7.5 Min. Quad. Mercator coordinates 568E, 4094.5N.
C2A1-C2A3		NW1/4, NE1/4, SE1/4, Mine Mountain 7.5 Min. Quad. Mercator coordinates 567.5E, 4093N.
C3A1-C3A4 C4D-C3D	106-107	NE1/4, NE1/4, SE1/4, Ammonia Tanks 7.5 Min. Quad. Mercator coordinates 566E, 4115N. South Rattlesnake Ridge Area.

APPENDIX 2. Summary of sample preparation methods.

The method used to make the glass wafers for XRF analysis is as follows: 1.0000 grams of crushed and leached sample is added to 9.0000 grams of lithium tetraborate (flux), and ~0.160 grams of ammonium nitrate (oxidant). This preparation is heated and gently shook in a platinum crucible at approximately 1100° C for a period of thirty minutes. This produces a homogenous liquid which can then be poured into a platinum mold. Wafers prepared in this manner are ready for analysis on a Rigaku XRF spectrometer.

The method used to leach carbonate from the pumice samples is as follows: A carbonate leach solution is prepared. This solution consists of 41.0 grams of sodium acetate, 13.5 grams of glacial acetate, and enough distilled water to make up a 500 milliliter solution. The crushed sample is added to this solution and vigorously boiled and periodically stirred for thirty minutes. The sample is then flushed four times with distilled water, allowing for settling between flushes. Random small samples were then oil mounted on slides and checked for carbonate using transmitted light microscopy.

APPENDIX 3. Outline of the methods used to obtain the chemistry of the phenocrysts, including a summary of the chemistry of the minerals obtained by this study. Symbols are; TPP = Pah Canyon Member, TPY = Yucca Mountain Member, TPC = Tiva Canyon Member.

The methods used to prepare the minerals for analysis are: The minerals were first separated from the crushed and leached glassy pumice. The heavy minerals, pyroxene, hornblende, biotite, magnetite, and illmenite, were separated from the light fraction of the pumice by a flotation processes. In this process, the heavy liquid bromoform was placed in a stopper flask, and the pumice The heavy fraction sinks and is drained off sample added. of the bottom. The light fraction floats and is drained off after the heavies. The lights, which are composed of plagioclase, alkali feldspar, quartz and glass, are further separated by magnetic separation. The glass contains some magnetic iron, and will catch on a magnet, leaving the minerals. The light and heavy minerals for each sample were placed inside individual bolts and were sealed in a standard epoxy mount, three bolts (samples) per mount. The mounts were polished and carbon coated at Lawrence Livermore National Laboratory, and ready for microprobe analysis.

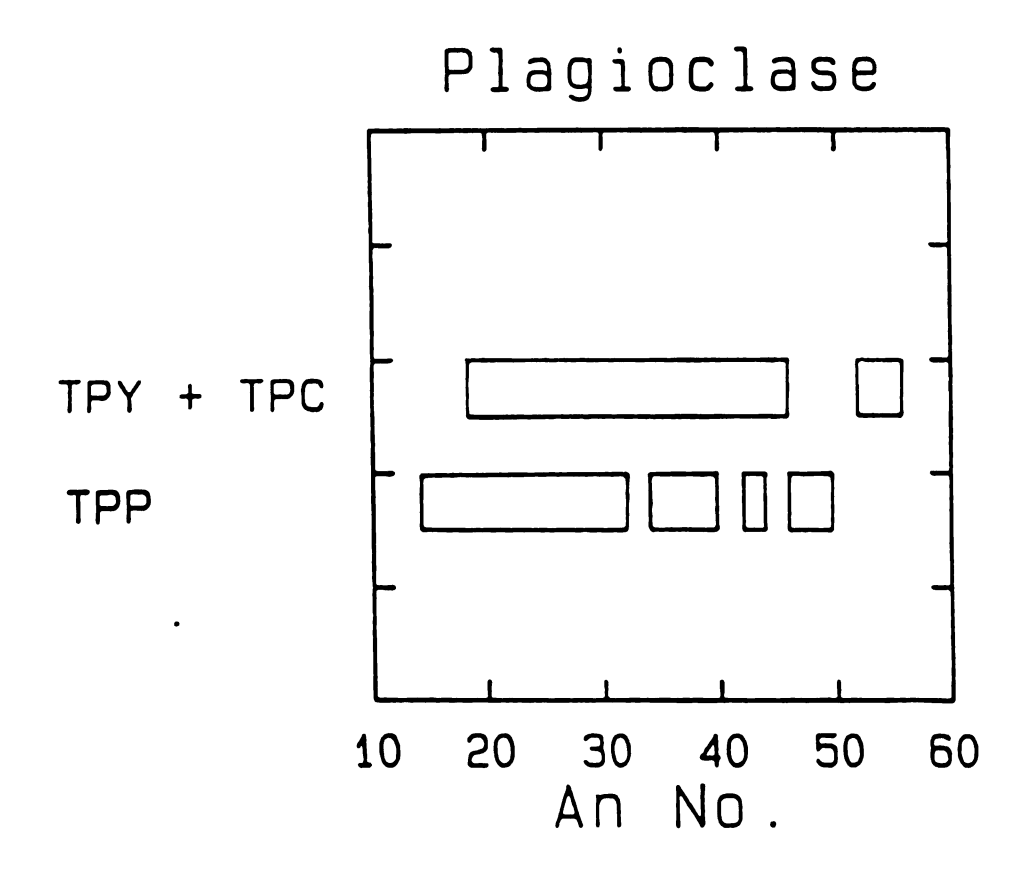
All mineral analyses were performed on a JEOL 733 superprobe at Lawrence Livermore National Laboratory. Two mineral codes were used, one for the heavy minerals, and one for the light minerals and glass. The codes are:

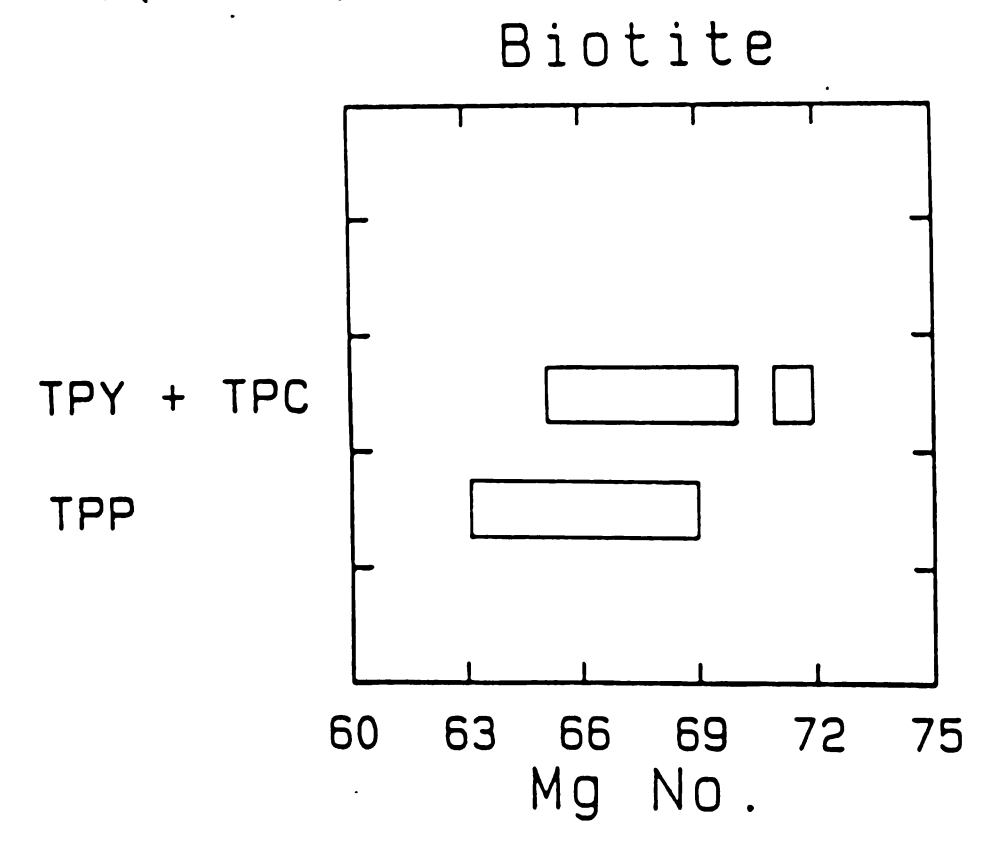
Element Standard	Counting Time (sec)	Calibration
	Heavy Code	
Ti Al Si Cr Mg Mn Fe Ni	20 20 5 20 7 20 20 40	illmenite kyanite diopside chromite olivine spessartine illmenite Ni-olivine
	Light code	
K Na Ti Ca Mg Ba Al Mn Si Fe	15 15 15 15 15 15 10 15 5	orthoclase albite rutile wollastinite olivine bentionite orthoclase spessartine diopside hematite

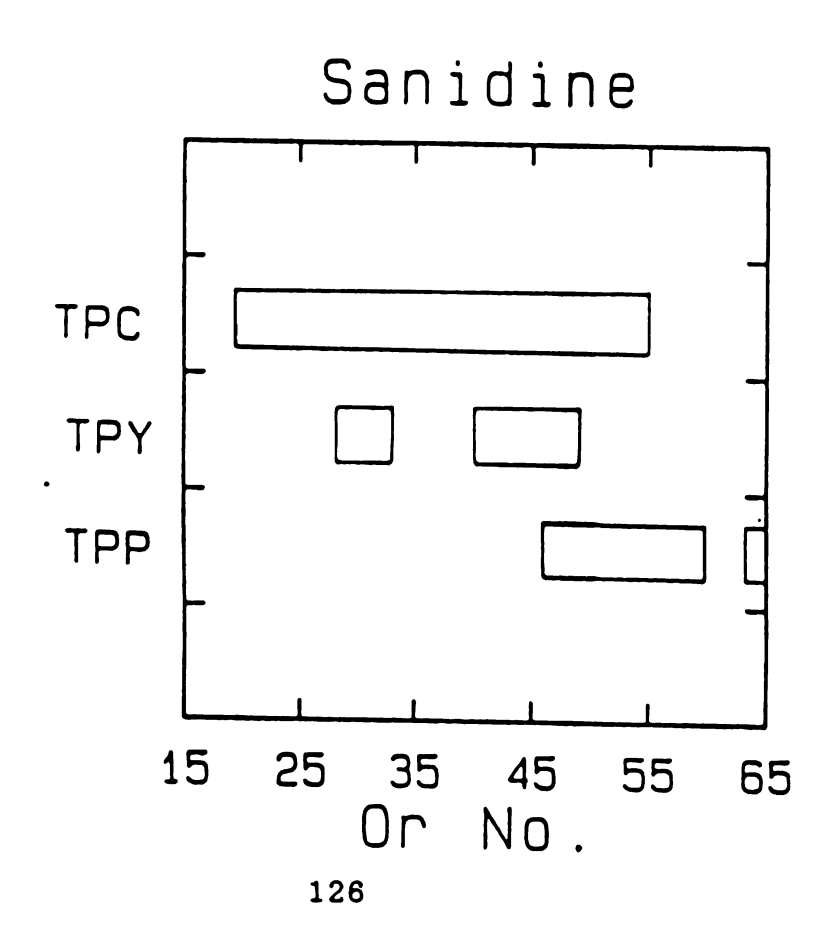
Mineral standards were periodically analyzed to calibrate the element intensity/concentration. Accuracy and precision were determined by measuring standards mineralogically similar to the analyte matrix. For example, an illmenite standard treated as an unknown was used to statistically

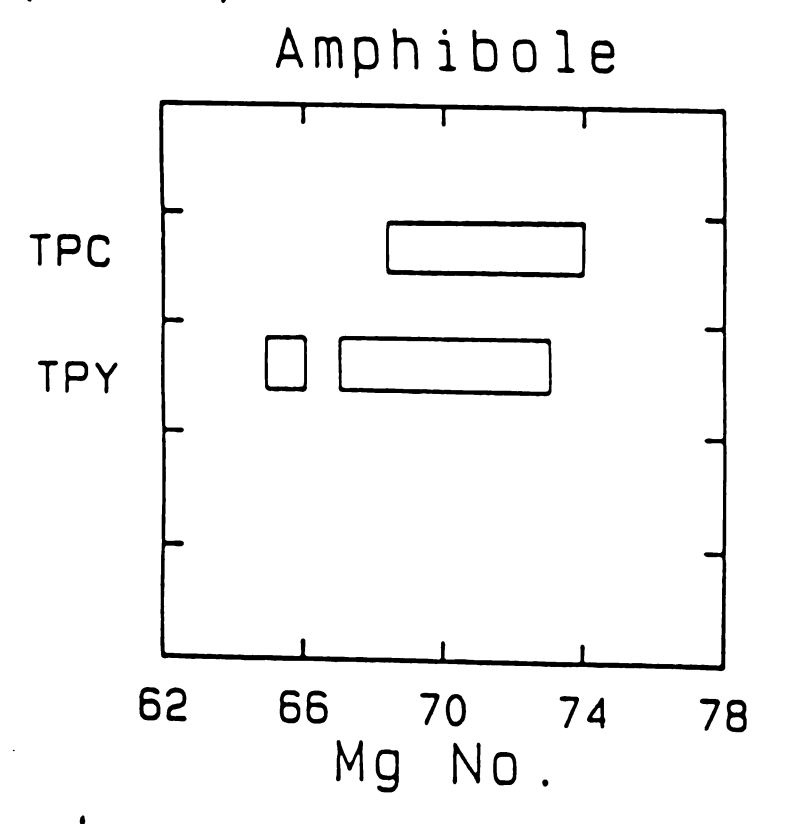
evaluate magnetite concentrations and calculate accuracy and precision.

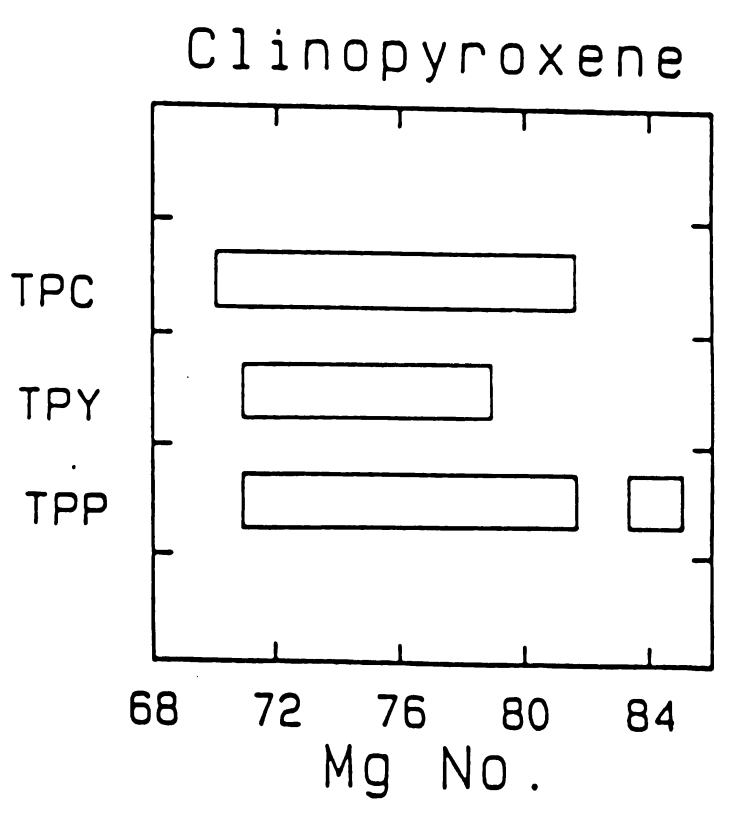
A summary of the chemistry of the major phases, plagioclase, alkali feldspar, biotite, amphibole, and clinopyroxene for the Pah Canyon (TPP), Yucca Mountain (TPY), and the Tiva Canyon (TPC) Members is presented below.



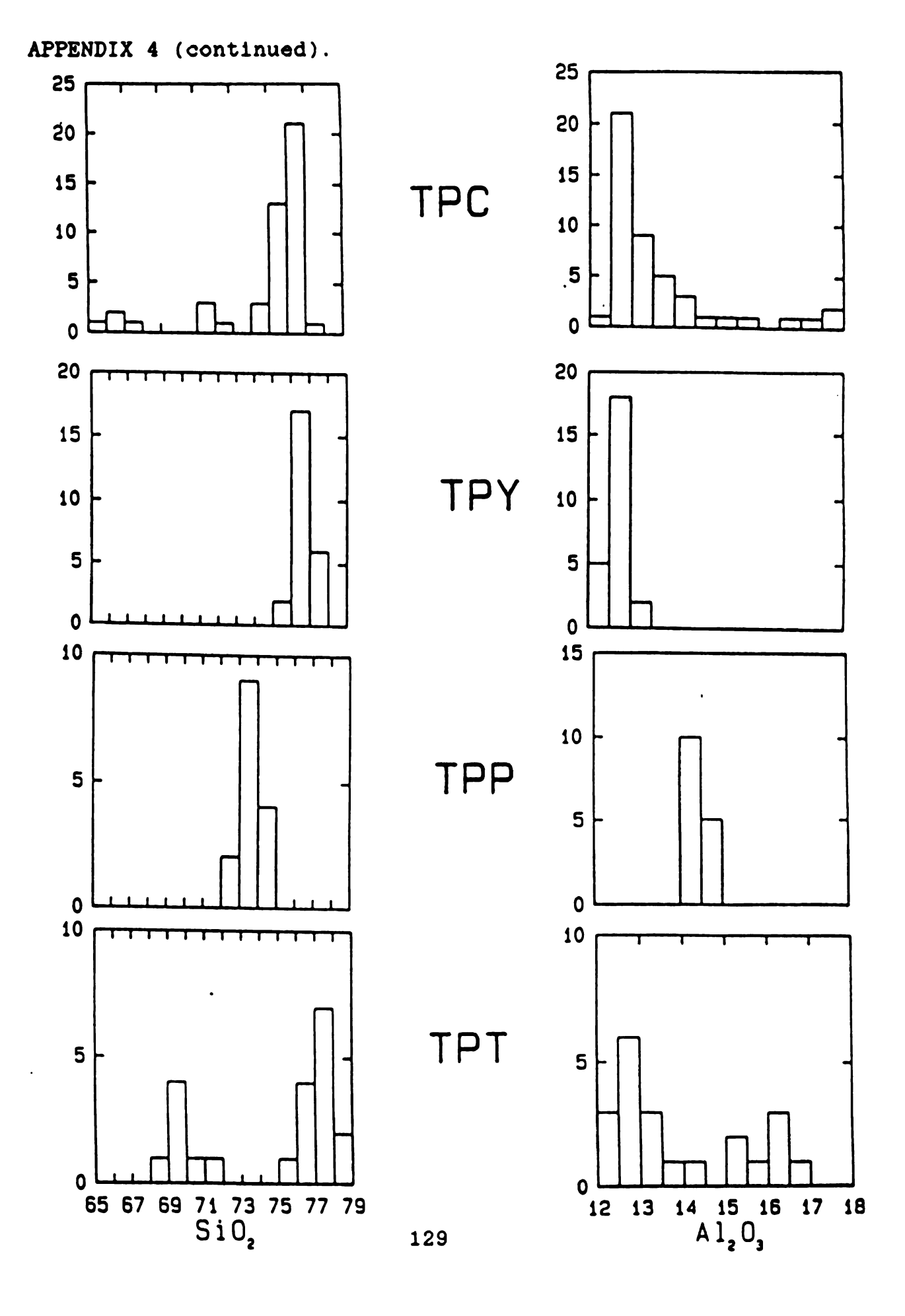


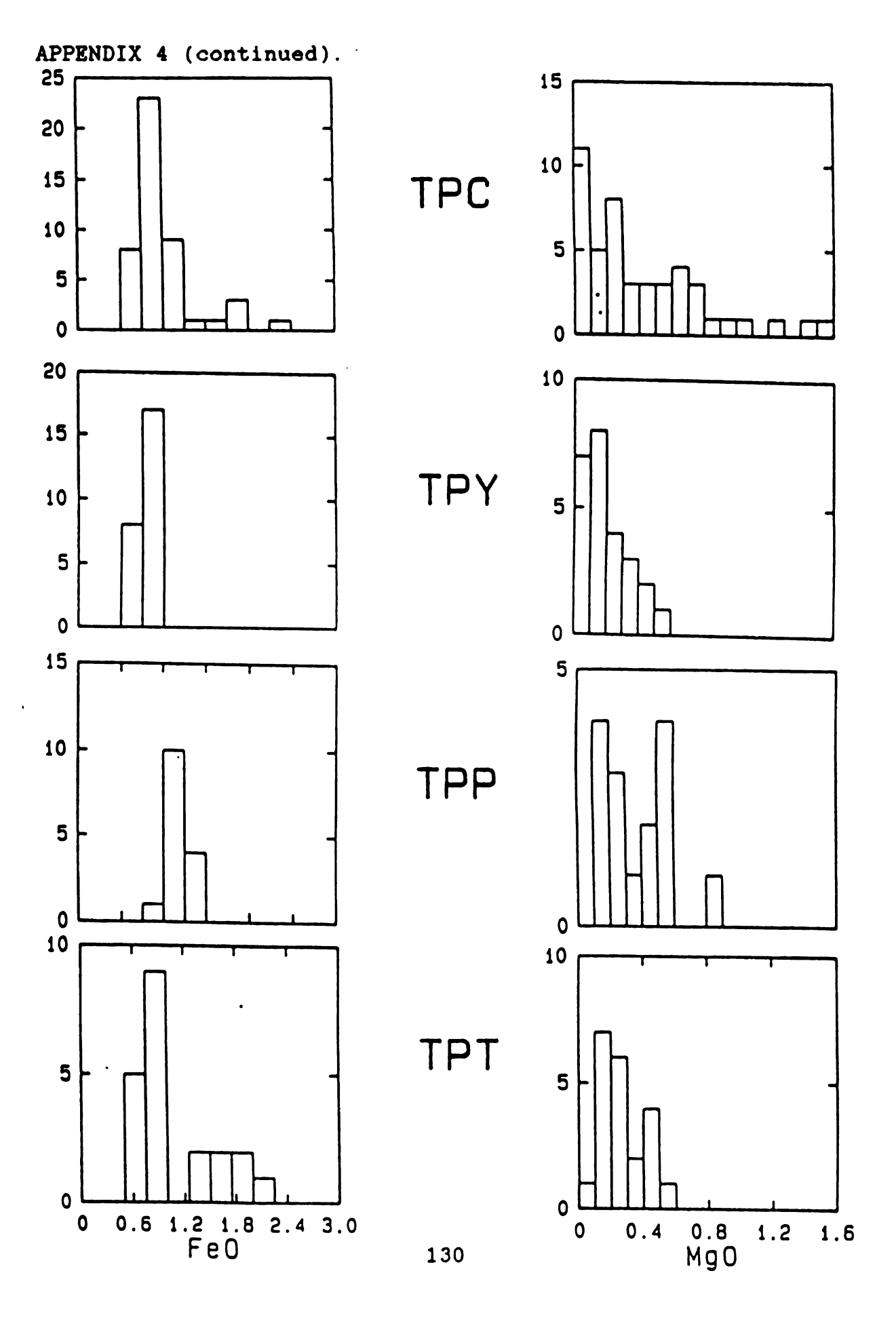


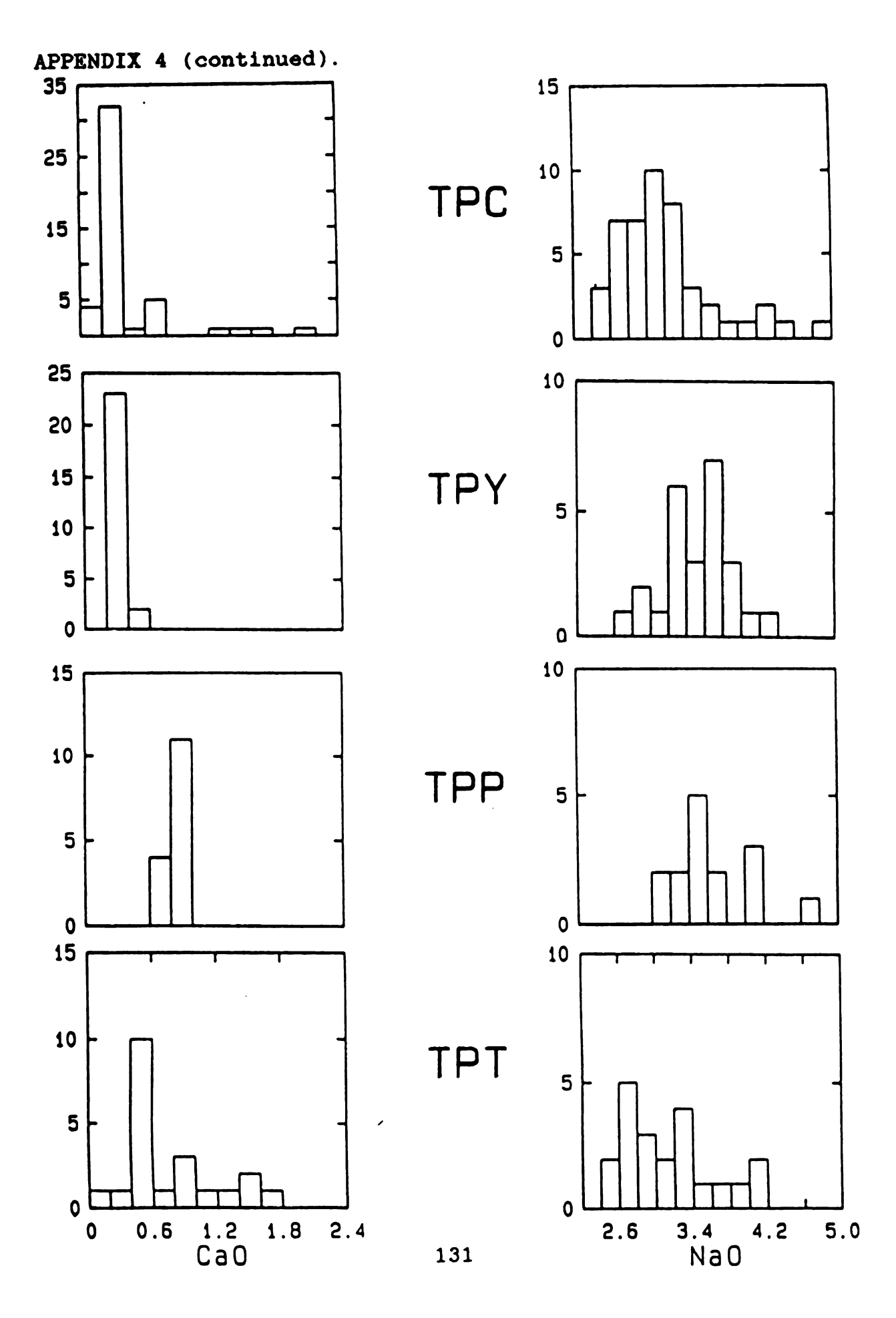


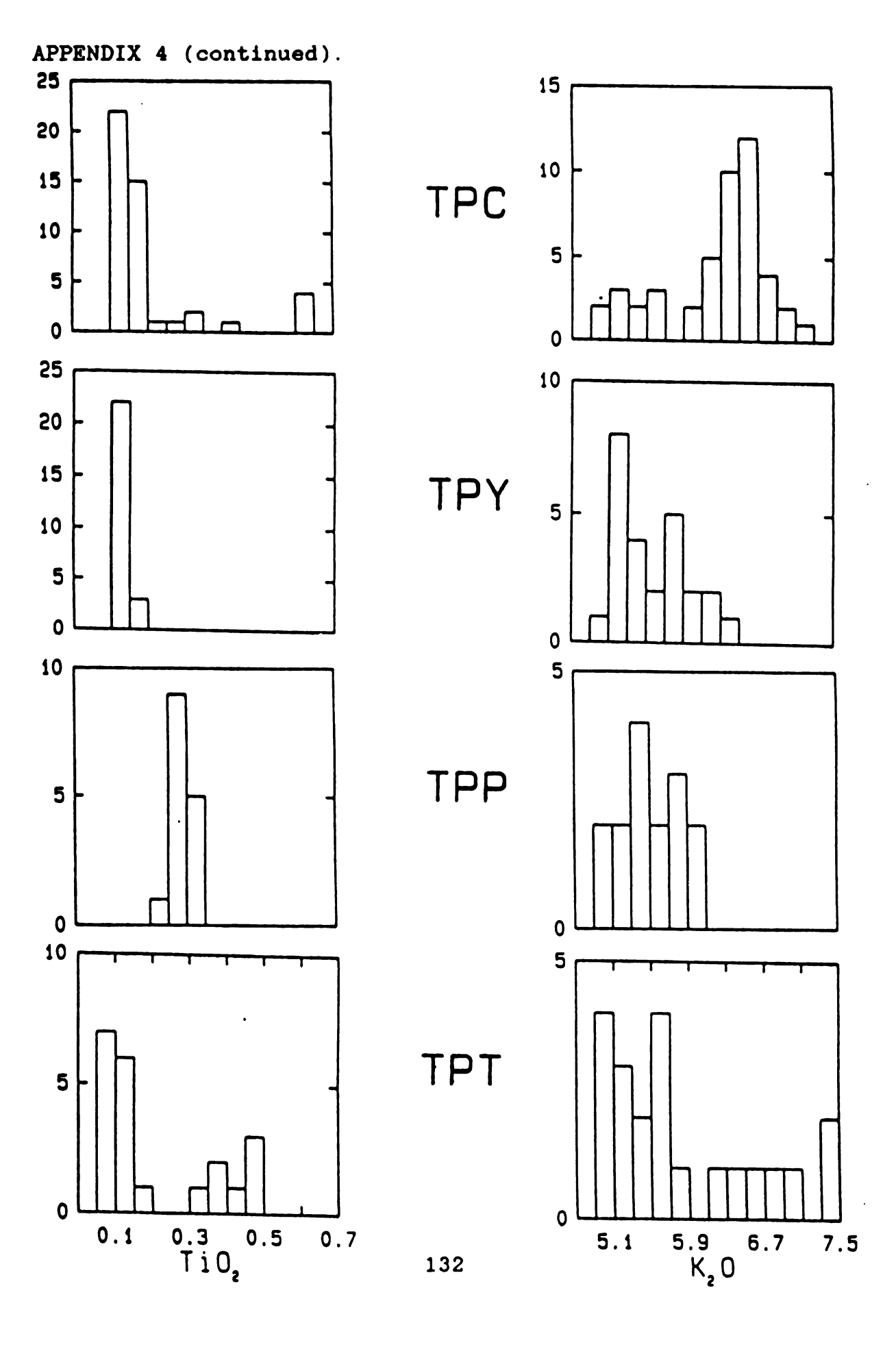


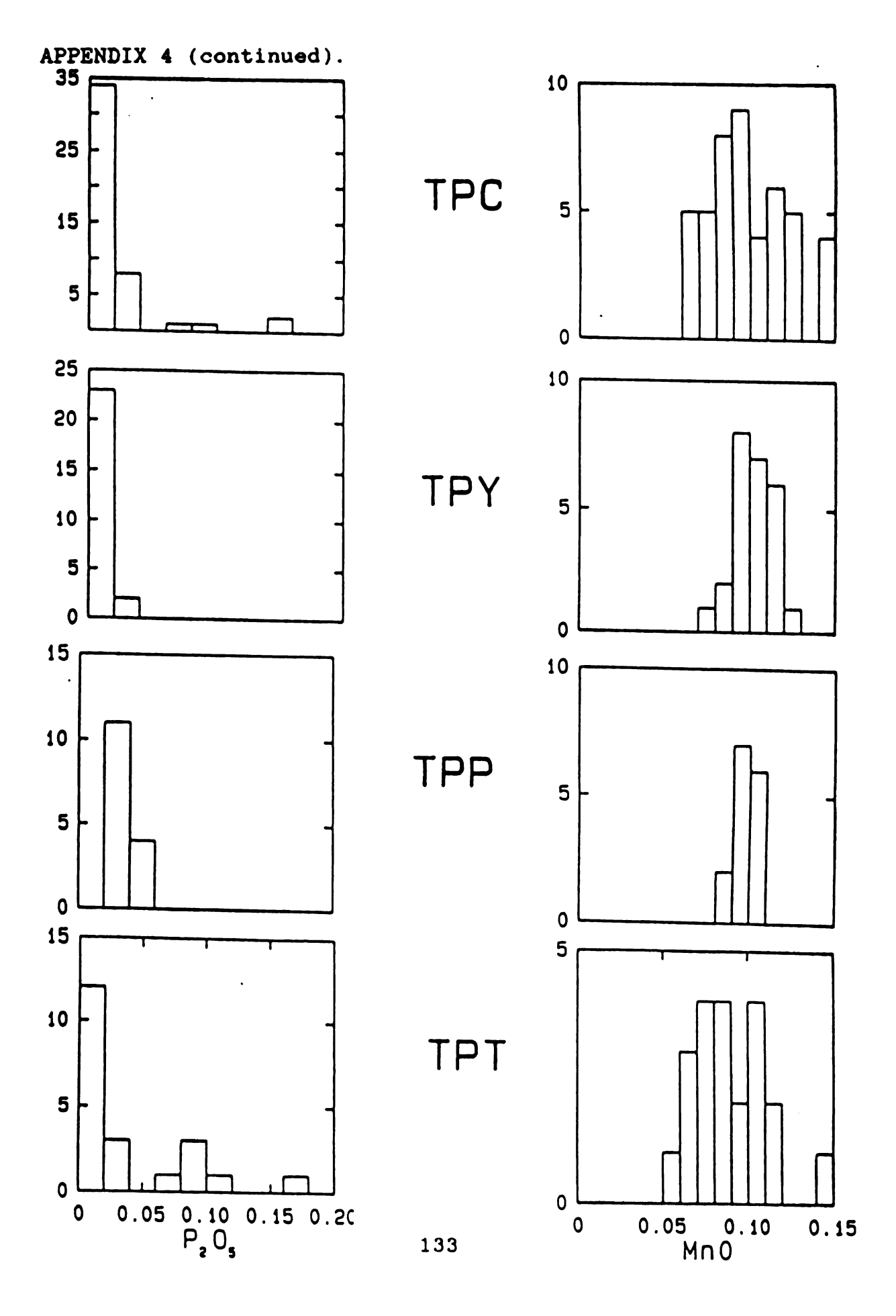
APPENDIX 4. Histograms of major and trace elements for the four ash-flow sheets of the Paintbrush Tuff. Symbols for the Members are; TPT = Topopah Spring, TPP = Pah Canyon, TPY = Yucca Mountain, and TPC = Tiva Canyon.

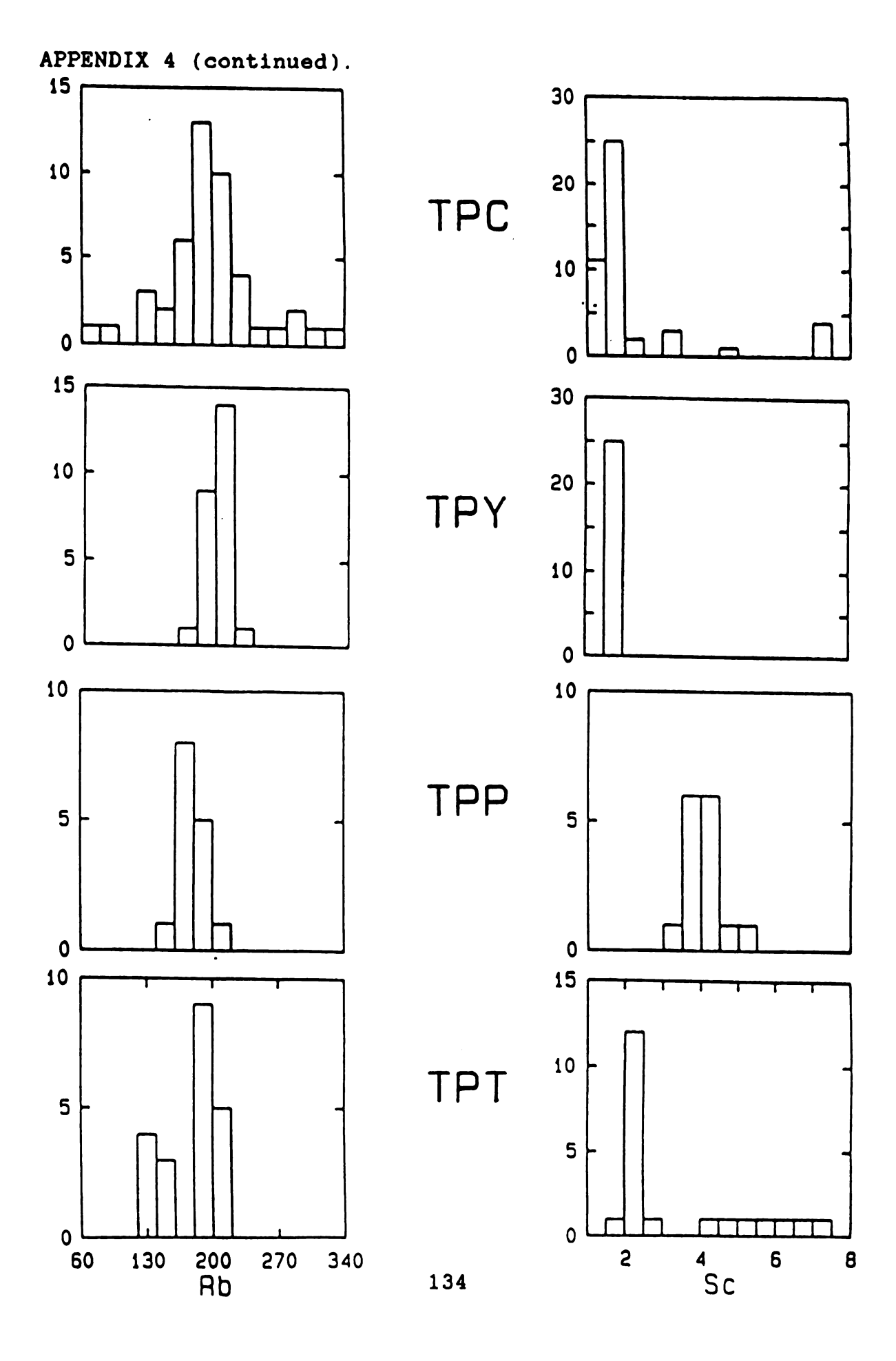


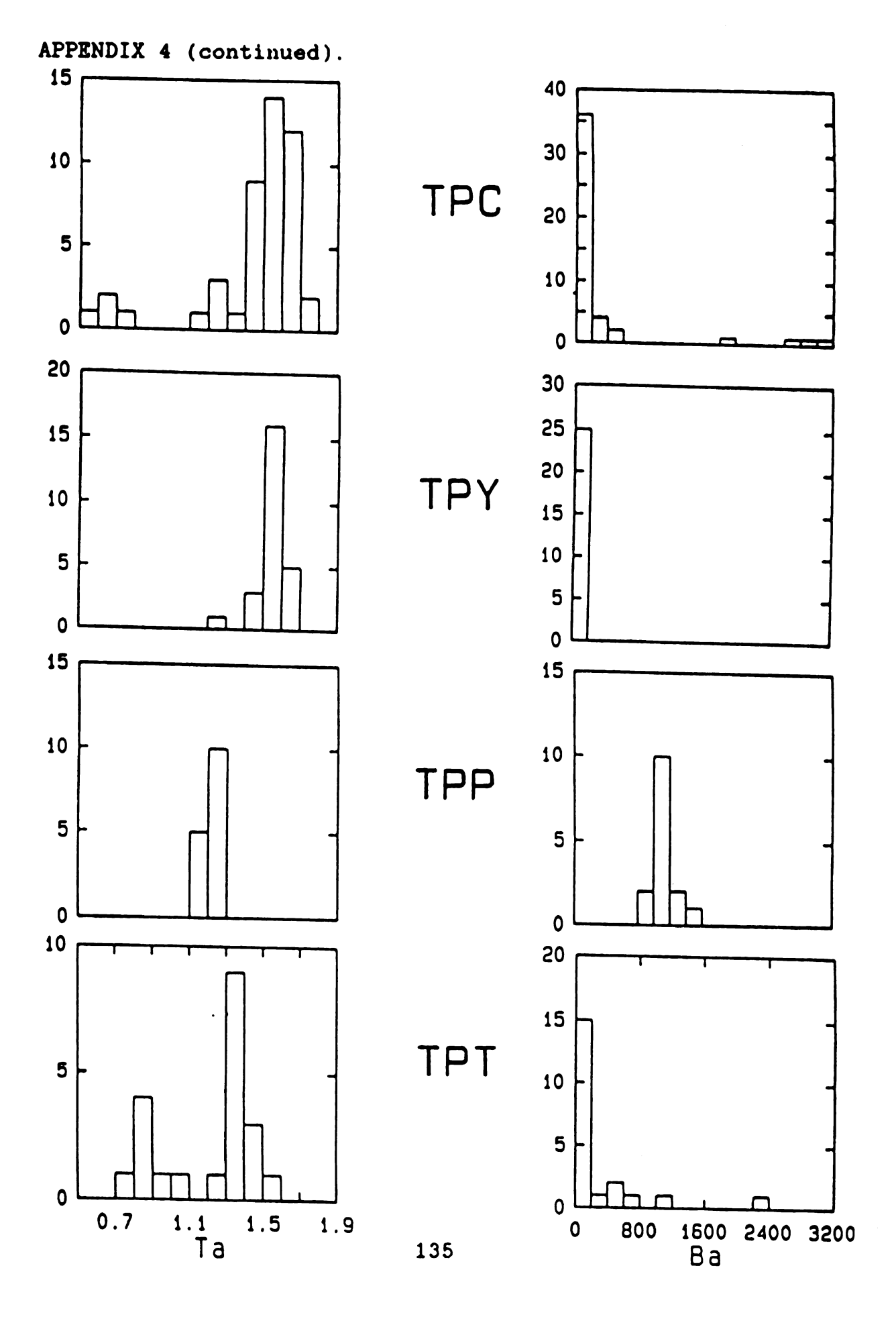


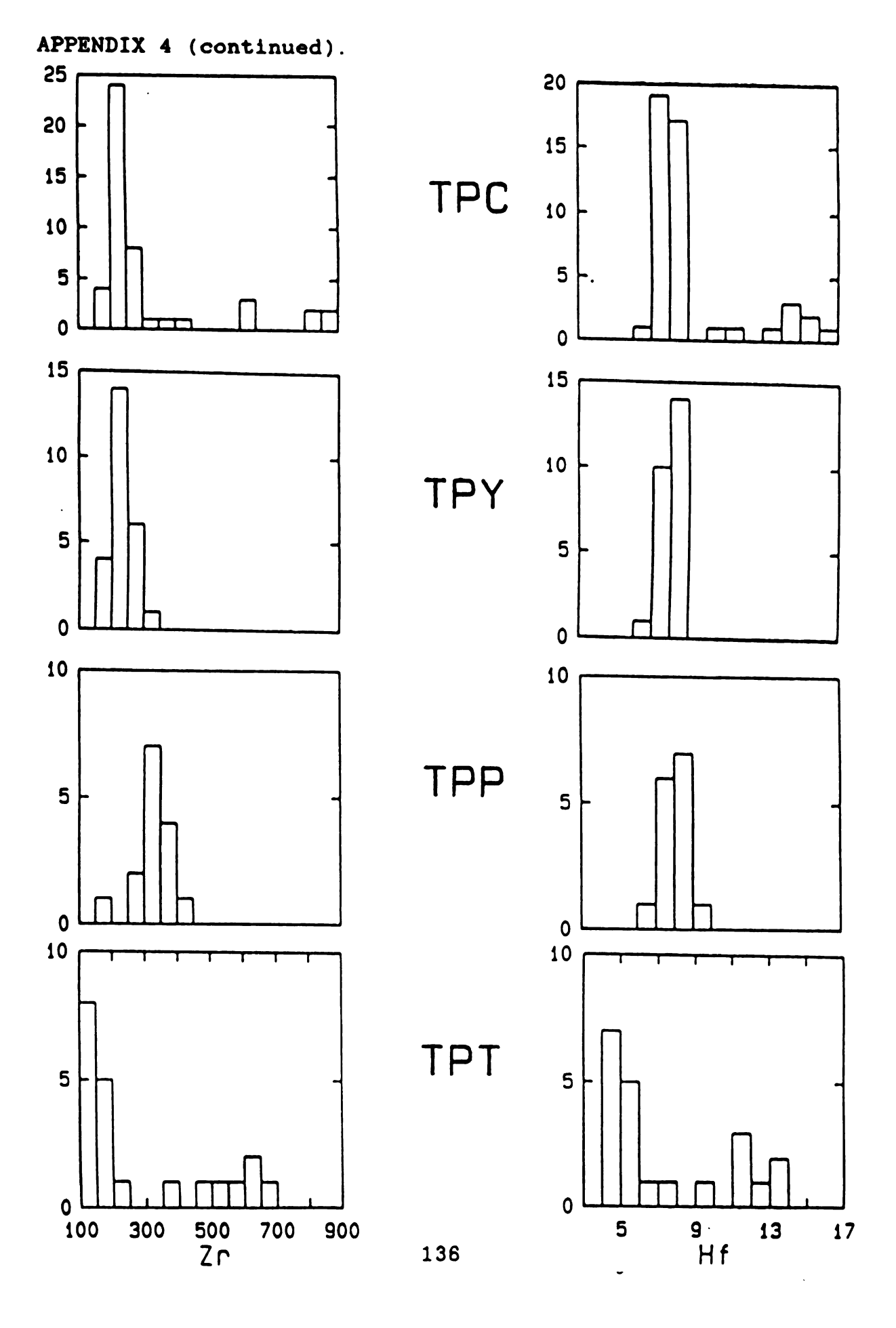


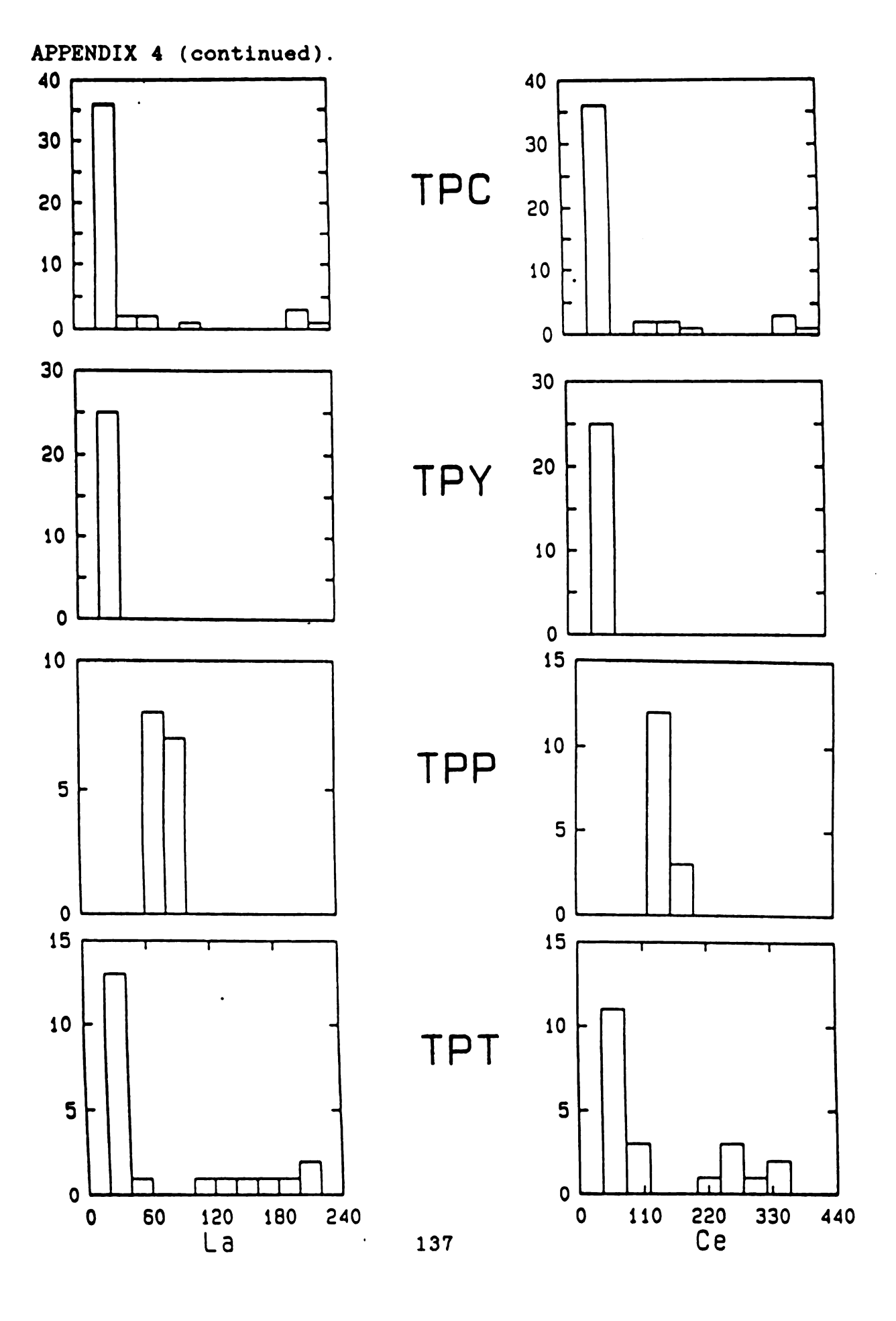


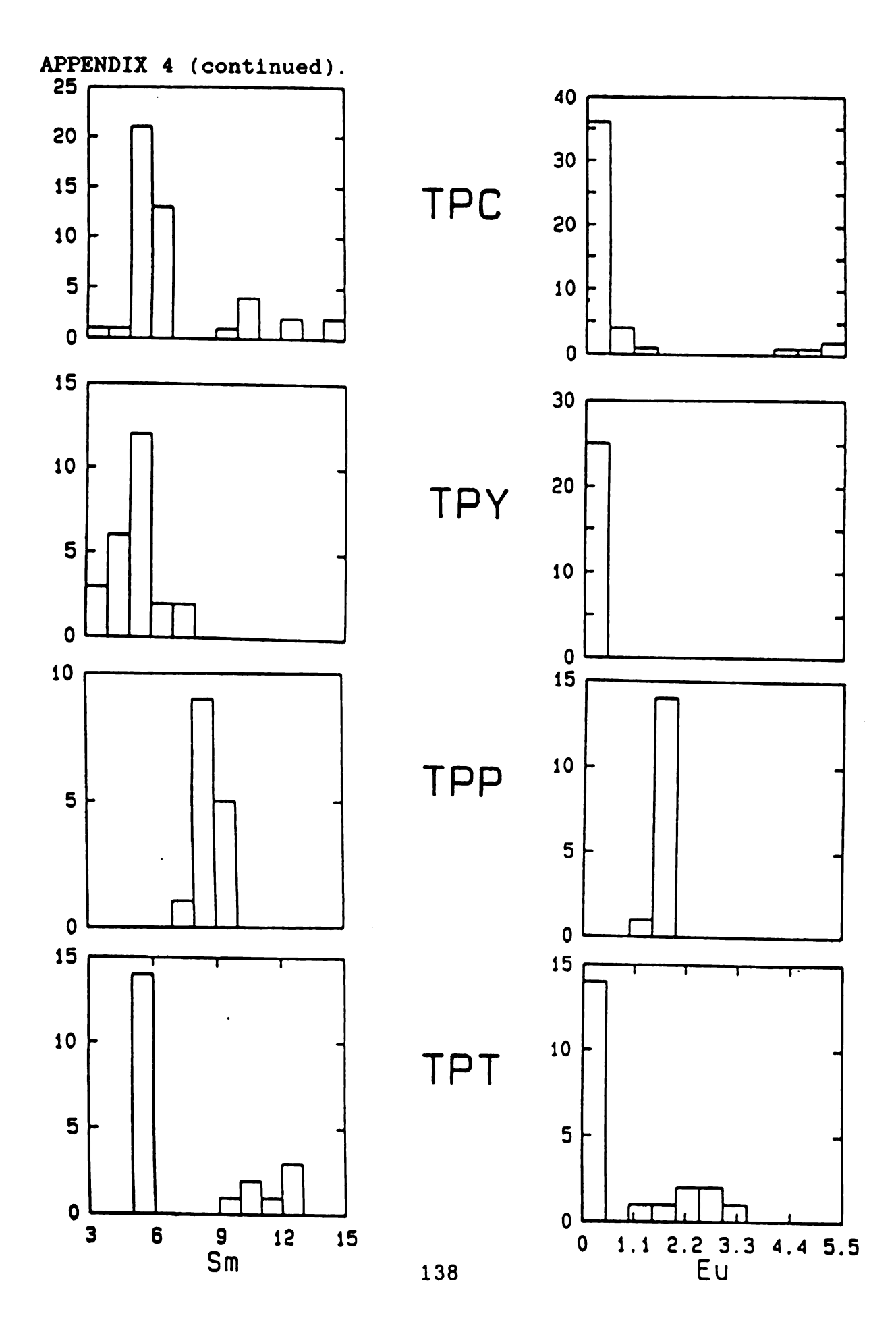


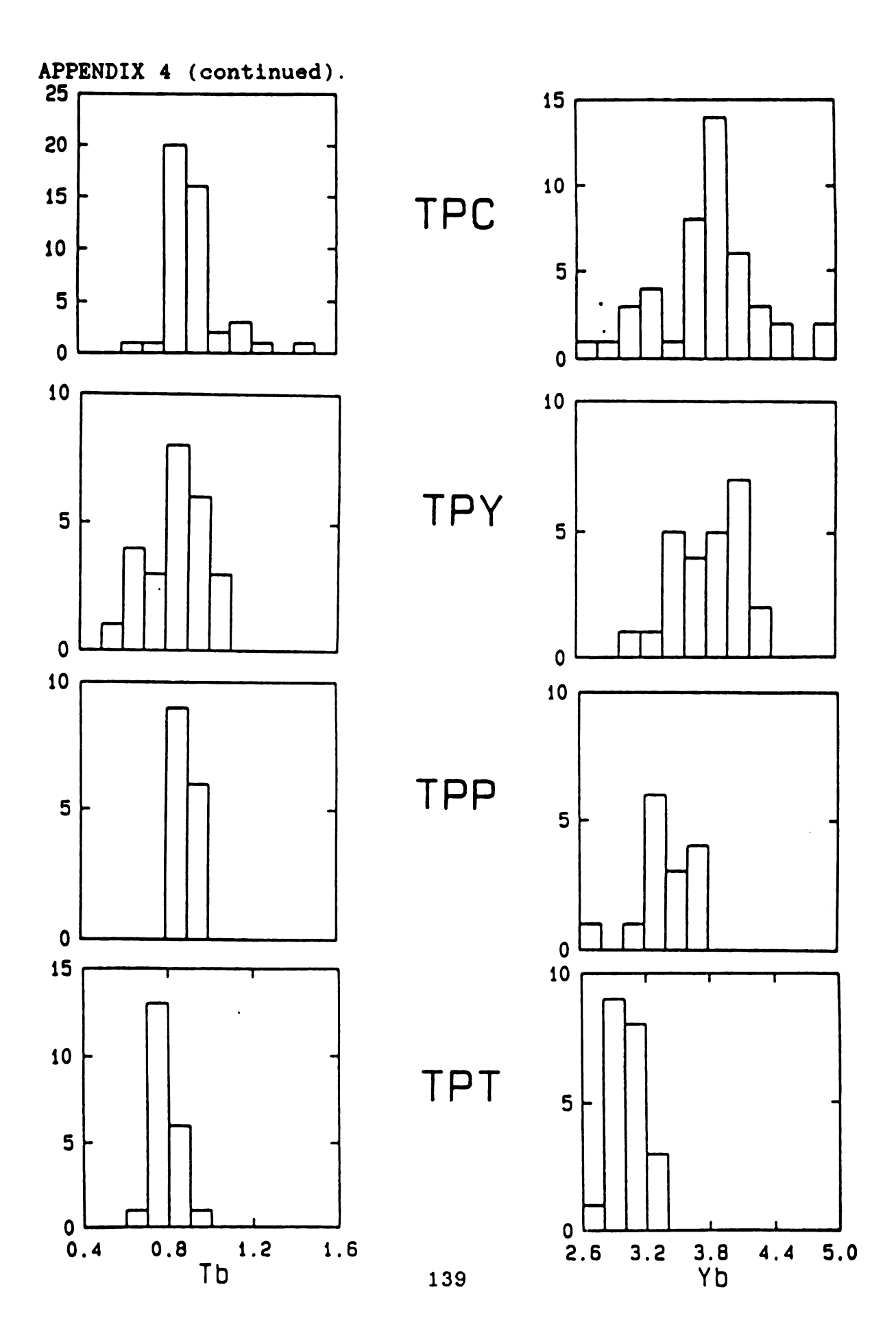




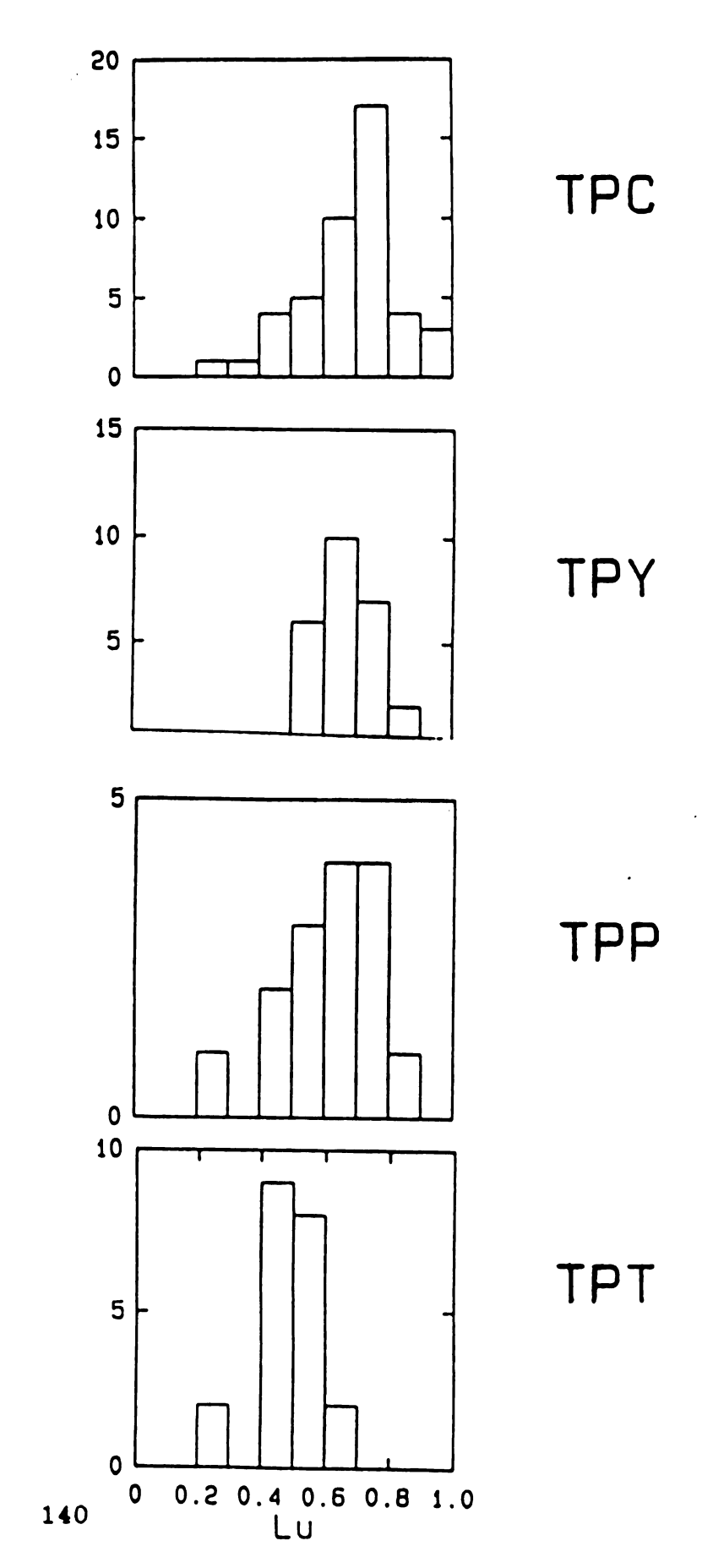








APPENDIX 4 (continued).



APPENDIX 5. Methods used for temperature calculations

The temperatures used in this study were determined using the magnetite/illmenite geothermometer of Spencer and Lindsley (1981). Magnetite and illmenite grains were concentrated and mounted as discussed in Appendix 3. average of three grains of magnetite and three grains of illmenite were analyzed per sample, with an average of three analyses per grain. The microprobe beam was rastered over an area of 100 microns squared. These raw analyses were recalculated to the appropriate stochiometric oxide phase according to Stormer (1983). All analyses which failed to fit into a stochiometric oxide phase or totaled less than 95% when recalculated stochiometrically were rejected. mole fraction of ulvospinel and the mole fraction illmenite were averaged for each grain, and each grain averaged to give a mean value for each sample. Temperatures and oxygen fugacities for each averaged sample were calculated according to the method of Stormer (1983) using a computer program called NEWSTFO2.

REFERENCES

- Anderson, A.T., 1976. Magma mixing: Petrological processes and volcanological tool. J. Volcanol. Geotherm Res., 1: 3-33.
- Bacon, C.R., Macdonald, R., Smith, R.L. and Baedecker, P.A., 1981. Pleistocene high-silica rhyolites of the Coso volcanic field, Inyo County, California. J. Geophys. Res., 86: 10223-10241.
- Baker, B.H. and McBirney A.R., 1985. Liquid fractionation. Part III: Geochemistry of zoned magmas and the compositional effects of liquid fractionation. J. Volcanol. Geotherm. Res., 24: 55-81.
- Blake, S., 1981. Eruptions from zoned magma chambers. J. Geol. Soc. Lond., 138: 281-287.
- Blake, S. and Ivey G.N., 1986. Magma-mixing and the dynamics of withdrawal from stratified resevoirs. J. Volcanol. Geotherm. Res., 27: 153-178.
- Broxton, D.E., Byers, F.M., Jr. and Warren, R.G., 1985.
 Trends in phenocryst chemistry in the Timber
 Mountain-Oasis Valley volcanic field, SW Nevada:
 Evidence for episodic injection of primitive magma into an evolving magma system (abstract). Geol. Soc. Am.
 Abstr. Programs, 17: 345.
- Brown, W.L., and Parsons, I., 1981. Towards a more practical two-feldspar geothermometer. Contrib. Mineral. Petrol., 76: 369-377.
- Byers, F.M., Jr., Carr, W.J., Christiansen, R.L., Lipman, P.W., Orkild, P.P., and Quinlivan, W.D. 1976a, Geologic map of the Timber Mountain caldera area, Nye County, Nevada: U.S. Geol. Surv. Miscellaneous Geologic Investigations Map I-891.
- Byers, F.M., Jr., Orkild, P.P., Quinlivan, W.D. and Sargent, K.A., 1976b. Volcanic suites and related cauldrons of Timber Mountain-Oasis Valley caldera complex, southern Nevada. U.S. Geol. Surv. Prof. Pap. 919: 70 pp.
- Carr, W.J., Byers, F.M., Jr., and Orkild, P.P., 1984. Stratigraphic and volcano-tectonic relations of Crater Flat Tuff and some older volcanic units, Nye County, Nevada. U.S. Geol. Surv. Open-File report 84-114: 42 pp.
- Christiansen, R.L., and Lipman, P.W., 1972. Cenozoic volcanism and plate-tectonic evolution of the Western United States. II. Late Cenezoic: Phil. Trans. R. Soc. London, A 271: 249-284.

- Christiansen, R.L., Lipman, P.W., Carr, W.J., Byers, F.M., Jr., Orkild, P.P. and Sargent, K.A., 1977. Timber Mountain-Oasis Valley caldera complex of southern Nevada. Geol. Soc. Am. Bull., 88: 943-959.
- Cox, K.G., Bell, J.D. and Pankhurst, R.J., 1979. The interpretation of igneous rocks. George Allan and Unwin, London, p. 358.
- Crecraft, H.R., Nash, W.P., and Evans, S.H., Jr., 1981. Late Cenozoic volcanism at Twin Peaks, Utah; Part I: Geology and Petrology. J. Geophys. Res., 86: 10303-10320.
- Criss, J., 1980. Fundamental parameter calculations on a labboratory microcomputer. Advances in X-Ray analysis, 23: 93-97
- Eichelberger, J.C., 1978. Andesite volcanism and crustal evolution. Nature, 275: 21-27.
- Eichelberger, J.C., 1980. Vesiculation of mafic magma during replenishment of silicic magma reservoirs. Nature, 228: 446-450.
- Ekren, E.B., Rogers, C.L., Anderson, R.E., and Orchild, P.P., 1968. Age of basin and range normal faults in Nevada Test Site and Nellis Air Force Range, Nevada. In Nevada Test Site, edited by E.B. Eckel, Mem. Geol. Soc. Am., 110: 247-250.
- Ekren, E.B., Anderson, R.E., Rogers, C.L., and Noble, D.C., 1971. Geology of northern Nellis Air Force Base Bombing and Gunnery Range, Nye County, Nevada. U.S. Geol. Survey Prof Paper 651: 91p.
- Flood, T.P., Schuraytz, B.C., Vogel, T.A. and Younker, L.W., 1985a. Constraints on the evolution of a high-level silicic system based on whole-pumice geochemistry. Eos Trans. AGU, 66: 396.
- Flood, T.P., Schuraytz, B.C., Vogel, T.A. and Younker, L.W., 1985b. Cyclic evolution of a magmatic system: the Paintbrush Tuff, SW Nevada volcanic field. Geol. Soc. Am. Abstr. Programs, 17, 7: 584.
- Govindaraju, K. (Ed.), 1984. Geostandards Newsletter, 8:1-39.
- Hildreth, W., 1981. Gradients in silicic magma chambers: Implications for lithospheric magmatism. J. Geophys. Res., 86: 10153-10192.

- Hagan, R.C., 1982. X-ray fluorescence analysis: Major elements in silicate minerals: Los Alamos-9400-MS: 1-13.
- Hofmann, A.W. and Feigenson, M.D., 1983. Case studies on the origin of basalt. Part I: Theory and reassessment of Grenada basalts. Contrib. Mineral. Petrol., 84: 382-389.
- Huppert, H.E. and Sparks, R.S.J., 1984. Double-diffusive convection due to crystallization in magmas. Ann. Rev. Earth Planet. Sci., 12: 11-37.
- Huppert, H.E., Sparks, R.S.J. and Turner, J.S., 1982. Effects of volatiles on mixing in calc-alkaline magma systems. Nature, 297: 554-557.
- Huppert, H.E., Sparks, R.S.J. and Turner, J.S., 1984. Some effects of viscosity on the dynamics of replenished magma chambers. J. Geophys. Res., 89: 6857-6877.
- Huppert, H.E. and Turner, J.S., 1981. A laboratory model of a replenished magma chamber. Earth Planet, Sci. Lett., 54: 144-152.
- Kouchi, A. and Sunagawa, I., 1983. Mixing basaltic and dacitic magmas by forced convection. Nature, 304: 527-528.
- Kouchi, A. and Sunagawa, I., 1985. A model for mixing basaltic and dacitic magmas as deduced from experimental data. Contrib. Mineral. Petrol., 89: 17-23.
- Langmuir, C.H., Vocke, R.D., Hanson, G.N. and Hart, S.R., 1977. A general mixing equation: applied to the petrogenesis of basalts from Iceland and Reykjanes Ridge. Earth Plan. Sci. Lett., 37: 380-392.
- Lipman, P.W., 1971. Iron-titanium oxide phenocrysts in compositionally zoned ash-flow sheets from southern Nevada. J. Geol., 79: 438-456.
- Lipman, P.W., Christiansen, R.L. and O'Conner, J.T., 1966. A compositionally zoned ash-flow sheet in southern Nevada. U.S. Geol. Surv. Prof. Pap. 524-F: 47 pp.
- Lipman, P.W. and Friedman, I., 1975. Interaction of meteoric water with magma: An oxygen-isotope study of ash-flow sheets from southern Nevada. Geol. Soc. Am. Bull., 86: 695-702.
- Mahood, G.A., Gilbert, C.M. and Carmichael, I.S.E., 1985. Peralkaline and metalaluminous mixed-liquid ignimbrites of the Guadalajara region, Mexico. J. Volcanol. Geotherm. Res., 25: 259-272.

- Mahood, G.A. and Hildreth, E.W., 1983. Large partition coefficients for trace elements in high-silica rhyolites. Geochem. Cosmochim. Acta, 47:11-30.
- McBirney, A.R., Baker, B.H. and Nilson, R.H., 1985. Liquid fractionation. Part I: Basic principles and experimental simulations. J. Volcanol. Geotherm. Res., 24: 1-24.
- Nash, W.P. and Crecraft, H.R., 1985. Partition coefficients for the trace elements in silicic magmas. Geochem. Cosmochim. Acta, 49: 2309-2322.
- Noble, D.C. and Hedge, C.E., 1969. Sr87/Sr86 variations within individual ash-flow sheets. U.S. Geol. Surv. Prof. Pap. 650-c: 133-139.
- Noble, D.C., Kistler, R.W., Christiansen, R.L., Lipman, P.W., and Poole, F.G., 1965. Close association in space and time of alkalic, calc-alkalic, and calcic volcanism in southern Nevada (abtract). Geol. Soc. Am. Spec. Paper 82, 143-144.
- Noble D.C., Vogel, T.A., Weiss, S.I., Erwin, J.W., McKee, E.H., and Younker, L.W., 1984. Stratighraphic relations and source areas of ash-flow sheets of the Blach Mountain and Stonewall Mountain Volcanic Centers, Nevada. J. Geophys. Res., 89: 8593-8602.
- Poole, F.G., Carr, W.J., and Elston, D.P., 1966. Salyer and Wahmonie Formation of southeastern Nye County, Nevada. Bull. U.S. Geol. Surv. 1224-A: A36-A44.
- Quinlivan, W.D., and Byers, F.M., Jr., 1977. Chemical data and variation diagrams of ingeous rocks from the Timber Mountain-Oasis Valley caldera complex, southern Nevada. U.S. Geol. Surv. Open-File Report 77-724, 9 pp.
- Schuraytz, B.C., Vogel T.A., and Younker L.W., 1983. Pumice heterogeneity in the Topopah Spring Member of the Paintbrush Tuff: Implications for ash-flow eruption dynamics (abstract). Eos Trans. AGU, 64: 896.
- Schuraytz, B.C., Vogel, T.A. and Younker, L.W., 1985. Inflections in elemental and mineralogical gradients within the Topopah Spring Member of the Paintbrush Tuff: Evidence for the resolution of compositional and thermal properties across a magmatic interface (abstract). Eos Trans. AGU, 66: 391.
- Schuraytz, B.C., Vogel, T.A. and Younker, L.W., 1986. Geochemical gradients in the Topopah Spring Member of the Paintbrush Tuff: Evidence for eruption across a magmatic interface. (In prep.).

- Scott, R.B., Byers F.M., Jr. and Warren, R.G., 1984. Evolution of magma below clustered calderas, southwest Nevada volcanic field (abstract). Eos Trans. AGU 65: 1126-1127.
- Smith, R.L., 1979. Ash-flow magmatism. Geol. Soc. Am. Spec. Pap., 180: 5-27.
- Sparks, R.S.J., Huppert, H.E. and Turner, J.S., 1984. The fluid dynamics of evolving magma chambers. Phil. Trans. R. Soc. London, A 310: 511-534.
- Sparks R.S.J., and Marshall, L.A., 1986. Thermal and mechanical constraints on mixing between mafic and silicic magmas. J. Volcanol. Geotherm. Res., 29: 99-124.
- Spencer, K.J., and Lindsley, D.H., 1981. A solution model for coexisting iron-titanium oxides. Am. Mineral., 66: 1189-1201.
- Spera, F.J., 1984. Some numerical experiments on the withdrawal of magma from crustal reservoirs. J. Geophys. Res., 89: 8222-8236.
- Spera, F.J., Yuen, D.A., Greer, J.C., and Sewell, G., 1986. Dynamics of magma withdrawl from stratified magma chambers. Geology, v. 14, no.9: 723-726.
- Stormer J.C., and Whitney J.A., 1985. Two feldspar and iron-titanium oxide equilibria in silicic magmas and the depth of origin of large volume ash-flow tuffs. Am. Mineral., 70: 52-64.
- Turner, J.S., and Campbell, I.H., 1986. Convection and mixing in magma chambers. Earth Sci. Rev., 23: 255-352.
- Turner, J.S., Huppert, H.E. and Sparks, R.S.J., 1983. An experimental investigation of volatile exsolution in evolving magma chambers. J. Volcanol. Geotherm. Res., 16: 263-277.
- Tuttle, O.F., and Bowen, N.L., 1958. Origin of granite in the light of experimental studies in the system NaAlSi3O8-KAlSi3O8-SiO2-H2O. Geol. Soc. America Mem. 74:153p.
- Vogel, T.A., Younker, L.W., Wilband, J.T. and Kampmueller, E., 1984. Magma mixing: the Marsco suite, Isle of Skye, Scotland. Contrib. Mineral. Petrol., 87: 231-241.
- Vogel, T.A., 1982. Magma mixing in the acidic-basic complex of Ardnamurchan: Implications on the evolution of shallow magma chambers. Contrib. Mineral. Petrol., 79: 411-423.

- Warren, R.G., Byers, F.M. and Caporusio F.A., 1984.
 Petrography and mineral chemistry of units of the Topopah Spring, Calico Hills and Crater Flat tuffs, and older volcanic units, with emphasis on samples from drill hole USW G-1, Yucca Mountain, Nevada Test Site. Rep. La-10003-MS: 1-78.
- Warren, R.G., and Byers, F.M., 1985. The petrologic unit: a useful tool in deciphering a complex volcanic terrane in SW Nevada (absract). Geol. Soc. Am. Abstr. Programs, 17:270.
- Whitney J.A., and Stormer, J.C. Jr., 1986. Model for the intrusion of batholiths associated with the eruption of large-volume ash-flow tuffs. Science, 231: 483-485.
- Wright, T.L. and Doherty, P.C., 1970. A linear programming and least squares computer method for solving petrologic mixing problems. Bull. Geol. Soc. Amer., 81: 1995-2008.